Synthesis and Characterization of Ni-based Layered Cathode Materials by Carbonate Co-precipitation Method

(共沈炭酸塩を原料とするNi系層状化合物の合成とその電池特性に関する研究)

September, 2005

Division of Energy and Materials Science
Graduate School of Science and Engineering
Saga University

Tae-hyung Cho

Contents

Chapter 1

Introduction

1.1 Introduction

During the past several decades the electronics industry has been rapidly developed. In recent year, outstanding growth in portable electronic products, such as notebook computer, cellular phones, PDA's and camcorder, is leading an increasing demand for energy storage system. As the portable products become more advanced and their size and weight continue to reduce, the demands for energy storage device, such as smaller size, higher energy density and lighter weight also continuously increased. As energy storage device for the mobile electronic devices, there are two kinds of battery, i.e. primary and secondary battery. However, the secondary battery is better than primary battery in the viewpoint of economy and environment.

There are several kinds of secondary battery for the portable electronic device, such as lead-acid, nickel cadmium (Ni-Cd), nickel metal hydride and lithium ion. Among these, lithium ion secondary battery has mainly used nowadays as an energy storage device for its special merits, such as high working voltage of 3.6 V, which is three times higher than that of Ni-Cd and Ni-MH secondary battery, longer cycle life, lower self discharge rate and higher energy density than Ni-Cd, Ni-MH secondary battery (see Fig. 1.1).

1.2 The history of lithium battery

Since Li element is light and possesses a relatively lower potential, many research groups tried to apply this element to high power density battery material [1]. Obviously, lithium, an anode, can give higher energy density than other anodes. However, metallic lithium easily reacts with water and emits hydrogen gas. Therefore the aqueous electrolyte cannot be used for metallic lithium anode. The research of

lithium battery was activated since it was reported that the metallic lithium can be stable in some electrolyte such as molten salt, liquid SO_2 and organic electrolyte like PC (propylene carbonate) / $LiClO_4$. The primary lithium battery had been developed in 1970's [2].

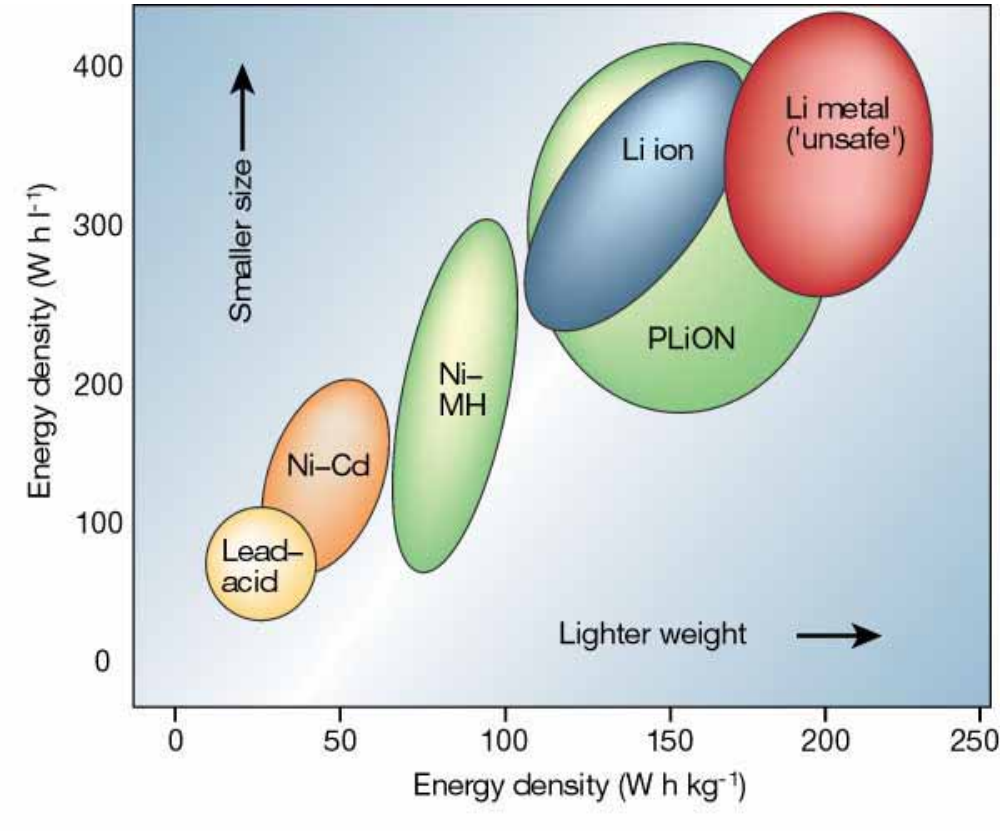

Figure 1.1 Specific energy densities (per weight and per volume) of several secondary batteries.

Attempt to develop rechargeable lithium batteries have been carried out from the beginning of 1970's, and extensive research allow the commercialization of the lithium secondary batteries. However, the lithium secondary battery has a severe problem such as dendrite formation of lithium metal during charge process as shown in Fig. 1.2. As a matter of fact, several cellular phones, which are mounted lithium

secondary batteries as power sources, were recalled at the end of 1980's with respect to several undesirable accidents, such as firing or explosion during use. In the early stage of 1980's, a new concept, "Rocking chair", was proposed [3] and demonstrated by some research groups [4-6]. However, cathode material should have high redox potential in order to compensate the decrease in cell voltage.

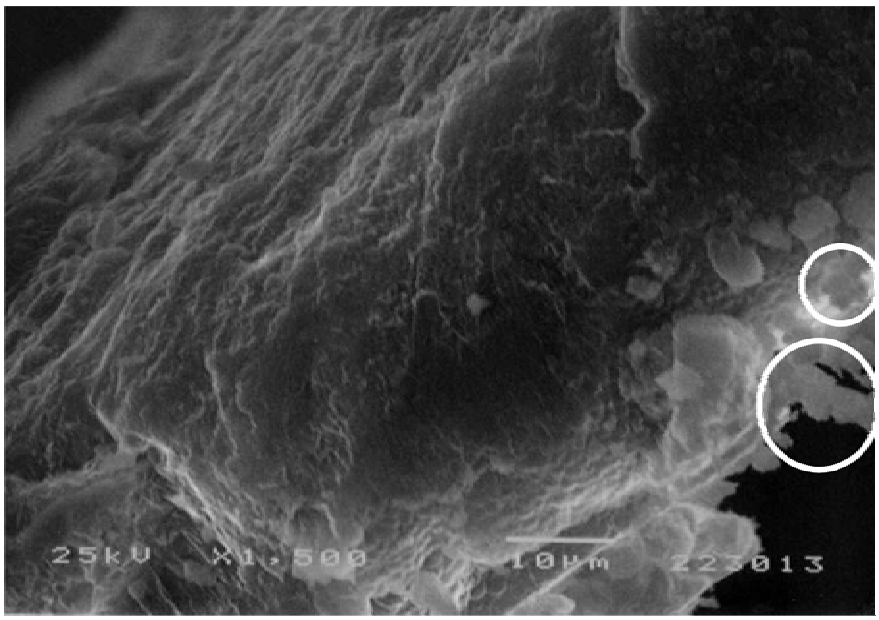

Figure 1.2 The growth of lithium dendrites on the surface of Cu foil. The dendrite is shown in the circles.

In 1990's, lithium ion battery have commercialized by Sony Energytech based on a carbon (non-graphitic) as an anode and $LiCoO_2$ as a cathode. The name of "lithium ion battery" was given by T. Nagaura and K. Tozawa[7], and the concept of "lithium ion battery" was firstly introduced by Asahi Kasei Co. Ltd and they obtained patents around the world [8]. Sony has made several interactive improvements on the performance of their particular rocking chair battery (RCB) system. Today, the lithium

ion battery is the fastest growing and the most promising battery.

1.3 General concept of lithium battery

1.3.1 Lithium metal battery

The discharge process of this battery involves three main steps in the metallic lithium anode; i) dissolution of lithium ion from lithium metal anode, ii) the migration of lithium ions across the electrolyte and separator and iii) insertion of lithium ions into the host structure of the cathode. Common cathode materials for lithium metal battery are inorganic compounds, such as transition metal dechalcogenides and oxides. They are characterized by layered or tunneled structure, which can provide channels in order to transfer lithium ions reversibly and faster in the host matrix. In fact, it is well known that Li/V_6O_{13} [9], Li/TiS_2 [10] and Li/MoS_2 [11] cells have been proved to have a reversible behavior. The Li/MoS_2 cell was commercialized by Moli Energy.

In the view point of reversibility, I believe that the lithium secondary battery with lithium metal anode is capable of very long cycle life and supplies a fairly stable operation voltage and capacity. However, practical cyclability of the battery is limited due to the dendritic growth of lithium metal, which causes short circuit of cell, followed a drastic increase in volume of the anode [12,13]. The abrupt changes in the anode would bring about safety hazard or explosion by thermal abuse.

1.3.2 Lithium ion battery

Lithium ion battery (LIB) has emerged from lithium metal battery to eliminate its un-safety. The principle of the Li-ion battery is explained in the Fig. 1.3. The inorganic compound, $LiCoO_2$, is used as the cathode material. This material has a

rhombohedral structure where Li and Co cations fill alternating layers of edge-sharing octahedral sites in a close packed oxygen array. During charging, lithium is extracted from the layers, then transported and doped into the carbonaceous anode. In the discharge process, the lithium ions are un-doped from the anode and return again to the space between layers in the cathode. Thus, this battery is sometimes called as the "Rocking Chair Battery" or the "Swing Battery" in the view point of lithium transfer. The reaction scheme of the lithium ion battery is expressed in Figure 1.3, where $LiCoO_2$ is used as cathode material. When a cell is assembled, lithium ions are not doped into carbon. Therefore, the battery has low voltage near 0 V.

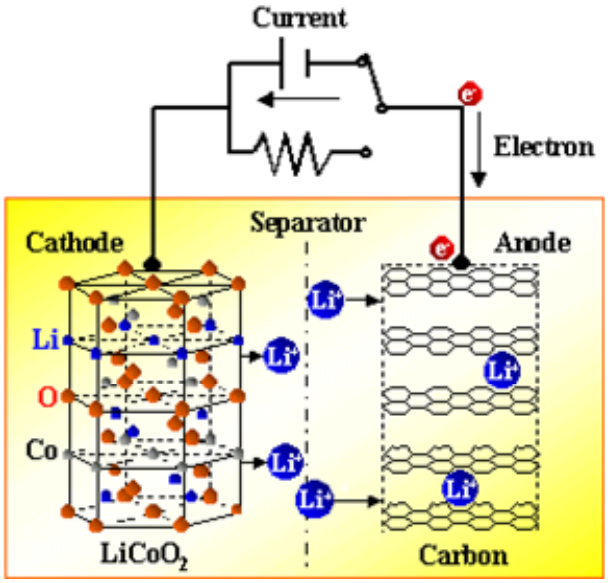

(+, Positive electrode):

$$LiCoO_2 \underset{\text{discharge}}{\overset{\text{charge}}{\rightleftharpoons}} Li_{1-x}CoO_2 + xLi^+ + xe^-$$

(-, Negative electrode):

$$C + xLi^+ + xe^- \underset{\text{discharge}}{\overset{\text{charge}}{\rightleftharpoons}} Li_xC$$

Figure 1.3 Basic structure of electroactive material and its redox reaction in lithium ion battery.

1.4 Components for lithium ion battery

1.4.1 Requisites for electrode materials [14]

High specific energy density (related to both average working voltage and reversible capacity) and long cyclic life (related to the stability of structure and electrode-electrolyte interface) are simultaneously required for a high performance Li-ion battery. Therefore, some aspects should be considered in the design of new electrode materials for lithium rechargeable batteries. In general, structure, chemical stability and the available redox couple of electroactive materials are the primary points. Ideally, it should simultaneously match following conditions:

a) An open structure to permit reversible lithium migration

In brief, the working principle of lithium rechargeable battery is the reversible migration of lithium between cathode and anode accompanied by a redox process, whose reversibility is prerequisite to Li secondary battery. Thus, the structure of the compound should be open for lithium insertion in its lattice.

b) Stability of electrode and electrolyte

This is the requirement for a long cycle life. The insertion/extraction reaction has a topotactic character and both insertion and extraction of guest lithium ions into and from host compound should ideally not modify the host structure. On the other hand, the oxidation of electrolyte should be avoided for oxidation and reduction.

c) A higher specific energy density

The specific energy density (per weight or per volume) is related to both the working voltage and the reversible capacity. The former depends on the potential of the redox process and the latter is restricted by the reversible amount of lithium intercalation. The available redox pair should locate in a suitable energy and the

structure of material should be stable in wide composition range in order to obtain a high specific energy density.

d) Higher electrode conductivities

The lithium insertion/extraction involves both lithium ions diffusion in the lattice and charge transfer process on the particle surface. Thus, electrode's conductivity includes both bulk lithium ion conductivity in active material and electronic conductivity of electrode. Higher electronic conductivity is helpful to keep the inner resistance low and gives an excellent rate capability. Beside this, lower interfacial resistance for electrochemical reaction is desirable for lower the polarization of electrode.

e) A low cost and environment benign.

The cost and environmental impact should be always kept in mind for new battery design. It is one of the future challenges to develop cheaper and hazardless electrode materials with excellent battery performances.

Fig. 1.4 shows the working potential and capacity of the various electrode materials [15]. Compounds with a working potential of above 3 V can be used as cathode materials in lithium ion battery. They include lithium containing transition metal oxides, such as $LiCoO_2$, $LiMn_2O_4$, $LiNiO_2$, $LiMnO_2$ and their derivatives, and polyanionic compounds, for example, $LiFePO_4$ compound.

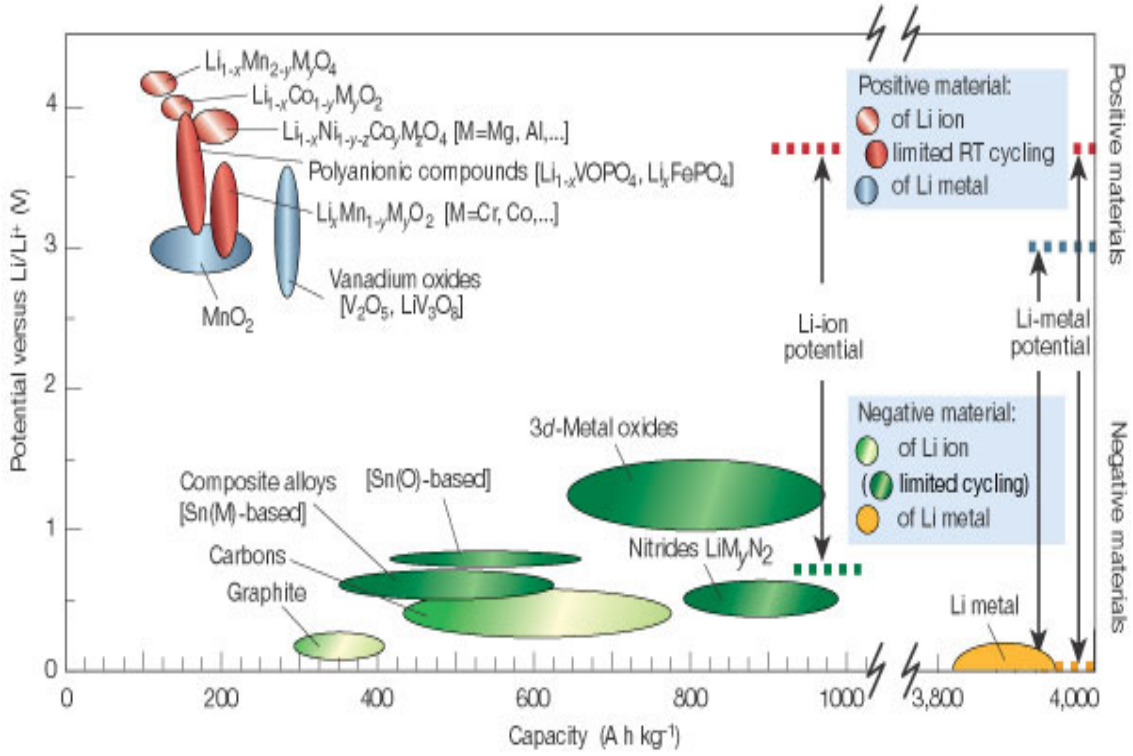

Figure 1.4 Voltage vs. capacity of some electrode materials.

1.4.2 Cathode materials for lithium ion battery

1.4.2.1 Layered transition metal oxide cathode

The layered metal oxides with a general formula of $LiMeO_2$ (Me = Transition metal elements such as Co, Ni and Mn), in which the Li ion and Me ion occupy the alternate (111) planes of the rock salt structure. The structure has an oxygen stacking sequence of ···ABCABC··· along the c axis of hexagonal setting and the Li and Me ions occupy the octahedral sites. There are three MeO_2 sheet per unit cell. This structure can be described as a layered structure with a space group of $R\bar{3}m$, and the unit cell parameters are conveniently defined in terms of the hexagonal setting [16]. A schematic layered structure is presented in the Fig. 1.5. The structure with MeO_2 layers

allows a reversible extraction/insertion of lithium ions from/into the lithium planes.

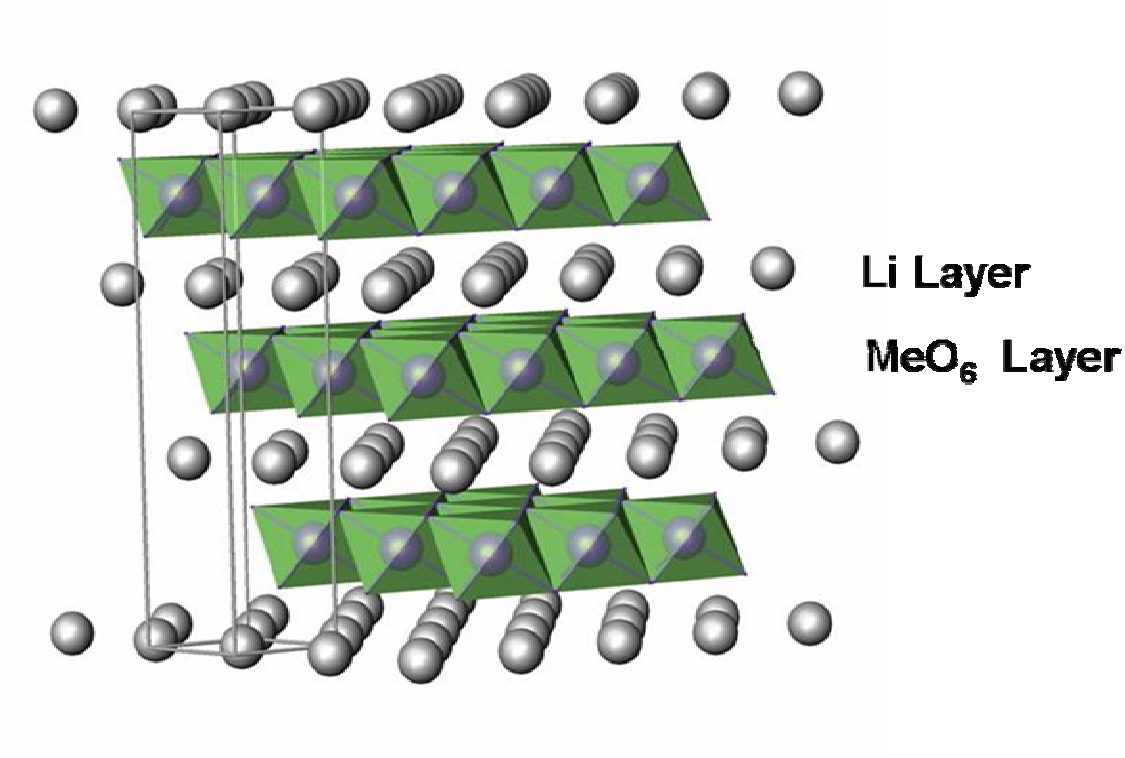

Figure 1.5 Schematic model of an ideal $LiMeO_2$ structure with $R\bar{3}m$.

Layered $LiCoO_2$

The most of the commercial lithium ion batteries are built with the $LiCoO_2$ cathode material. The $LiCoO_2$ has a hexagonal structure with cell parameters of a = 2.82 Å and c = 14.08 Å [16-20]. The cathode synthesized at higher temperature above 800 ^oC shows O3 type stacking with a regular ordering of Li^+ and Co^{3+} ions in the alternate (111) planes of the rock salt lattice. On the other hand, synthesis at lower temperatures (~400 ^oC) results in a considerable disordering in distribution of the Li^+ and Co^{3+} ions, which lead to the formation of a spinel like $LiCoO_2$ phase with poor electrochemical properties.

$LiCoO_2$ has a theoretical capacity of 274 mAh g^{-1}, corresponding to extraction

of 1 mole of Li^+ from $LiCoO_2$ and its average working voltage is about 4 V. The cathode undergoes serious phase transformation between hexagonal and monoclinic when the cathode charged above 4.2 V [21-23]. Since this phase transformation leads deterioration of cycling performance, practical capacity is restricted as half of theoretical capacity. A phase transformation corresponding to the lithium extract amount from host structure is schematically given in the Fig. 1.6 (a). This structural change leads volume change, and it could be cause of the defects of particles. Moreover, the capacity fading can be attributed to side reaction, Co dissolution at higher voltage > 4.2 V, from oxide compound into electrolyte.

In order to suppress phase transformation, substitution of foreign elements such as Mg [24-26], Al [27-32], Fe [33-35], Ni [36-43], Cr [44], Mn [45,46] and Li [47-49] for Co has been extensively studied. Recently, Zou et al reported that small amount of foreign element can give stable cycling performance due to suppression of phase transformation during intercalation/deintercalation process at higher cut-off voltage of 4.5 V [50-52]. Nowadays, Mg doped $LiCoO_2$ is used for commercial lithium ion battery. Moreover, it has been found that the cyclability of the cathode material could be improved significantly by modifying its surface with metal oxide such as Al_2O_3 and ZrO_2 [53,54]. However, drawbacks of $LiCoO_2$, such as higher price and toxicity of cobalt element accelerate extensive studies to investigate alternatives to $LiCoO_2$.

Layered $LiNiO_2$

The $LiNiO_2$ cathode material is considered to be one of the best cathode materials for Li-ion battery. It has same crystal structure with $LiCoO_2$ and belongs to hexagonal system ($R\bar{3}m$) with cell constant of a = 2.88 Å and c = 14.18 Å [55-59]. Its

working voltage is more than 3.7 V and theoretical capacity is 275 mAh g^{-1}. The $LiNiO_2$ provides important advantages, such as less toxicity, lower price and higher reversible capacity of about 200 mAh g^{-1}, compared to $LiCoO_2$. However, it suffers from a few problems, i.e. irreversible phase transformation, difficulty in synthesis and safety concerns.

The cathode material shows topotatic reaction consisting of three single phase reactions for the $0 \leq x \leq 0.75$ in $Li_{1-x}NiO_2$ and two phase reaction, in $0.75 < x < 1$ [60-62]. A schematic representation of the phase transformation during the delithiation is given in Fig. 1.6 (b). This phase transformation could cause capacity fading. Moreover, the Li-Ni-O system is characterized by the existence of a $Li_{1-z}Ni_{1+z}O_2$ ($0 < z \leq 0.2$) solid solution. Although the structure can still be described as a layered structure at low z value ($z \leq 0.2$), it has cation mixing, i.e. presence of extra Ni^{2+} cations in the Li layers. The extra nickel ions in the Li layer hinder the diffusion of lithium ions during electrochemical cycling and resulting in poor battery performance.

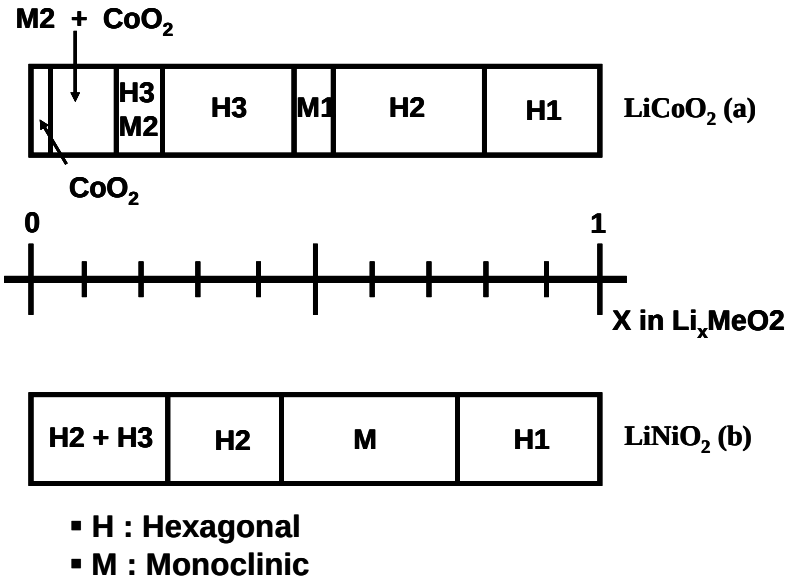

Figure 1.6 A schematic diagram of phase transition for the (a) $LiCoO_2$ and (b) $LiNiO_2$.

In order to overcome these drawbacks, the $LiNi_{1-x}Co_xO_2$ solid solution has been widely studied because these materials seem to combine the advantages of both $LiNiO_2$ and $LiCoO_2$. For instance, the presence of more than 20 % of Co in the $LiNiO_2$ can stabilize an ideal layered structure without cation mixing, thus $LiCo_{0.2}Ni_{0.8}O_2$ shows excellent electrochemical behavior [63-66]. However, Co content should be less than 15 % in order to compensate cost problem. Although the reversible capacity is decreased, the thermal stability of the cathode can be improved by partly substitution of small amount of Mn [67,68] and Fe [69,70] for Ni. Though small amount of Mg doping [71] leads slight decrease in initial capacity, and a strong increase in electronic conductivity by hole formation. Further suppression of phase transformation during de-intercalation process results in excellent cycle stability.

1.4.2.2 Li - Mn - O system

Spinel $LiMn_2O_4$ compound

A spinel compound, $LiMe_xMn_{1-x}O_4$ (Me = Metal element), is an attractive cathode material for replacing Co or Ni based layered cathode materials in the next generation of Li-ion batteries. Especially, it has been extensively studied as positive electrode materials of large-size lithium ion batteries for power sources of hybrid electric vehicles (HEV) [72,73] because they have several advantages such as lower cost, high-rate capability and higher thermal stability compared to those of Co or Ni based layered materials (e.g. $LiCoO_2$ or $LiNiO_2$).

As shown in the Fig. 1.7, the $LiMn_2O_4$ crystallizes in space group, $Fd\bar{3}m$, with Li and Mn present in 8a tetrahedral sites and 16d octahedral sites in the cubic close-packed oxygen array, respectively. All other sites, such as tetrahedral 8b and 48f sites

and octahedral 16c sites, are empty [74]. MnO_6 octahedra share edges to build a rigid three-dimensional framework. Li ions diffuse through 8a-16c-8a path [75].

From the spinel cathode, about 1 mole of lithium can be reversibly extracted in two steps, at 4.05 V and 4.15 V, leading to the delithiated λ-MnO_2 [76]. On the other hand, the spinel $LiMn_2O_4$ is changed to tetragonal $Li_2Mn_2O_4$ when more lithium ions are inserted into the 16c site at 2.8 V.

The cathode was firstly used in a commercial Li-ion cell in 1996. However, this compound shows poorer performance than the layered cathodes. The main problem for the application of Mn spinel is the capacity fading upon cycling which become serious at elevated temperature (above 60 ^oC). Many possible sources had been proposed, such as structural instability [77-79], Mn dissolution into the electrolyte [80,81], the cooperative Jahn-Teller effect [82].

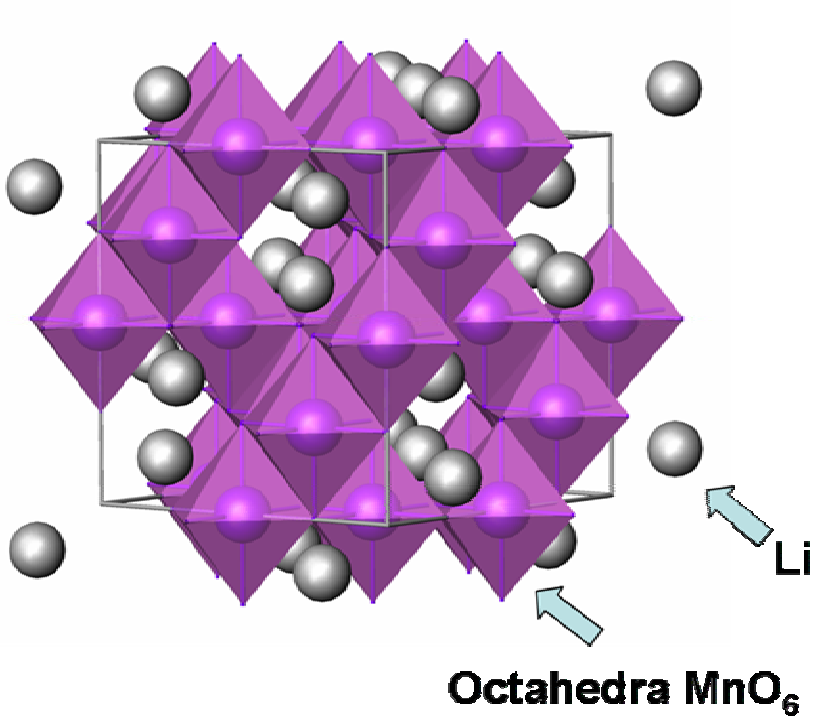

Figure 1.7 Structure of cubic spinel $LiMn_2O_4$.

Recently, M. Yoshio et al. elucidated that main reason for capacity fading of spinel, $LiMe_xMn_{1-x}O_4$ (Me = Metal element), is closely related to oxygen deficiency [78,83-85]. In the charge-discharge profiles, this kind of sample shows a 3.2 V discharge plateau together with 4.5 V charge plateau, and the charge-discharge plateaus delivering the equivalent capacity [83,84]. They also have reported that oxygen deficient spinel brings the phase transformation from cubic to orthorhombic phase at around lower than room temperatures [78]. Consequently, preparing oxygen stoichiometric spinel compound is critical point to overcome capacity fading.

Main drawback in application of oxygen stoichiometric $LiMe_xMn_{1-x}O_4$ (Me = Metal element) for $LiMe_xMn_{1-x}O_4$/graphite cell at elevated temperature (over than 50 ^oC) is dissolution [86] of Mn ions because the dissolved Mn ions from cathode material [87,88] attack graphite anode thereby degradation of anode. In order to reduce the solubility of Mn ions at the elevated temperature, surface encapsulation [89], reducing specific surface area [85,90] have been suggested and investigated.

$LiMnO_2$ compound

Since this compound shows higher theoretical capacity of 285 mAh g^{-1} than spinel $LiMn_2O_4$ 148 mAh g^{-1}, $LiMnO_2$ as cathode materials is of interest. $LiMnO_2$ is polymorphous, mainly orthorhombic (zigzag layered structure, P_{mmn}) and monoclinic (layered structure, $C_{2/m}$) structure as shown in Fig. 1.8 (a) and (b), respectively.

Orthorhombic $LiMnO_2$ crystallizes in the space group P_{mnm} where Mn (y=5/8) and Li (y=1/8) occupies in octahedral 2a sites in the distorted cubic close packed oxygen array, respectively [91,92]. Generally, this cathode material is prepared by solid state reaction method by using manganese oxide and lithium hydroxide at various

temperatures under inert atmosphere. When the material is synthesized at low temperature, this compound can deliver higher capacity about 200 mAh g^{-1}. On the other hand, the sample synthesized at higher temperature displays lower capacity with better cycle stability than low temperature product [93-98]. The cathode material undergoes irreversible phase transformation to spinel-like structure during cycling in the voltage range between 2 and 4.3 V.

Monoclinic $LiMnO_2$ has iso-structural with layered $LiCoO_2$. It is not thermodynamically stable, thus it can be prepared by ion exchange from α-$NaFeO_2$. It also undergoes phase transformation to spinel as orthorhombic $LiMnO_2$.

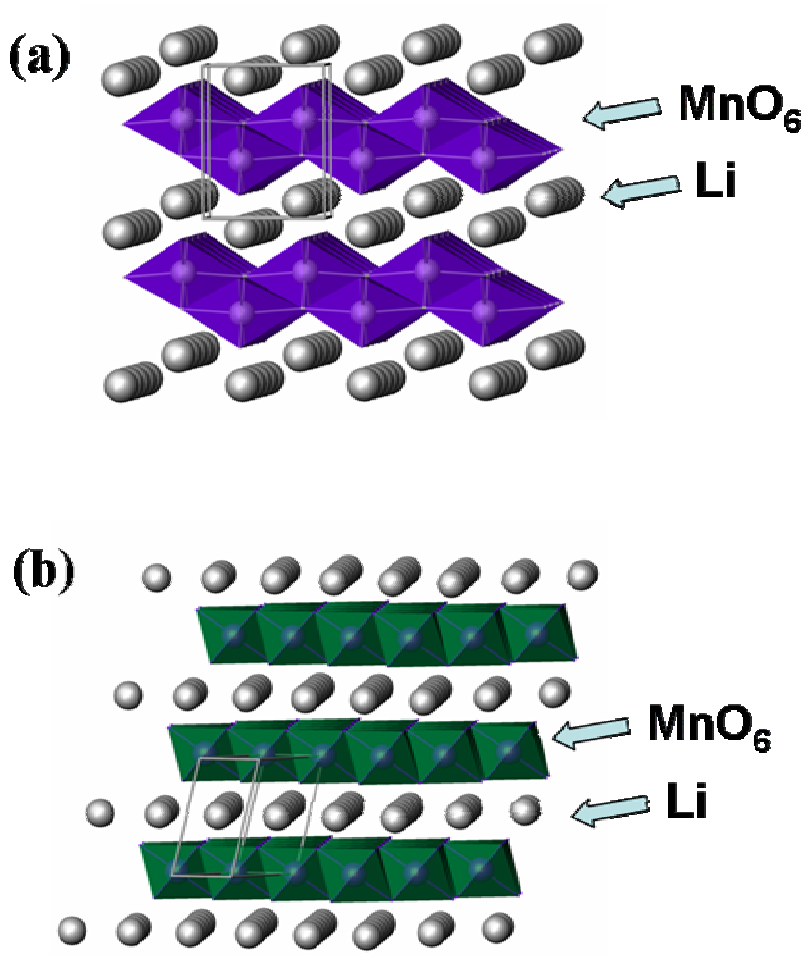

Figure 1.8 The structure of (a) orthorhombic and (b) monoclinic $LiMnO_2$.

1.4.2.3 $LiFePO_4$ with olivine structure

Padhi first demonstrated that orthorhombic $LiFePO_4$ could be used as a cathode for rechargeable lithium battery [99]. It has a theoretical capacity of 170mAh g^{-1} and is environmentally benign and inexpensive. Further it shows excellent cycle stability due to structural similarity between charged/discharged states. Especially, this material exhibits very good thermal stability [100,101]. These properties make it an attractive candidate for large scale batteries, such as power source for an electric vehicle.

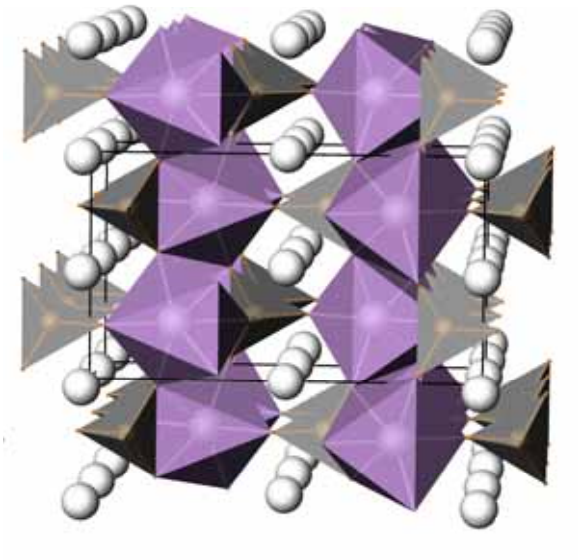

Figure 1.9 Structure of $LiFePO_4$.

Olivine type $LiMPO_4$ (M = transition metal) is one of polyanionic compounds, such as NASICON $Li_3Fe_2(PO_4)_3$ [102] and monoclinic (or rhombohedral) $Fe_2(SO_4)_3$ [103]. The polyanionic compounds can be viewed as replacement of O^{2-} anions by larger size $(XO_4)^{m-}$ polyanions such as PO_4^{3-}, SO_4^{2-}, MoO_4^{2-}, WO_4^{2-} and so forth. Olivine type $LiFePO_4$ (orthorhombic structure, P_{nma}) allows two-dimensional Li^+

diffusion pathway as shown in Fig. 1.9. The problem for this material is low electrical (electronic and ionic) conductivity, so electrochemical properties depend on charge/discharge rate and operating temperature [104]. In order to overcome this drawback, many works have been done and it is found that reduction of particle size and increase in electronic conductivity by coating of conducting agent are quite effective [105-108]. However, reducing particle size leads to lower electrode density and lower energy density, and coating process requires too much carbon. Therefore, the drawbacks, such as lower conductivity, lower operating voltage and poor rate capability, prevent the cathode material from commercial application.

1.4.3 Carbonaceous anode materials

The types of carbonaceous materials used in lithium ion battery are roughly divided into three: graphite, soft carbon and hard carbon. The structure of graphite is quite regular, namely constructed from regular stacking of grapheme sheet. Lithium ions are doped into the layers to form the substance of graphite intercalation compound (GIC) during the charge. The composition of fully lithiated Li-GIC is expressed as LiC_6, so the theoretical discharge capacity is calculated to be 372 mAh g^{-1}. It is well known that it can not be used in PC (propylene carbonate) based electrolyte for the sake of predominant decomposition of PC on graphite surface. Moreover, EC (ethylene carbonate) based electrolyte also gradually decompose. Therefore, only hard carbon was used along PC and EC based solvent before 1997. With invention of electrolyte additive, which suppress decomposition of EC based solvent, graphite can be used as anode. As shown in Fig. 1.10, soft carbons have fairly developed layered structures, but crystal growth is poorer than graphite. The soft carbon can be used in EC based

electrolyte. This also shows 372 mAh g^{-1} as theoretical discharge capacity.

On the other hand, hard carbon is quite different from above two. The anode particle is an aggregate of small crystallites randomly oriented, in which there are small irregular spaces. Each crystallite has a layer structure like a broken piece of graphite. It is smoothly capable of storing and releasing lithium ion. This material may show more than 372 mAh g^{-1} of discharge capacity.

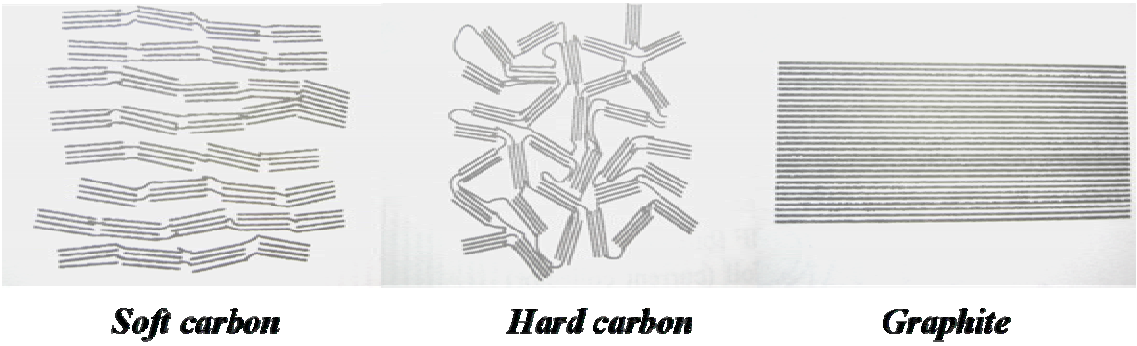

Figure 1.10 Three types of carbon used in lithium ion battery.

1.4.4 Electrolytes

The most popular electrolytes are the liquid-type ones where carbonates or esters of simple alcohol and glycol are frequently used as solvents which contain $LiPF_6$ as an electrolyte. Sometimes a combination of γ-butyllactone and $LiBF_4$ is utilized. Propylene carbonates is an excellent solvent, but it decomposes vigorously on the surface of graphite.

Recently, polymer electrolytes have attracted much attention because they enable us to be free from electrolyte leakage and to make a very thin battery. Many kinds of polymer electrolytes have been proposed, but only a few are utilized in practical

batteries. Basically, these are not a true solid polymer, but a polymer gel containing liquid electrolyte as a plasticizer. The gel contains a lot of liquid, however, it strongly resists leakage of the liquid electrolyte which is kept stably in the matrix.

1.4.5 Separators

The separator used in LIB has two important functions: one is to avoid the direct contact between the anode and cathode, while it allows a free mass transfer of the electrolyte, and the other is a shutter action to stop the mass transfer in the case of accidental heat generation, which cause it melt down, resulting in shut down of a cell. The material should be soft and flexible enough to act as buffer between the both sheets of cathode and anode. The material should be sufficiently stable for a long time while it is kept in contact with the electrolyte. Orientated polyolefin film is commonly used. Stretching of film is an important process for obtaining a high porous film. Examples of SEM images of this film are shown in Fig. 1. 11.

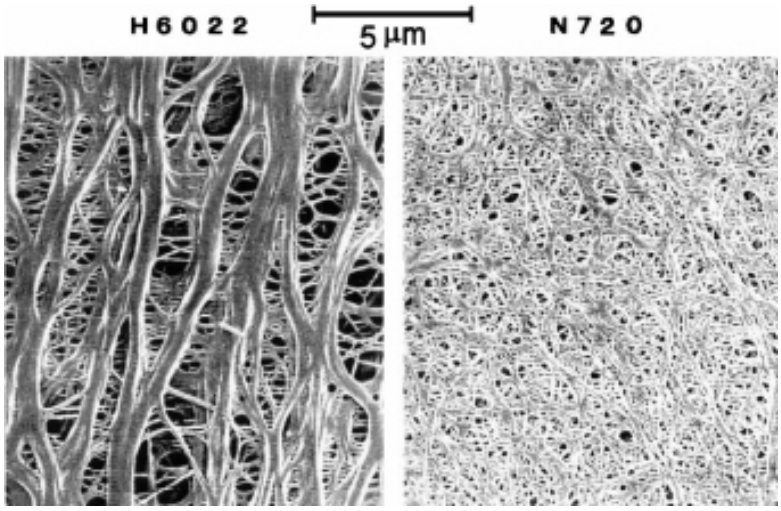

Figure 1.11 SEM images of the two type of olefin-based separator sheets.

1.5 Targets of this research

Recently, layered transition metal oxides with hexagonal structure, $LiMn_{1/2}Ni_{1/2}O_2$ and $LiMn_{1/3}Ni_{1/3}Ni_{1/3}O_2$, were introduced by Ohzuku et al [109,110] as a promising cathode material to be replaced $LiCoO_2$. The combination of Ni, Mn and Co can provide better thermal stability and higher reversible capacity than $LiCoO_2$. Moreover, these compounds showed lower cost and less toxicity [111]. Although $LiMn_{1/2}Ni_{1/2}O_2$ and $LiNi_{1/3}Mn_{1/3}Co_{1/3}O_2$ were attractive cathode materials, the material have a difficulty to prepare. A proper synthesis route should be selected in order to produce the cathode material successfully. Many researchers have applied hydroxide co-precipitation method to prepare the cathode material [111-114]. In this method, Mn ion precipitate as $Mn(OH)_2$ (Mn is 2+), but it is oxidized easily in aqueous solution by air (oxygen) gradually, so a part of Mn^{2+} would change to Mn^{3+} (MnOOH) or Mn^{4+} (MnO_2). Formation of these product leads to the decomposition of mixed hydroxide solid solution. Therefore, preparation of homogeneous mixed hydroxide precursor with high reproducibility is very difficult even if it is prepared under inert atmosphere. So, only Tanaka chemical Co. LTD. can provide homogeneous mixed hydroxide precursor.

I have proposed new synthesis route which can replace mixed hydroxide method. I use carbonate ion for the preparation of homogeneous precursor instead of OH^- ion and named as “carbonate co-precipitation method”. Important advantage of this method is that valence of Mn ion is easily kept as Mn^{2+}, thereby this method is applicable for industrial application.

This thesis consists of two parts. In the first part (chapter 2 and 3), I have applied novel powder preparation route, carbonate co-precipitation method, to prepared $Li[Mn_{x/2}Ni_{x/2}Co_{1-x}]O_2$ (x = 1, 2/3) solid solution and studied the influence of

synthesis conditions on structural and electrochemical properties of cathode materials.

In the second part, I have suggested novel application of carbonate co-precipitation method as surface modification technique to improve electrochemical performance of cathode materials. There are two chapters in the second part. In chapter 4, I have tried to improve cycle stability of $LiCoO_2$ at higher cut-off voltage of 4.5 V by surface modification with $LiMn_{1/2}Ni_{1/2}O_2$. In chapter 5, I have discussed about enhancement of rate capability of $LiNi_{1/2}Mn_{1/2}O_2$ by surface modification with Co element.

References

[1]. J. M. Tararascon, in "Rencet Advances in Rechargeable Li Batteries", *special Issue of Solid State Ionics,* eds. M. S. Whittingham, **69,** No. 3-4 (1994).

[2]. H. Ikeda, T. Saito, and H. Tamura, in *Proc. Manganese Dioxide Symp.* **Vol.1,** eds. A. Kozawa and R. H. Brodd (IC sample Office, Cleveland. OH.1975).

[3]. M. Armand, "*Materials for Advanced Batteries*", eds. D. W. Murphy, J. Broadhead and B. C. H. Steele (Plenum press, New York, **1980**) P. 145.

[4]. B. di Pietro, M. Patriarca, and B. Scrosati, *J Power Sources*, **8** (1982) 289.

[5]. M. Lazzari, and B. Scrosati, *J. Electrochem. Soc.*, **127** (1980) 773.

[6]. S. Morzilli, B. Scrosati, and F. Sgarlata, *Electrochim. Acta*, **30** (1985) 1271.

[7]. T. Nagaura, and K. Tozawa, *Prog. Batt. Solar cells*, **9** (1990) 209.

[8]. A. Yoshino, K. Sanechika, and T. Nakashima, Japan Kokai Shou 62-90863 (1987).

[9]. A. Hooper, and B. C. Tofield, *J. Power Sources,* **11** (1984) 33.

[10]. F. Croce, S. Passerini, and B. Scrosati, *J. Power Sources*, **43** (1993) 481.

[11]. R. R. Haering, J. A. R. Stile, and K. Brandt, US patent (1982) No. 4,281,048.

[12]. Y. Toyoguchi, T. Matsui, T. Yamaura, and T. Iijima, *3rd International Meeting on Lithium Batteries*, **1986**, 117.

[13]. J. J. Auborn, and Y. L. Barberio, *J. Electrochem. Soc*., **134** (1987) 638.

[14]. J. B. Goodenough, and V. Manivannan, *DENKI KAGAKU*, **66** (1998) 1173.

[15]. J. M. Tarascon, and M. Armand, *Nature*, **414** (2001) 359.

[16]. K. Mizushima, P. C. Jones, P. J. Wiseman, and J. B. Goodenough, *Mater. Res. Bull*., **17** (1980) 783.

[17]. J. N. Reimers, and J. R. Dahn, *J. Electrochem. Soc.*, **139** (1992) 2091.

[18]. T. Ohzuku, A. Ueda, M. Nagayama, Y. Inakoshi, and H. Konori, *Electrochim. Acta*, **38** (1993) 1159.

[19]. E. Plichta, S. Slane, M. Uchiyama, M. Saloman, D. Chua, W. B. Ebner, and W. H. Lin, *J. Electrochem. Soc*., **136** (1989) 1865.

[20]. T. Nohma, H. Kurokawa, M. Uehara, M. Takahashi, K. Nisio, and T. Sato, *J Power Sources*, **54** (1995) 522.

[21]. J. N. Reimers, and J. R. Dahn, *J. Electrochem. Soc.*, **139** (1992) 2091.

[22]. M. Zou, M. Yoshio, S. Gopukumar, and J. Yamaki, *Electrochem. Solid-State Lett.*, **7** (2004) A176.

[23]. T. Ohzuku, and A. Ueda, *J. Electrochem. Soc.*, **141** (1994) 2972.

[24]. A. Van der Ven, M. K. Aydinol, and G. Ceder, *J. Electrochem. Soc.*, **145** (1998) 2149.

[25]. H. Tukamoto, and A.R. West, *J. Electrochem. Soc.*, **144** (1997) 3164.

[26]. S. Levasseur, M. Ménétrier, and C. Delmas, *J. Power Sources*, **112** (2002) 419.

[27]. G. Ceder, Y.-M. Chiang, D. R. Sadoway, M. K. Aydinol, Y. I. Jang, and B. Huang, *Nature*, **392** (1998) 694.

[28]. Y. I. Jang, B. Huang, H. Wang, D. R. Sadoway, G. Ceder, Y. M. Chiang, H. Liu, and H. Tamura, *J. Electrochem. Soc.*, **146** (1999) 862.

[29]. H. Huang, G. V. Subba Rao, and B.V. R. Chowdari, *J. Power Sources*, **81** (1999) 690.

[30]. W. Yoon, K. K. Lee, and K. B. Kim, *J. Electrochem. Soc.,* **147** (2000) 2023.

[31]. S. T. Myung, N. Kumagai, S. Komaba, and H. T. Chung, *Solid State Ionics*, **139** (2001) 47.

[32]. N. Amdouni, H. Zarrouk, F. Soulette, and C. Julien, *Mater. Chem. Phys.*, **80** (2003) 205.

[33]. R. Alcantara, J. C. Jumas, P. Lavela, J. O. Fourcade, C. P. Vincente, and J. L. Tirado, *J. Power Sources*, **81- 82** (1999) 547.

[34]. H. Kobayashi, H. Shigemura, M. Tabuchi, H. Sakaebe, K. Ado, H. Kageyama, A. Hirano, R. Kanno, M. Wakita, S. Morimoto, and S. Nasu, *J. Electrochem. Soc.*, **147** (2000) 960.

[35]. M. Holzapfel, R. Schreiner, and A. Ott, *Eletrochim. Acta*, **46** (2001) 1063.

[36]. C. Delmas, and I. Saadoune, *Solid State Ionics*, **53-56** (1992) 370.

[37]. I. Saadoune, and C. Delmas, *J. Mater. Chem.*, **6** (1996) 193.

[38]. T. Ohzuku, and A. Ueda, *J. Electrochem. Soc.*, **144** (1997) 2780.

[39]. J. Cho, G. Kim, and H. S. Lim, *J. Electrochem. Soc.*, **146** (1999) 3571.

[40]. C. Delmas, M. Menetrier, L. Croguennec, I. Saadoune, A. Rougier, C. Pouillerie, G. Prado, M. Grune, and L. Fournes, *Electrochim. Acta*, **45** (1999) 243.

[41]. J. Cho, H. S. Jung, Y. C. Park, G. B. Kim, and H. S. Lim, *J. EIectrochem. Soc.*, **147** (2000) 15.

[42]. S. Madhavi, G. V. Subba Rao, B. V. R. Chowdari, and S. F. Y. Li, *J. Power Sources*, **93** (2001) 156.

[43]. R. J. Gummow, and M. M. Thackeray, *Solid State Ionics*, **53-56** (1992) 681.

[44]. S. Madhavi , G. V. Subba Rao , B. V. R. Chowdari, and S. F. Y. Li, *Electrochim. Acta*, **48** (2002) 219.

[45]. R. Stoyanova, E. Zhecheva, and L. Zarkova, *Solid State Ionics*, **73** (1994) 233.

[46]. A. R. Armstrong, A. D. Robertson, R. Gitzendanner, and P. G. Bruce, *J. Solid*

State Chem., **145** (1999) 549.

[47]. S. Lavassuer, M. Menetrier, E. Suard, and C. Delmas, *Solid State Ionics*, **128** (2000) 11.

[48]. N. Imanishi, M. Fujii, A. Hirano, and Y. Takeda, *J. Power Sources*, **97- 98** (2001) 287.

[49]. N. Imanishi, M. Fujii, A. Hirano, Y. Takeda, M. Inaba, and Z. Ogumi, *Solid State Ionics*, **140** (2001) 45.

[50]. M. Zou, M. Yoshio, S. Gopukumar, and J. Yamaki, *Chem. Mater.*, **15(25)** (2003) 4699.

[51]. M. Zou, M. Yoshio, S. Gopukumar, and J. Yamaki, *Mater. Res. Bull.*, **40** (2005) 708.

[52]. M. Zou, M. Yoshio, S. Gopukumar, and J. Yamaki, *Chem. Mater.*, **17(6)** (2005) 1284.

[53]. J. Cho, Y. J. Kim, and B. Park, *J. Electrochem. Soc.,* **148** (2001) A1110.

[54]. J. Cho, Y. J. Kim, and B. Park, *Chem. Mater.*, **12** (2000) 3788.

[55]. J. R. Dahn, U. Von Sacken, and C. A. Michal, *Solid State Ionics*, **44** (1990) 87.

[56]. T. Ohzuku, A. Ueda, and M. Nagayama, *J. Electrochem. Soc*., **140** (1993) 1862.

[57]. H. Arai, S. Okada, Y. Sakurai, and J. Yamaki, *Solid State Ionics*, **95** (1997) 275.

[58]. H. Arai, S. Okada, Y. Ohtsuka, M. Ichimura, and J. Yamaki, *Solid State Ionics*, **80** (1995) 261.

[59]. A. Rougier, I. Saadoune, P. Gravereau, P. Willmann, and C. Delmas, *Solid State Ionics,* **90** (1996) 83.

[60]. J. R. Dahn, U. von Sacken, and C. A. Michal, *Solid State Ionics*, **44** (1990) 87.

[61]. T. Ohzuku, A. Ueda, and M. Nagayama, *J. EIectrochem. Soc.*, **140** (1993)

1862.

[62]. W. Li, J. N. Reimers, and J. R. Dahn, *Solid State Ionics*, **67** (1993) 123.

[63]. A. Rougier, I. Saadoune, P. Gravereau, P. Willmann, and C. Delmas, *Solid State Ionics*, **90** (1996) 83.

[64]. E. Zhecheva, and R. Stouanova, *Solid State Ionics*, **66** (1993) 143.

[65]. A. Ueda, and T. Ohzuku, *J. EIectrochem. Soc.*, **141** (1994) 2010.

[66]. C. Delmas, I. Saadoune, and A. Rougier, *J. Power Sources*, **43-44** (1993) 595.

[67]. M. Yoshio, Y. Todorov, K. Yamato, H. Noguchi, J. Itoh, M. Okada, and T. Mouri, *J. Power Sources*, **74** (1998) 46.

[68]. M. Yoshio, H. Noguchi, J. Itoh, M. Okada, and T. Mouri, *J. Power Sources* **90** (2000) 176.

[69]. J. N. Reimers, E. Rossen, C. D. Jones, and J. R. Dahn, *Solid State Ionics*, **61** (1993) 335.

[70]. G. Prado, A. Rougier, L. Fournès, and C. Delmas, *J. Electrochem. Soc.*, **147** (2000) 2880.

[71]. C. Pouillerie, F. Perton, P. Biensan, J. P. Pérès, M. Broussely, and C. Delmas, *J. Power Sources*, **96** (2001) 293.

[72]. T. Kai, H. Ando, Y. Muranaka, T. Horiba, and K. Hironaka, Shin-Kobe Tech. Rep., **11** (2001) 9.

[73]. T. Horiba, K. Hironaka, T. Matsumura, T. Kai, M. Kosek, and Y. Muranaka, *J. Power Soreces*, **119-121** (2003) 893.

[74]. S. Megahed, and B. Scrosati, *J. Power Sources*, **51** (1994) 79.

[75]. M. M. Thackeray, P. J. Johnson, L. A. de Picciotto, P. G. Bruce, and J. B. Goodenough, *Mater. Res. Bull.*, **19** (1984) 179.

[76]. J. C. Hunter, *J. Solid State Chem.*, **39** (1981) 142.

[77]. Y. Xia, and M. Yoshio, *J. Electrochem. Soc.*, **143** (1996) 893.

[78]. Y. Xia, T. Sakai, T. Fujieda, X. Yang, X. Sun, Z. Ma, J. McBreen, and M. Yoshio, *J. Electrochem. Soc.*, **148** (2001) A723.

[79]. S. J. Wen, T. J. Richardson, L. Ma, K. A. Striebel, P. N. Ross, and E. J. Cairns, *J. Electrochem. Soc.*, **143** (1996) L136.

[80]. D.-H. Jang, Y.-J. Shin, and S.-M. Oh, *J. Electrochem. Soc.*, **143** (1996) 2204.

[81]. T. Inoue, and M. Sano, *J. Electrochem. Soc.*, **145** (1998) 3704.

[82]. M. M. Thackeray, Y. Shao-Horn, and A. J. Kahian, *Electrochem. Soc. Interface*, **1** (1998) 7.

[83]. X. Wang, H. Nakamura, and Masaki Yoshio, *J. Power Sources,* **110** (2002) 19.

[84]. M. Yoshio, H. Noguchi, H. Wang, and X. Wang, *J. Power Sources,* in press (2005).

[85]. B. Deng, H. Nakamura, Q. Zhang, M. Yoshio, and Y. Xia, *Electrochim. Acta*, **49** (2004) 1823.

[86]. S. Komaba, B. Kaplan, T. Ohtsuka, Y. Kataoka, N. Kumagai, and H. Groult, *J. Power Sources*, **119-121** (2003) 378.

[87]. N. Kumagai, S. Komaba, Y. Kataoka, and M. Koyanagi, *Chem. Lett.*, **2000**, 1154.

[88]. H. Tunekawa, S. Tanimoto, R. Marubayashi, M. Fujita, K. Kifune, and M. Sano, *J. Electorchem. Soc.*, **149** (2002) A1326.

[89]. Y.-K. Sun, Y.-S. Lee, M. Yoshio, and K. Amine, *Electrochem. Solid-State Lett.*, **5** (2002) A99.

[90]. B. Deng, H. Nakamura, and M. Yoshio, *Chem. Lett*., **32** (2003) 942.

[91]. R. Hoppe, G. Brachtel, M. Jansen, and Z. Anorg, *Allg. Chem.*, **417** (1975) 1.

[92]. A. R. Armstrong, and P. G. Bruce, *Nature*, **381** (1996) 499.

[93]. Y.-I, Jang, B. Huang, Y.-M. Chiang, and D. R. Sadoway, *Electrochem. Solid-State Lett.*, **1** (1998) 13.

[94]. Y.-I. Jang, B. Huang, H. Wang, D. R. Sadoway, and Y.-M. Chiang, *J. Electrochem. Soc.*, **146** (1999) 3217.

[95]. Y.-M. Chiang, D. R. Sadoway, Y.-I. Jang, B. Huang, and H. Wang, *Electrochem. Solid-State Lett.*, **2** (1999) 107.

[96]. Y.-I. Jang, and Y.-M. Chiang, *Solid State Ionics*, **130** (2000) 53.

[97]. H. Wang, Y.-I. Jang, and Y.-M. Chiang, *Electrochem. Solid-State Lett.*, **2** (1999) 490.

[98]. Y.-M. Chiang, H. Wang, and Y.-I. Jang, *Chem. Mater*., **13** (2001) 53.

[99]. A. K. Pahdi, K. S. Najundaswamy, and J. B. Goodenough, *J. Electrochem. Soc.*, **144** (1997) 1188.

[100]. D. D. MacNeil, Z. Lu, Z. Chen, J. R. Dahn, *J. Power Sources,* **108** (2002) 8.

[101]. M. Takahashi, S. Tobishima, K. Takei, and Y. Sakurai, *Solid State Ionics,* **148** (2002) 283.

[102]. A. K. Padhi, K. S. Nanjundaswamy, C. Masquelier, and J. B. Goodenough, *J. Electrochem. Soc.*, **144** (1997) 2581.

[103]. A. Manthiram, and J. B. Goodenough, *J. Power Sources*, **26** (1989) 403.

[104]. S. Andersson, J. O. Thomas, B. Kalska, and L. Häggström, *Electrochem. Solid-State Lett.*, **3** (2000) 66.

[105]. N. Ravet, J. B. Goodenough, S. Besner, M. Simoneau, P. Hovington, and M. Armand, Abstract 127, The Electrochemical Society and The Electrochemical

Society of Japan Meeting, Vol. **99-2**, Honolulu, HI, Oct 17-22, 1999.

[106]. H. Huang, S. C. Yin, and L. F. Nazar, *Electrochem. Solid-State Lett.*, **4** (2001) A170.

[107]. Z. Chen, and J. R. Dahn, *Electrochem. Soc.*, **149** (2002) A1184.

[108]. A. Yamada, S. C. Chung, and K. Hinokuma, *J. Electrochem. Soc.*, **148** (2001) A224.

[109]. T. Ohzuku, and Y. Makimura, *Chem. Lett.*, **2001**, 642

[110]. T. Ohzuku, and Y. Makimura, *Chem. Lett.*, **2001**, 744

[111]. N. Yabuuchi, and T. Ohzuku, *J. Power Sources*, **119–121** (2003) 171.

[112]. Z. Lu, D. D. MacNeil, and J. R. Dahn, *Electrochem. Solid-State Lett.*, **4** (2001) A200.

[113]. D. D. MacNeil, Z. Lu, and J. R. Dahn, *J. Electrochem. Soc.*, **149** (2002) A1332.

[114]. K. M. Shaju, G. V. Subba Rao, and B. V. R. Chowdari, *Electrochim. Acta*, **48** (2002) 145.

Chapter 2

Synthesis and characterization of layered $LiNi_{1/2}Mn_{1/2}O_2$

2.1 Objective of this research

Lithium transition metal oxides, $LiMeO_2$ (Me = Ni, Co and Mn) have been extensively studied as a cathode materials for lithium ion secondary battery [1-4]. $LiCoO_2$ has been used as a major cathode material for lithium battery because of easiness in preparation, stable cycling performance and high rate capability. However, a lot of attention has recently been paid to nickel based layered cathode materials as an alternative to $LiCoO_2$ in the view point of high cost and toxicity. Even though $LiNiO_2$ exhibits relatively higher reversible capacity, it shows phase transition during charge and discharge. Such phase transition may cause of deterioration of cycling performance. Moreover, the exothermic decomposition of highly delithiated product raises greater safety concerns [5]. Partial substitution of Ni sites by other elements, such as Mn, Mg, Al, Co, Ti and Zr, leads to enhancement of cycling performance [6-12]. According to previous studies [13,14], replace of Ni by Mn leads capacity decrease, though the structure was stabilized. Spahr et al [14,15] reported that 50% of Mn doping into Ni site delivered an increased specific capacity than lower level Mn doping into $LiNiO_2$.

Recently, a layered transition metal oxide with rhombohedral structure, $Li[Ni_{1/2}Mn_{1/2}]O_2$, was introduced by Ohzuku et al. as a promising cathode material to be replaced $LiCoO_2$ [16,17] . The compound can be prepared in air atmosphere at higher temperature of more than 800 ^oC with the rhombohedral structure (space group, $R\bar{3}m$). The valences of Ni and Mn in the compound are determined to be 2+ and 4+, respectively [18]. The electrochemical redox process is based on the two electron reaction of $Ni^{2+/4+}$, but Mn^{4+} is inactive. Thus, the electrochemically inactive Mn^{4+} is believed to support the host structure during redox process and contribute stable

cycling performance. Moreover, the combination of nickel and manganese can provide advantages such as lower cost and less toxicity than $LiCoO_2$.

Although $LiMn_{1/2}Ni_{1/2}O_2$ is an attractive cathode material, preparation of the $LiMn_{1/2}Ni_{1/2}O_2$ with excellent electrochemical performance is quite difficult. A hydroxide co-precipitation method has been used as a major preparation technique to get homogeneous solid solution [18-24]. Though the hydroxide co-precipitation is one of the powerful syntheses methods, precipitated transition metal hydroxide is easily oxidizes in the basic aqueous solution during the precipitation process. For example, $Mn(OH)_2$ oxidized gradually to MnOOH (Mn^{3+}) or MnO_2 (Mn^{4+}) under the precipitation conditions by oxygen. Such reaction decreases the homogeneity of final product. Therefore, the control of Mn valence in aqueous solution is to be a critical point to obtain pure product. In contrast, the Mn valence in the carbonate can be stable as +2 even in the basic aqueous solution. This implies that the homogeneous solid solution containing Mn could be readily prepared using carbonate co-precipitation method. Therefore, I selected carbonate co-precipitation method for the precursor to prepare $LiMn_{1/2}Ni_{1/2}O_2$. In this study, I report the structural integrity, morphology and electrochemical performances of the $LiMn_{1/2}Ni_{1/2}O_2$ cathode material prepared by newly developed carbonate co-precipitation method. I also tried to optimizing synthesis condition for preparing the $LiMn_{1/2}Ni_{1/2}O_2$ cathode material with excellent electrochemical performance.

2.2 Experimental

I used $MnSO_4 \cdot 4\text{-}5H_2O$, $NiSO_4 \cdot 6H_2O$, and Na_2CO_3 as the starting materials for preparing transition metal carbonate powder, $Mn_{1/2}Ni_{1/2}CO_3$. I prepared two aqueous

solutions, 1 M transition-metal sulfate and a 1 M sodium carbonate. Bright green $Mn_{1/2}Ni_{1/2}CO_3$ sediment was obtained by feeding these solutions into hot reaction bath (60 ^oC) under a CO_2 atmosphere. During precipitation process, the amount of equimolar Mn and Ni fed is controlled and pH of the reaction bath was fixed at 7.2. After the formation of precipitate, the sediment was washed with distilled water several times. The precipitates were dried at room temperature after filtration. The co-precipitated carbonate powder $Mn_{1/2}Ni_{1/2}CO_3$ was pre-heated at 500 ^oC for 5 h in air. The mixed carbonate powder decomposes into spinel Me_3O_4 (Me = metal) during pre-heat process. I applied EDTA titration to decide exact amount of transition metal ions in the pre-heated spinel powder. A stoichiometric amount of lithium hydroxide was added into the pre-heated spinel powder and the mixture was calcined at various temperature for 15h in air. The experimental procedure is schematically presented in the Fig. 2.1.

X-ray diffraction analysis for the precursors and the final $LiMn_{1/2}Ni_{1/2}O_2$ products were carried out using Rigaku Rint 1000 diffractormeter with a CuKα radiation. The XRD data for the Rietveld analysis were carefully collected by step of 0.03° with a constant counting time of 10 seconds per step. I applied Rietveld refinements analysis using the FullProf 2000 program [25] in order to investigate the structural change. The contents of metal ion in the products were determined by an inductively coupled plasma spectrometer (ICP : SPS 7800, Seiko instruments, Japan). The specific surface areas of the synthesized materials were determined using a Micromeritics Gemini 2375 (USA) by the B.E.T method. Scanning electron microscopy (SEM : JSM-5300E, JEOL, Japan) was carried out to observe the morphologies of the synthesized materials. X-ray photoelectron spectra of the

transition metals in the products were measured using PHI 5800 (ULVAC-PHI INC, USA) spectrometer with monochromatic Al-Kα radiation. Charge referencing was done with carbon C_{1s} binding energy of 284.5 eV.

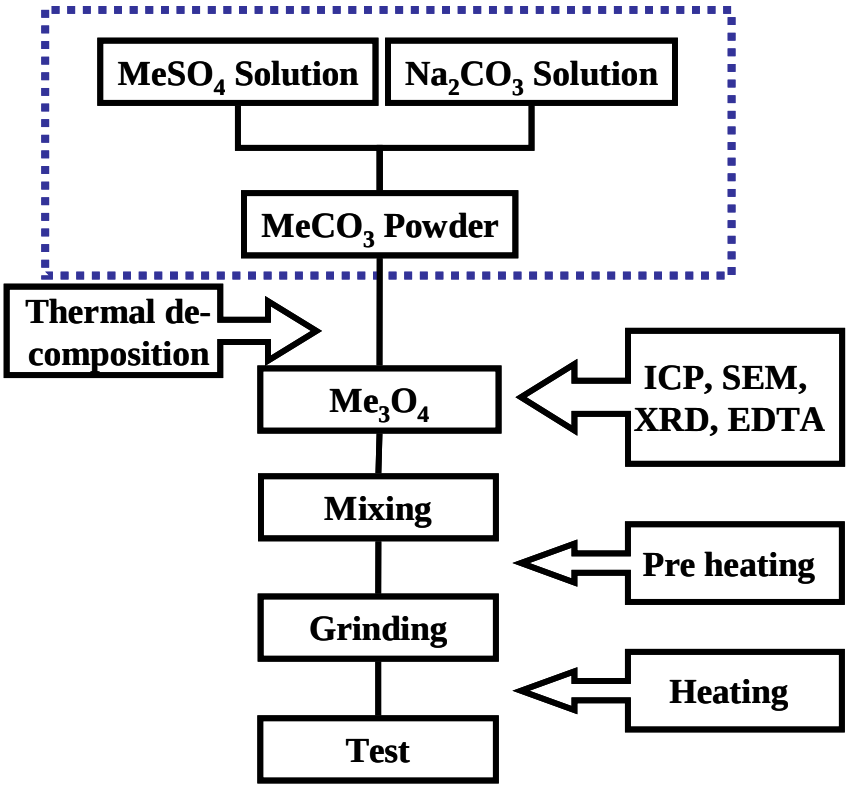

Figure 2.1 A schematic flow-chart of experimental procedure for preparing $LiMn_{1/2}Ni_{1/2}O_2$.

The electrochemical characterizations were carried out using the CR-2032-type coin cell. A cathode was prepared by pressing active material film, which is consist of 20 mg active material and 12 mg conducting binder (Teflonized acetylene black), on the stainless steel mesh. The cell was composed of the cathode, the lithium foil as an anode and 1M $LiPF_6$-EC/DMC (1:2 in volume) as an electrolyte. The electrochemical cycling tests were performed at room temperature. Cyclic voltammetry study (CV) was

conducted using a three-electrode cell with 1M $LiPF_6$-EC/DMC (1:2 in volume) as electrolyte and lithium foil was used as both counter and reference electrode. CV experiments were carried out at a scan speed of 0.1 mV s^{-1} between 2.8 and 4.6 V.

2.3 Results and Discusstions

2.3.1 Characterization of carbonate precursor

The structure of the precursor prepared by carbonate co-precipitation method was investigated by X-ray diffraction experiment. Figure 2.2 shows XRD patterns of the precursor and standard $MnCO_3$ (JCPDS 07-0268), respectively.

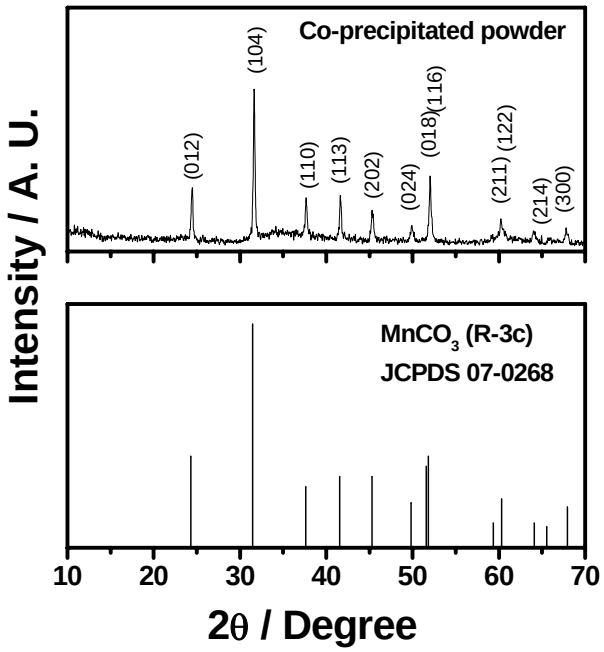

Figure 2.2 X-ray diffraction patterns of co-precipitatated precursor and standard $MnCO_3$ pattern as a reference.

As shown in the Fig. 2.2, we could get single phase of XRD pattern and all diffraction patterns can be indexed as transition metal carbonate with hexagonal

structure (space group 167; $R\bar{3}c$) in spite of mixed state of two different materials, such as $MnCO_3$ and $NiCO_3$. Therefore, The XRD analysis revealed that the homogeneous mixed carbonate precursor was successfully formed through co-precipitation process.

The chemical composition of the precursor was determined by ICP spectroscopy as $Mn_{0.49}Ni_{0.51}CO_3$, which is well coincided with a designed value ($Mn_{0.5}Ni_{0.5}CO_3$). I carried out SEM observation at different magnification in order to observe the morphology of the precursor. Fig. 2.3 (a) and (b) show micro and macro morphologies of the precursor, respectively. The SEM images show small primary particle is about 0.1-0.5 μm. On the other hand, the macro morphology shows secondary particle size is 15 μm. The SEM observation reveled that the small primary particles, less than 0.5 μm, aggregated each other to form large secondary particle.

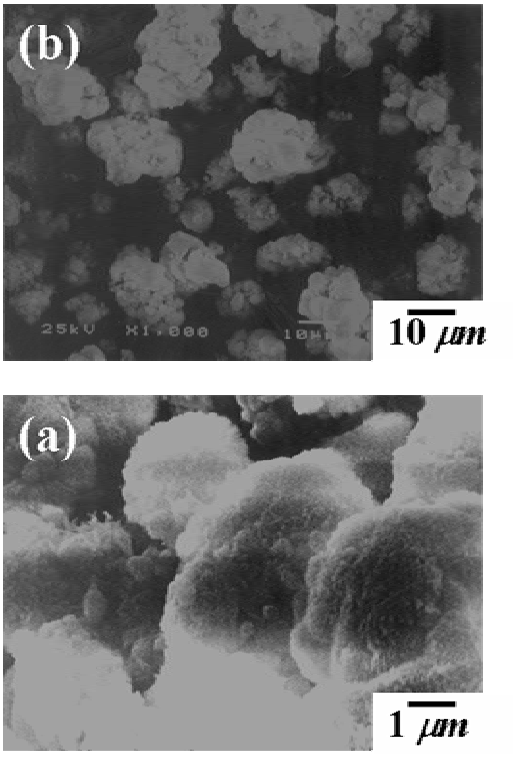

Figure 2.3 SEM photographs of (a) micro and (b) macro morphologies for the $Mn_{1/2}Ni_{1/2}CO_3$ precursor.

2.3.2 Post annealing

2.3.2.1 Structural characterization of $LiMn_{1/2}Ni_{1/2}O_2$

The $LiMn_{1/2}Ni_{1/2}O_2$ compounds were synthesized at various calcination temperatures viz., 500, 700, 800, 850, 900, 950 and 1000 ^oC for 15h in air. I carried out X-ray diffraction analysis for the synthesized cathode materials in order to investigate the dependence of phase evolution on the calcination temperature. Figure 2.4 shows XRD patterns of the products as a function of calcination temperature.

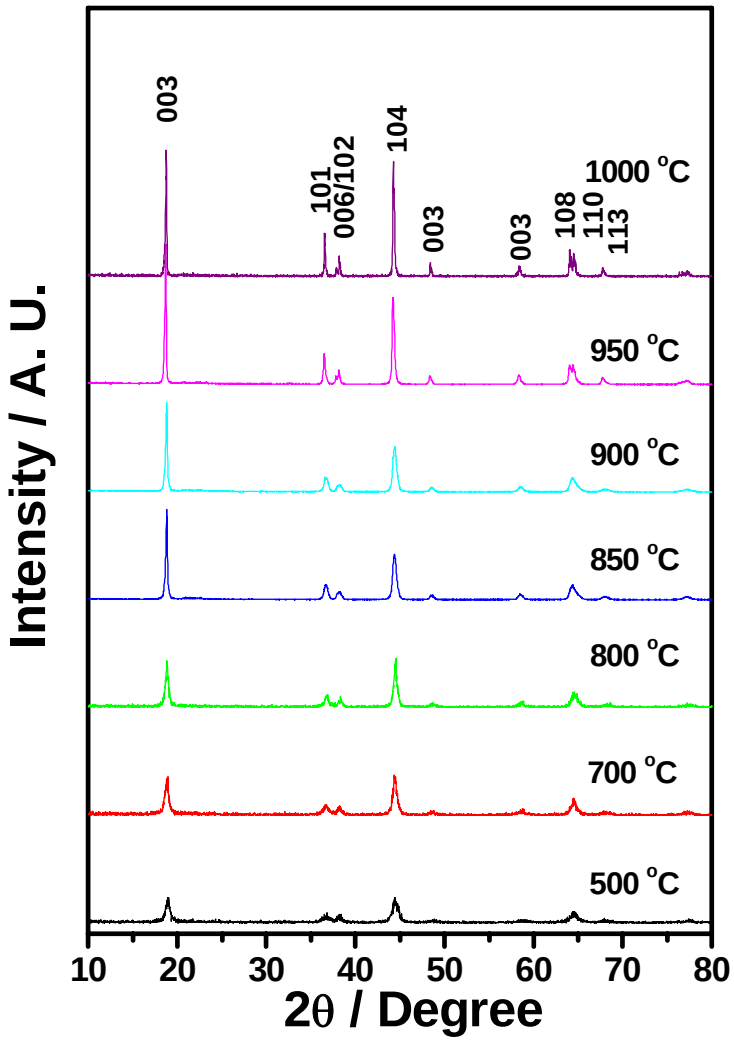

Figure 2.4 XRD patterns for the cathode materials synthesized at various calcinations temperatures.

All diffraction lines can be indexed based on the α-$NaFeO_2$ structure. However, the compounds synthesized below 850 ^oC show broad diffraction lines and unclear splitting in (006)/(102) and (108)/(110) peaks. This indicates that the compounds synthesized below 850 ^oC are not fully ordered.

The hexagonal lattice parameters of the $LiMn_{1/2}Ni_{1/2}O_2$ compounds were determined by Rietveld analysis and plotted in the Fig. 2.5. Unfortunately, the lattice parameters for the compounds synthesized at less than 800 ^oC can not be refined successfully because the diffraction patterns are too broader to fit well the profile. The lattice parameters, *a* and *c*, of the sample prepared at 800 ^oC are 2.879 Å and 14.23 Å, which is smaller than those of reported values [26]. Lattice parameters of samples, *a* and *c*, gradually increase with increase in calcinations temperature, then the obtained *a* and *c* values for 900 ^oC sample (a = 2.885 Å, c = 14.286 Å) were very closer to reported value [26]. The sample prepared at 950 and 1000 ^oC shows bigger lattice parameters than those reported values [26]. It is well known that higher peak intensity ratio of $I_{(003)}/I_{(104)}$ indicate low cation mixing and well ordered hexagonal structure [16,17]. By increasing calcinations temperature up to more than 850 ^oC the intensity ratio was abruptly increased up to 1.97 and the sample synthesized at 900 ^oC shows almost same ratio to that of 850 ^oC. The highest $I_{(003)}/I_{(104)}$ values are obtained in the temperature range of 850-900 ^oC. Further increasing of calcinations temperature leads decrease in intensity ratio. The *c/a* value also shows similar trend with the variation of intensity ratio. Therefore, I conclude that the structural integrity and hexagonal ordering are changed sensitively by the calcination temperature, and the calcination temperature range between 850 and 900 ^oC is recommended to prepare the well ordered $LiMn_{1/2}Ni_{1/2}O_2$.

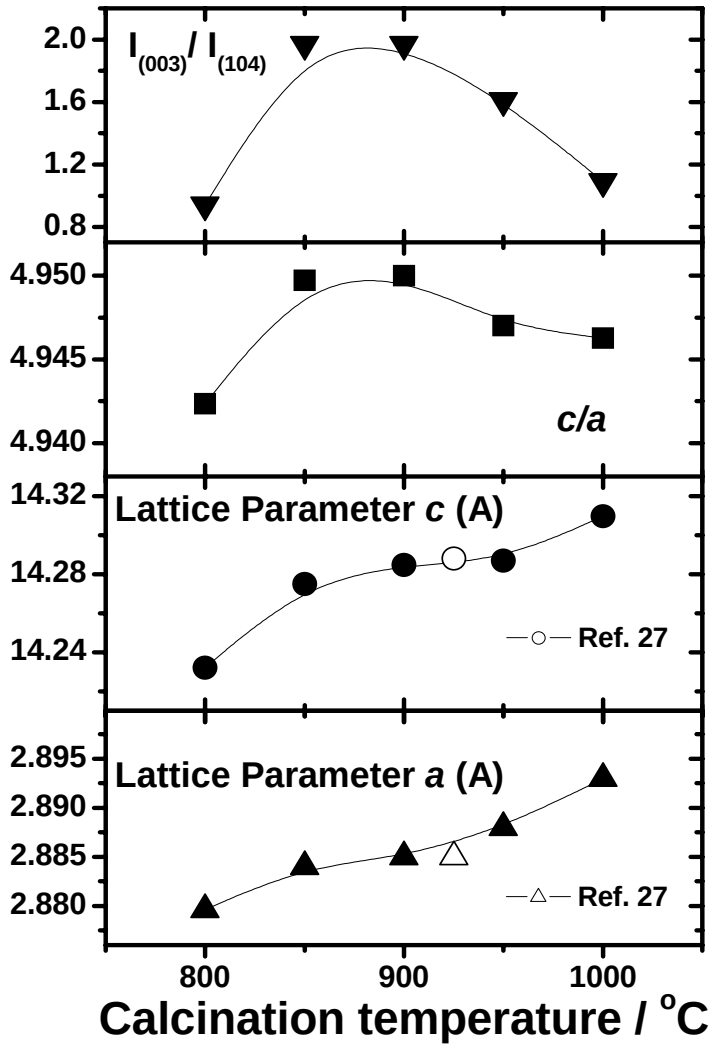

Figure 2.5 The variation in structural parameters depending on the calcination temperature.

2.3.2.2 Electrochemical properties of $LiMn_{1/2}Ni_{1/2}O_2$

The initial charge discharge profiles for the cathode materials synthesized at various temperatures, viz., 500, 700, 800, 850, 900, 950 and 1000 ^{o}C, are shown in Fig. 2.6. The cell were charged up to 4.5 V and then discharged to 2.8 V with a constant

current density of 20 mA g^{-1}. The initial charge profile is quite different and depends extremely on the calcination temperature. The cathode synthesized between 800 and 950 ^{o}C show monotonous voltage profiles and smaller polarization. On the other hand the samples prepared under 800 ^{o}C show relatively lower discharge capacities and higher irreversible capacities. Moreover, those samples show clear voltage plateau at around 4.4 V.

The initial charge-discharge capacities are gradually increased with the increase in calcination temperature up to 850 ^{o}C, while irreversible capacity loss decreases. However, further increase in calcinations temperature, above 950 ^{o}C leads deterioration of cell performance, i.e. the charge and discharge capacities were decreased and the irreversible capacity was increased. It is likely that there is close relation between structural integrity and electrochemical performance. Thus, I summarized the relation between the structural parameters and electrochemical performances in Fig. 2.7 in order to elucidate the relationship between them. It clearly shows the tight relationship between structural integrity ($I_{(003)}/I_{(104)}$) and electrochemical performances. The samples with higher structural integrity, such as 850 and 900 ^{o}C samples, can deliver excellent electrochemical performance than those of samples with lower structural integrity.

Figure 2.8 shows cycling performances of the prepared powders. The cells were charged to 4.5 V and then discharged to 2.8 V with a constant current density of 20 mA g^{-1}. All the samples show very stable cycling performance except for 1000 ^{o}C sample. The obtained discharge capacities clearly depend on the structural integrity. The sample calcined at 850 and 900 ^{o}C for 15 h delivered the highest discharge capacities of about 170 mAh g^{-1} as well as excellent cycle stability. I found

that the temperature range, 850 – 900 ^{o}C, is proper for synthesis of $LiMn_{1/2}Ni_{1/2}O_2$ by post annealing. Therefore, I have tried to discuss about those cathode materials in detail.

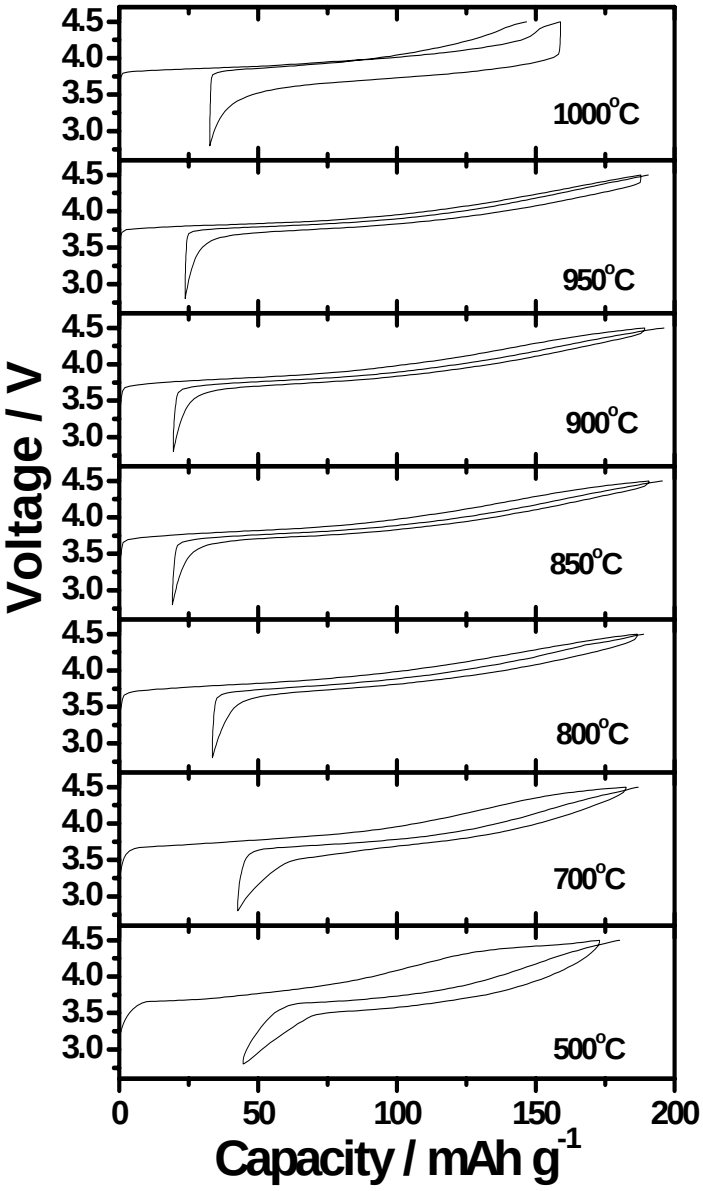

Figure 2.6 Charge-discharge curves of the $LiMn_{1/2}Ni_{1/2}O_2$ compounds prepared at temperature range 500 – 1000 ^{o}C.

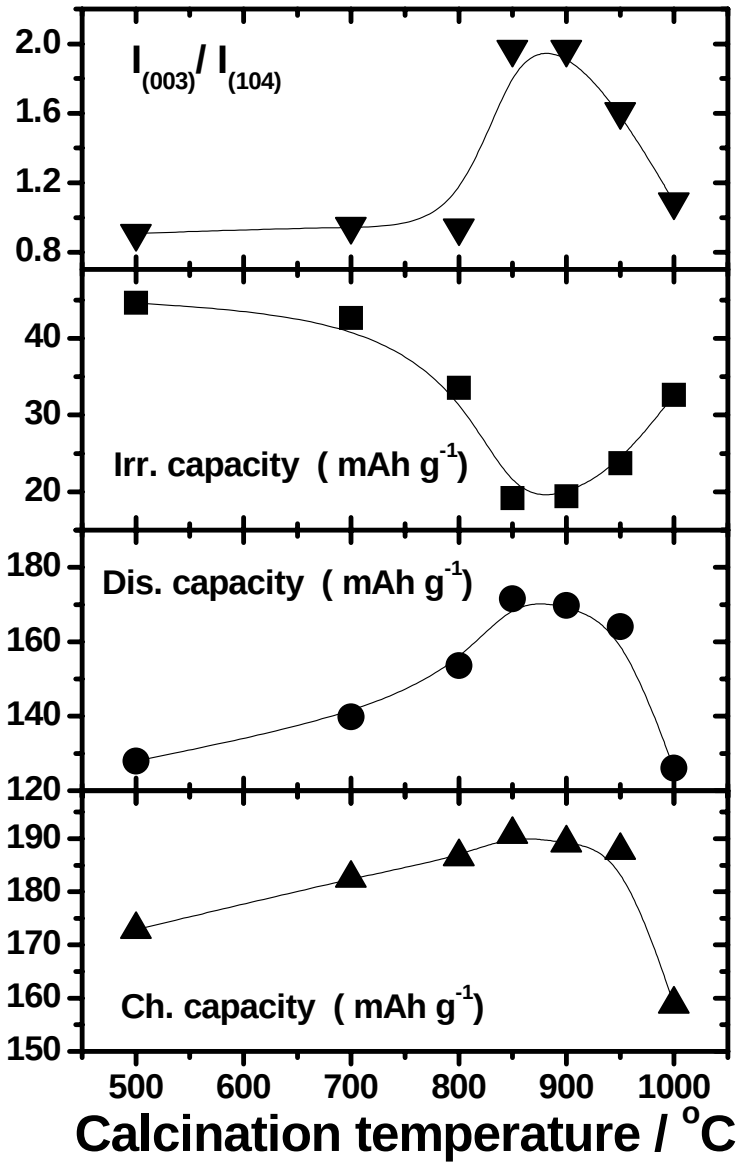

Figure 2.7 Relationship between structural integrity and electrochemical performances.

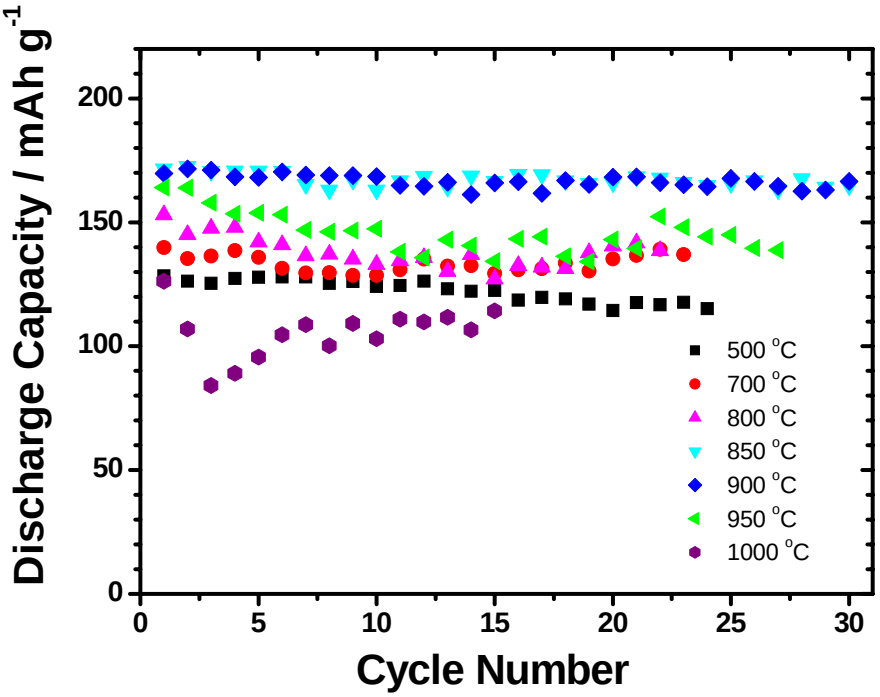

Figure 2.8 Discharge capacities as a function of cycle number.

2.3.3 Effect of calcination temperature on morphology and specific surface area

A SEM observation was carried out to investigate morphology of product. Figure 2.9 (a), (b) and (c) show morphologies of the samples prepared at 850, 900 and 950 ^{o}C, respectively. The sample prepared at 850 ^{o}C is composed of nano-scale primary particles (~100 nm) with higher specific surface area of 7.6 m^2 g^{-1}. The primary particle size became larger and specific surface area was decreased as increase in calcination temperature. The relatively larger specific surface area without any grinding process can be easily explained by smaller primary particles and the formation of loosely agglomerated secondary particle.

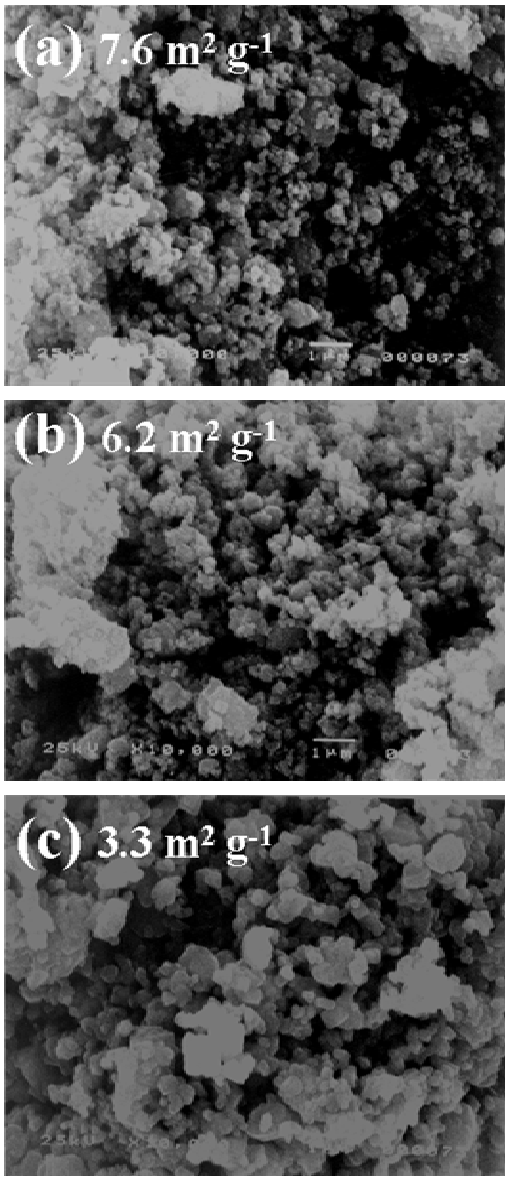

Figure 2.9 SEM photographs and specific surface areas of the $LiMn_{1/2}Ni_{1/2}O_2$ prepared at (a) 850 ^oC, (b) 900 ^oC and (c) 950 ^oC.

Figure 2.10 shows element distribution maps of Mn and Ni in the $LiMn_{1/2}Ni_{1/2}O_2$ prepared at 900 ^oC. It was confirmed that Mn and Ni distribute uniformly throughout the oxide particles. This indicates that the carbonate co-precipitation method is very effective to prepare single phase product.

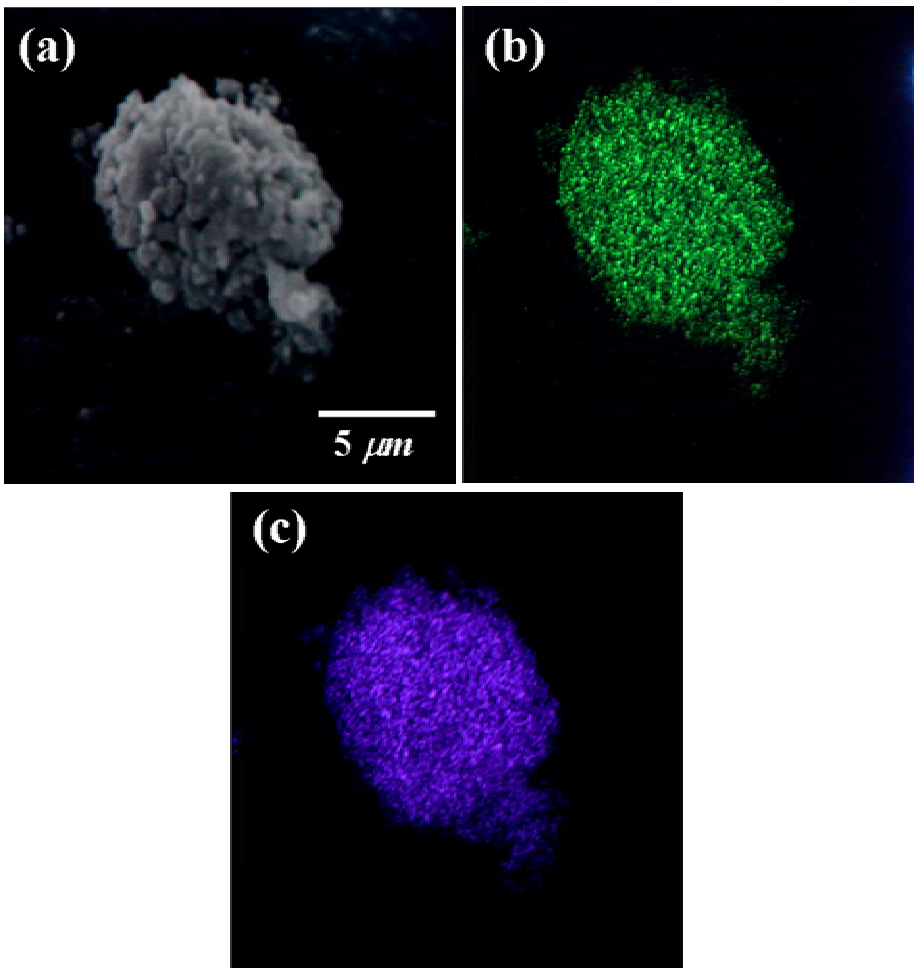

Figure 2.10 (a) SEM photograph and mapping of (b) Ni and (c) Mn elements in $LiMn_{1/2}Ni_{1/2}O_2$ synthesized at 900 ^oC.

In order to deduce the oxidation state of the Mn and Ni, X-ray photoelectron spectroscopy analysis was employed and the spectra for Ni $2p_{3/2}$ and Mn $2p_{3/2}$ in sample are given in the Fig. 2.11. The binding energies of Mn and Ni in the sample prepared at 900 ^oC were 641.8 and 854.2 eV, respectively. These values are well coincided with the binding energy of Mn^{4+} (642.0 eV) and Ni $^{2+}$ (854.04 eV) [27]. Therefore, the valences of Mn and Ni in the compound would be estimated to be 4+ and 2+, respectively.

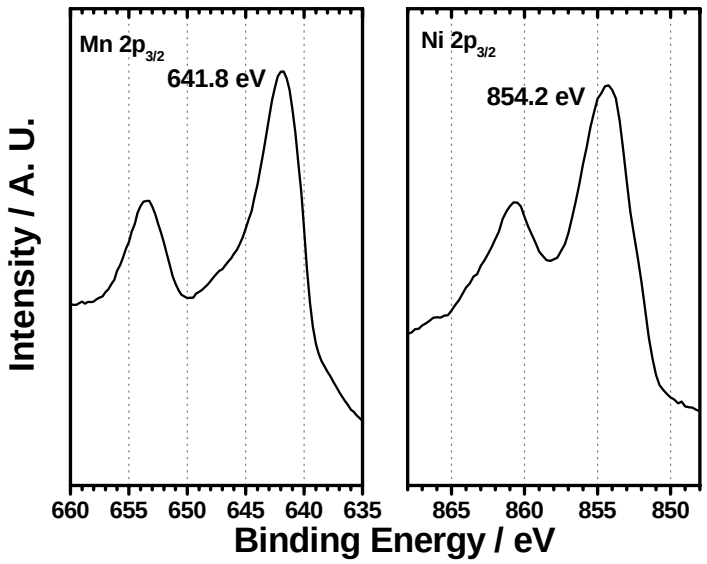

Figure 2.11 XPS spectra for Ni $2p_{3/2}$ and Mn $2p_{3/2}$ in $LiMn_{1/2}Ni_{1/2}O_2$ prepared at 900 ^oC.

Figure 2.12 (a), (b) and (c) show typical cyclic voltammogram of the $LiMn_{1/2}Ni_{1/2}O_2$ prepared at 850, 900 and 950 ^oC, respectively. The cyclic voltammograms of the cells were recorded with Li metal reference electrode at a scan rate 0.1 mV s^{-1}. As shown in (a), major oxidation peak shifted to the lower voltage in the second cycle and reproducible redox peaks are observed in subsequent cycles. The potential difference between the anodic and cathodic peak (ΔV) can give rough information of cathode material, i.e., resistance during lithium intercalation and deintercalation process. The smaller ΔV indicates smaller resistance of cathode material. The obtained ΔV for the sample prepared at 850, 900 and 950 ^oC are determined to be 0.15, 0.14 and 0.2 V, respectively. The ΔV values are smaller than previously reported values even at faster scan rate of 0.1 mV s^{-1} [27,28]. It means that

the samples prepared by carbonate co-precipitation would lead smaller resistance during cycling test.

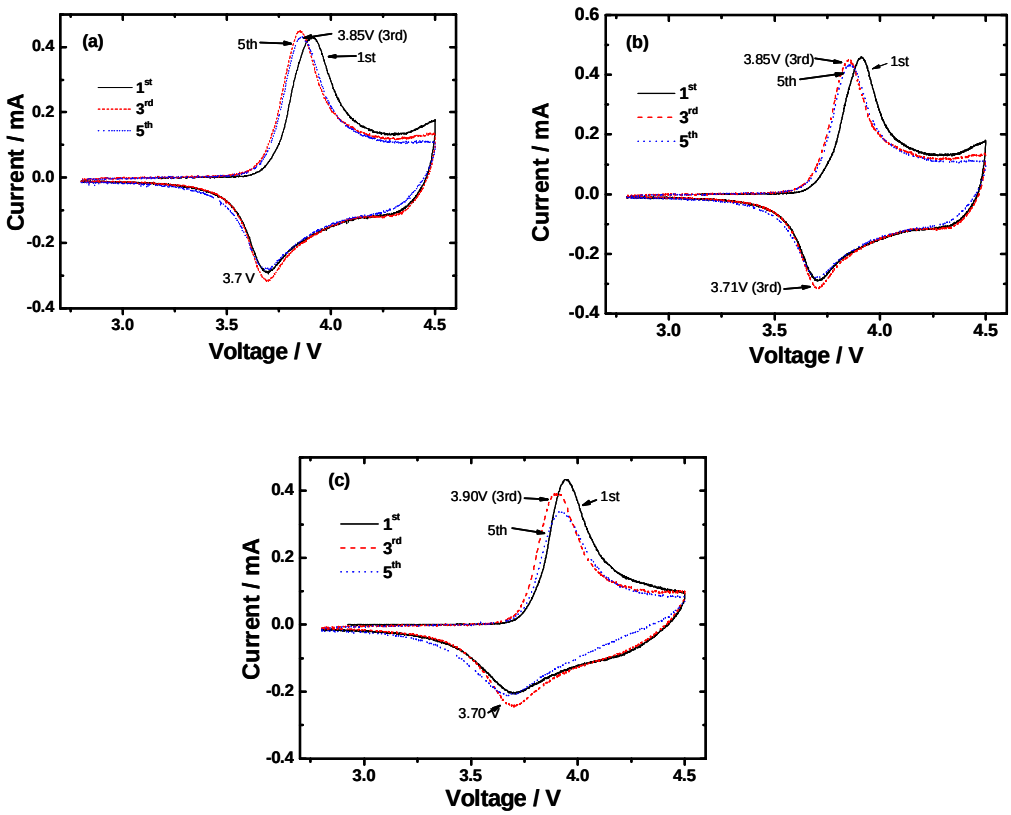

Figure 2.12 Cyclic voltammograms of $LiMn_{1/2}Ni_{1/2}O_2$ samples, synthesized at (a) 850 ^{o}C, (b) 900 ^{o}C and (c) 950 ^{o}C.

Figure 2.13 shows cycle stability of $LiMn_{1/2}Ni_{1/2}O_2$ prepared at 850, 900 and 950 ^{o}C in the various cut-off voltages of 4.4, 4.5 and 4.6 V (vs. Li/Li^{+}) at a current density of 0.2 mA cm^{-2} (20 mA g^{-1}). As shown in (a), all the samples delivered similar discharge capacity of 151.2 (850 ^{o}C), 154.1 (900 ^{o}C) and 151.4 mAh g^{-1} (950 ^{o}C) in the voltage range from 2.8 to 4.4 V. It is notable that all the samples show excellent capacity retention ratios of 99.3 %, 99.4 % and 98.5 % even after 30 cycles. However, the capacity retention ratio became difference for the cut-off voltage of 4.6 V. The

sample prepared at 850 °C showed the best capacity retention ratio of 95.4 % of initial discharge capacity and the samples prepared at 900 °C also showed stable cycling performance of 91.3 % of initial discharge capacity after 30 cycles. On the other hand, the sample prepared at 950 °C showed unstable cycling performance. The unstable cycling performance of the sample prepared at 950 °C might be attribute to lower structural integrity and higher resistance (ΔV) than the samples synthesized at 850 and 900 °C as confirmed by XRD anaylsis and cyclic voltammetry studies.

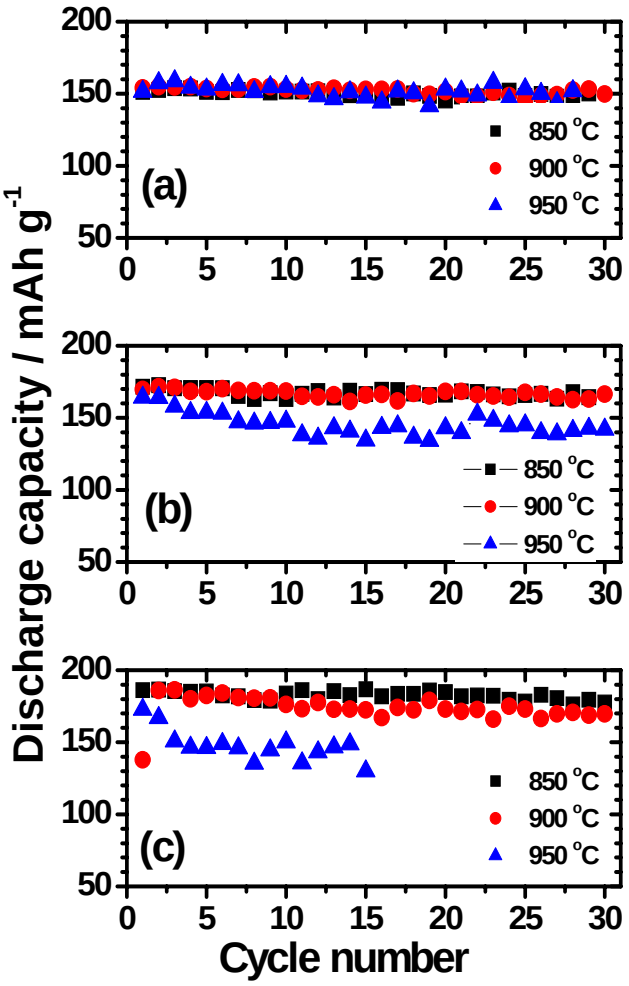

Figure 2.13 Cycling performances of the $LiMn_{1/2}Ni_{1/2}O_2$ cathode materials in the voltage range (a) 2.8 - 4.4 V, (b) 2.8 - 4.5 V and (c) 2.8 - 4.6 V.

Figure 2.14 shows rate capability test for $LiMn_{1/2}Ni_{1/2}O_2$ samples, synthesized at 850, 900 and 950 ^oC. The cells were charged with a constant current density of 0.2 mA cm^{-2} up to 4.5V and discharged to 2.8 V with various current density of 17 (0.1 C), 34 (0.2 C), 85 (0.5 C), 170 (1 C) and 340 mA g^{-1} (2 C). It is clear that rate capability becomes worse with the increase in synthesis temperature. Especially, discharge capacity of the sample synthesized at 950 ^oC more rapidly decreased than those of the other samples. I believe that the reason of the low rate capability of the sample prepared at higher temperature is the growth of primary particle as well as smaller specific surface area.

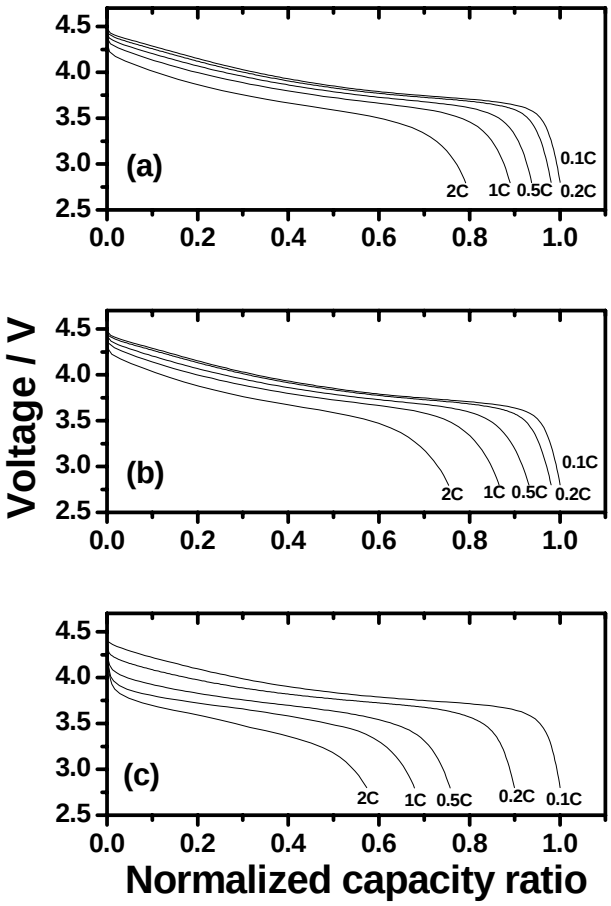

Figure 2.14 Rate capability of the samples prepared at (a) 850 ^oC, (b) 900 ^oC and (c) 950 ^oC.

2.3.4 Structural Changes during the first charge

Generally, the topotatic intercalation/deintercalation of lithium ions into/from the host structure leads a change in the lattice volume, and sometimes a structural breakdown or transformation to other stable phases. In order to investigate the structural change during lithium de-intercalation, ex-situ XRD analysis was carried out by using the sample synthesized at 900 ^{o}C. The graphite, KS-6, was used as internal standard, in this experiment. As shown in the Fig. 2.15, all diffraction patterns can be indexed based on the space group $R\bar{3}m$ in the all measured delithiation ranges. It would indicate that the original structure is maintained during charging up to 4.6 V. During the process, the lattice parameter, *a*, monotonously reduces in the range of $x \leq 0.53$ in $Li_{1-x}Mn_{1/2}Ni_{1/2}O_2$ and then slightly decreased up to further delithiation until $x \leq 0.76$. The decrease of lattice parameter, *a*, would be due to oxidation of nickel, accompanying Li extraction from the host structure. While the lattice parameter, *c*, which is correlated to the average metal-metal inter-slab distance, increases with increase of x value until x reaches the value of about 0.53. This phenomenon in lattice parameters is commonly observed in layered oxides and can be explained by electrostatic repulsive force between oxygen ions of two adjacent slabs. Further removal of Li gives rise to the decrease in parameter *c*. The decrease of lattice parameter, *c,* in the $x \geq 0.55$ range could be explained by anisotropic shrinkage. The unit cell volume, V, however, linearly reduces from 103 Å^3 (x = 0) to 99 Å^3 (x = 0.76) (about 2 % change in volume). The continuous shrinkage in cell volume could reflect the replacement of Ni^{2+} by Ni^{4+} and Li extraction. This small change in unit cell volume may give rise to excellent cycling performance.

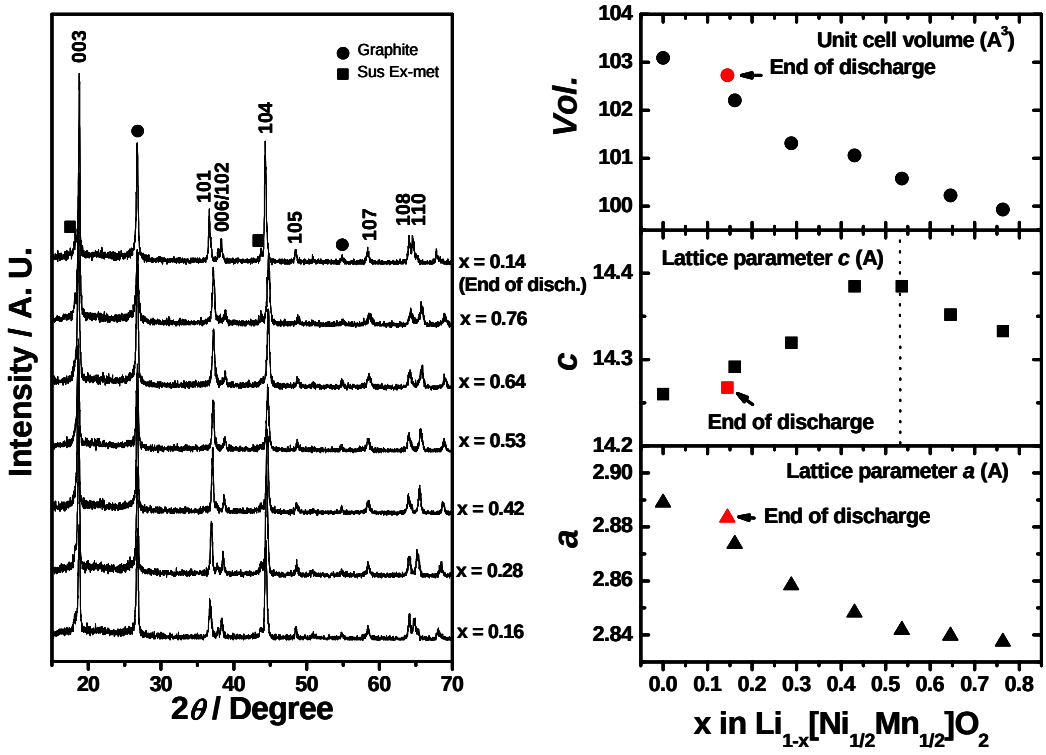

Figure 2.15 Ex-situ XRD patterns and variation of lattice parameters as a function of x in $Li_{1-x}Mn_{1/2}Ni_{1/2}O_2$.

2.3.5 Effect of lithium sources for structural and electrochemical performance on the $LiMn_{1/2}Ni_{1/2}O_2$ compound

Figure 2.16 shows the results of XRD studies for the $LiMn_{1/2}Ni_{1/2}O_2$ materials synthesized from various lithium sources at 900 ^oC. The XRD patterns of all materials can be indexed based on the α-$NaFeO_2$ structure (space group: 166, $R\bar{3}m$). A rough structural investigation by intensity ratio of $I_{(003)}/I_{(104)}$ reveals that the sample synthesized from LiOH has best structural integrity among three lithium sources.

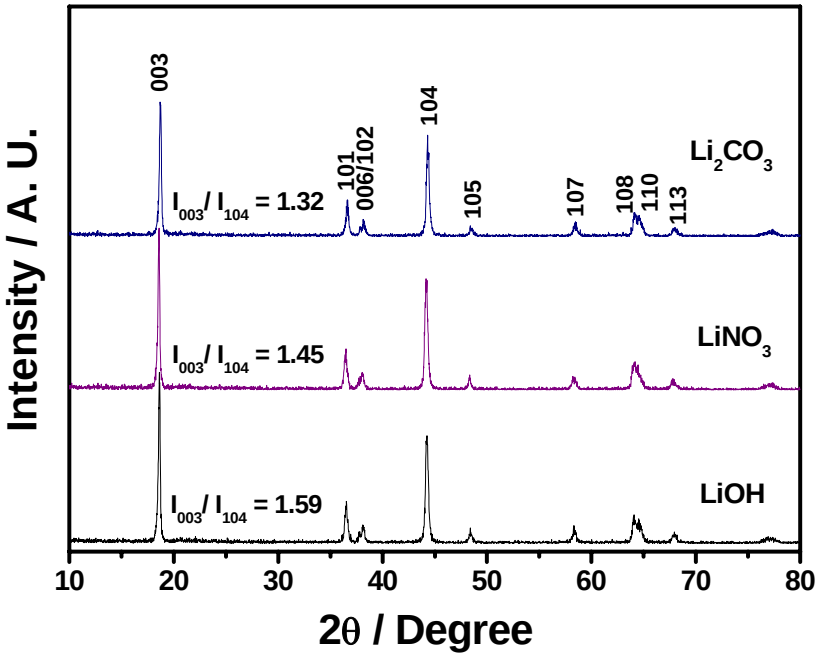

Figure 2.16 X-ray diffraction patterns of the $LiMn_{1/2}Ni_{1/2}O_2$ synthesized from various lithium sources at 900 ^{o}C.

I have used X-ray Rietveld refinement in order to elucidate structural change by the calcination temperature in detail. Here, I have also applied this technique to analysis the sample synthesized from various lithium sources.

Since X-ray scattering powers of Mn, Ni and Co are very similar, it is hard to distinguish individual transition metal ion in refinement. Nevertheless, in this refinement I assume only Ni ions could occupy the Li site because several studies have reported that only Ni ion could occupy the Li site by the refinement of neutron and X-ray diffraction profile refinement [28] because of similarity in ionic radius between Li^+ (0.72 Å) and Ni^{2+} (0.69 Å) [6]. Firstly, I have carried out the refinement using hexagonal $R\bar{3}m$ setting. The profile fitting results for the sample synthesized from

$LiNO_3$ was given in the Fig. 2.17 and obtained structural parameters are summarized in Table 3.1. Cation mixing amounts obtained by Rietveld refinements were slight different. The cation mixing obtained by refinement of the sample prepared by using LiOH, $LiNO_3$ and Li_2CO_3 were 9.2%, 7.9% and 8.4%, respectively. Generally, cation mixing is very important in the Ni-based hexagonal structure because diffusion rate of Li^+ suffers from cation mixing. Divalent nickels ions occupy lithium site in the case of cation mixing, which leads to formation of the $[Li_{1-x}Ni_x^{2+}][Mn_{0.5}Ni_{0.5-x}]O_2$ [6]. The divalent nickel ion in lithium site is oxidized to trivalent or tetravalent during initial charge process, then they cannot be readily reduced. Irreversible oxidation of nickel ion in the lithium site lead shrinkage of local interslab space with respect to difference of ionic radius Ni^{3+} (0.57 Å), Ni^{2+} (0.69 Å) and Li^+(0.72 Å) [6]. This local shrinkage of interslab hinders lithium re-intercalation into host structure, thereby electrochemical performance such as cycle stability and efficiency were deteriorated. Therefore, the sample synthesized from using $LiNO_3$ may be expected to show better reversible capacity with respect to the smaller cation mixing among these three samples.

Table 2.1 Structural parameters obtained by X-ray Rietveld refinement.

	LiOH	**$LiNO_3$**	**Li_2CO_3**
a	2.8854 ± 0.0001 Å	2.8881 ± 0.0001 Å	2.8880 ± 0.0001 Å
c	14.2961 ± 0.0009 Å	14.2941 ± 0.0009 Å	14.2981 ± 0.001 Å
c/a	4.9548	4.9615	4.9508
Vol.	103.077	102.748	103.277
Li_{3b}	0.908 ± 0.004	0.921 ± 0.003	0.916 ± 0.002
Ni_{3b}	0.092 ± 0.004	0.079 ± 0.003	0.084 ± 0.002
Z_{oxy}	0.2424 ± 0.0001	0.2434 ± 0.0001	0.2428 ± 0.0001
R_B	3.13	3.27	2.54
R_{wp}	16.9 %	17.1 %	17.4 %

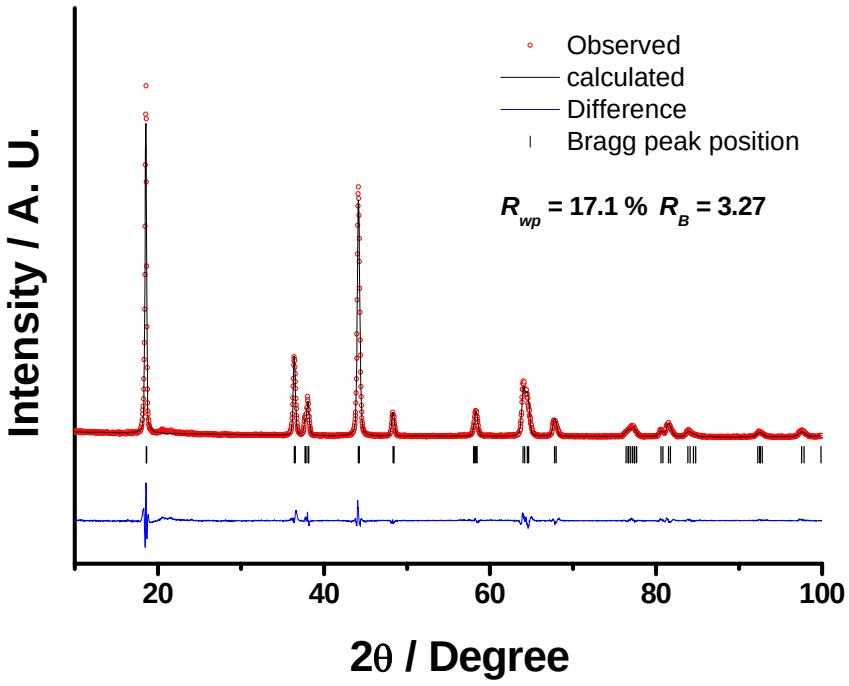

Figure 2.17 Rietveld refinement results for XRD data of sample synthesized from $LiNO_3$ obtained by using $R\bar{3}m$ setting as a model.

In order to observe the morphologies of the synthesized cathode materials, SEM observation was carried out. The SEM images of three samples are shown in Fig. 2.18. The three images are similar. However, the sample prepared by using lithium hydroxide shows slightly larger primary particle size, on the other hand sample prepared from lithium nitrate exhibits the smallest primary particle size of about 0.3 μm in diameter.

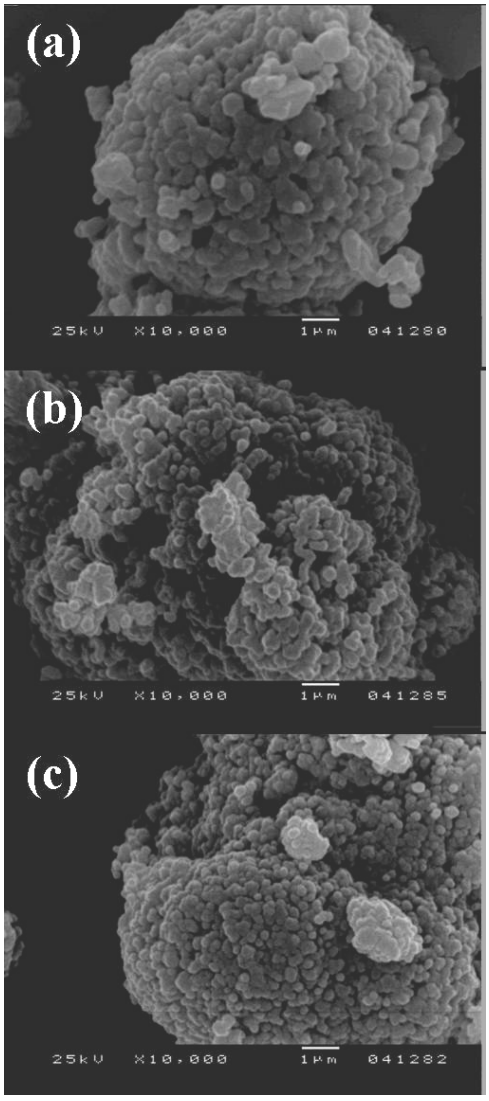

Figure 2.18 SEM Photographs of the sample synthesized by using (a) LiOH, (b) Li_2CO_3 and (c) $LiNO_3$

Figure 2.19 shows initial charge/discharge curves of the cathode materials in the voltage range between 2.8 and 4.4 V. All samples gives similar monotonous charge/discharge curves up to 4.4 V with relatively smaller polarization. The sample prepared from $LiNO_3$ shows higher charge/discharge capacity of 181.1/164.3 mAh g^{-1} as well as the smallest irreversible discharge capacity of 16.8 mAh g^{-1}. The sample synthesized by using Li_2CO_3 and LiOH delivered 175.4/157.8 mAh g^{-1} and 169.2/151.2 mAh g^{-1} as charge/discharge capacities, respectively.

Figure 2.20 shows the cycling stability of the cathode materials. Only the sample synthesized by using LiOH shows small reversible capacity loss about 2% after 30 cycles and the reversible capacity loss was not observed for the sample synthesized by using $LiNO_3$ and Li_2CO_3. The higher reversible capacity and excellent cycle stability might be due to its lower cation mixing and smaller primary particle size. Charge/discharge profile of this sample is extremely sensitive to operation temperature. This measurement was carried out under room temperature, thus the capacity is changed by the change of environmental temperature. If such condition is considered, there are no capacities fading in all three samples.

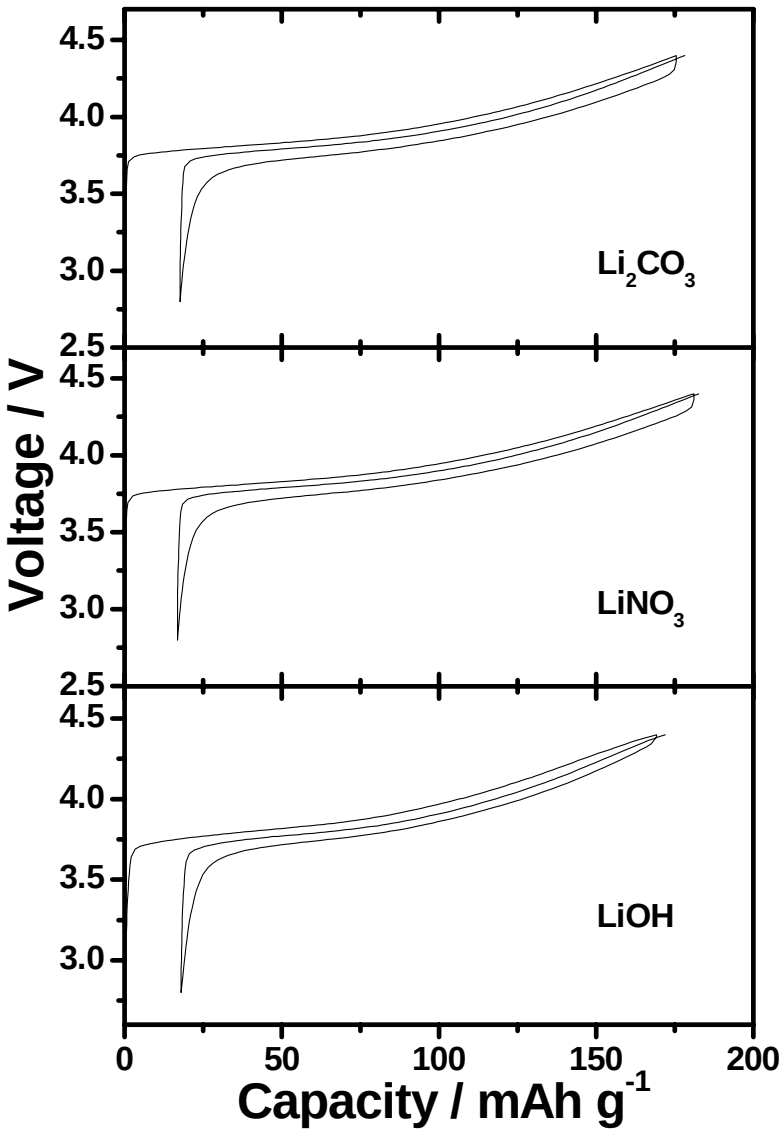

Figure 2.19 Initial charge-discharge curves for the $LiMn_{1/2}Ni_{1/2}O_2$ compounds prepared by using different lithium sources in the voltage range 2.8–4.5 V.

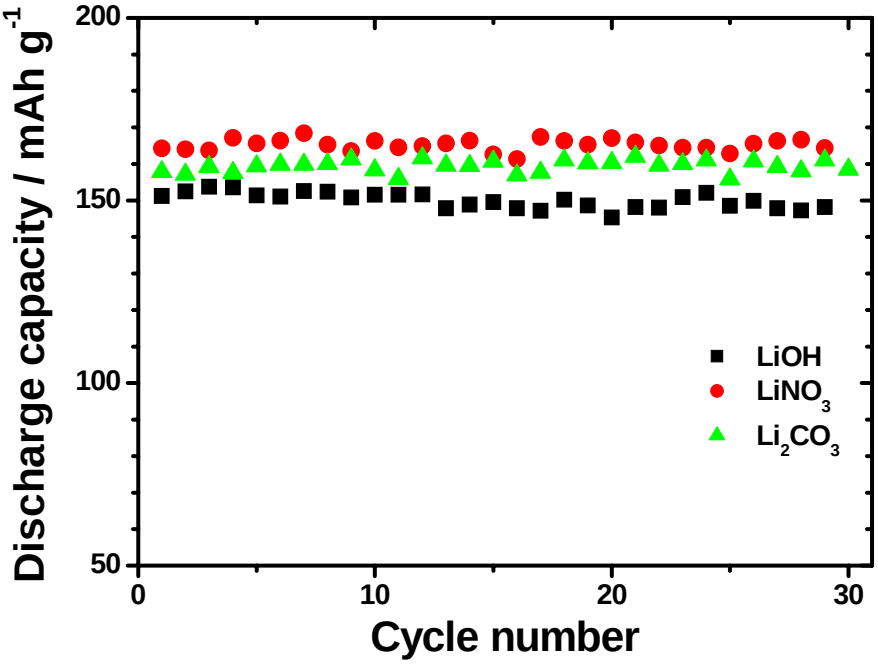

Figure 2.20 Cycling stability of the cathode materials synthesized from various lithium sources in the voltage range 2.8 - 4.5 V.

2.4 Conclusions

The layered $LiMn_{1/2}Ni_{1/2}O_2$ cathode materials were successfully synthesized by using homogeneous Mn and Ni mixture, which was prepared by the carbonate co-precipitation. It was founded that structural integrity of the cathode material depends strongly on the calcinations temperature from the XRD analysis. The temperature range between 850 ^{o}C and 900 ^{o}C is proper to obtain excellent cathode material. XPS spectroscopy and SEM-EDX observation reveled that Ni and Mn are homogeneously distributed in the cathode material with the valence of 2+ and 4+, respectively. The sample prepared at 850 ^{o}C shows the highest discharge capacity as well as the highest

rate capability due to higher structural integrity and larger specific surface area. The excellent electrochemical performance, such as higher discharge capacity and higher rate capability is tightly related to the higher structural integrity. The XRD experiment and SEM observation revels that structural integrity and morphology of the cathode materials synthesized by carbonate method depends slightly on the lithium sources. Sample prepared from lithium nitrate delivered better structural integrity and homogeneous particle distribution than those from lithium hydroxide and lithium carbonate.

References

[1]. Mizushima, P. C. Jones, P. J. Wiseman, and J. B. Goodenough, *Mater. Res. Bull.*, **15** (1980) 783.

[2]. C. Delmas, and I. Saadoune, *Solid State Ionics*, **53– 56** (1992) 370.

[3]. S.-T. Myung, S. Komaba, and N. Kumagai, *J. Electrochem. Soc.*, **149** (2002) A1349.

[4]. B. Ammundsen, and J. M. Paulsen, *Adv. Mater.*, **13** (2001) 943.

[5]. J. R. Dahn, E. W. Fuller, M. Obrovac, and U. von Sacken, *Solid State Ionics*, **69** (1994) 265.

[6]. A. Rougier, I. Saadoune, P. Gravereau, P. Willmann, and C. Delmas, *Solid State Ionics*, **90** (1996) 83.

[7]. J. N. Reimers, E. Rossen, C. D. Jones, and J. R. Dahn, *Solid State Ionics*, **61** (1993) 335.

[8]. Q. Zhong, and U. von Sacken, *J. Power Sources*, **54** (1995) 221.

[9]. A. Hirano, R. Kanno, Y. Kawamoto, Y. Nitta, K. Okamura, T. Izumi, and F. Izumi, *J. Solid State Chem.*, **134** (1997) 1.

[10]. J. Kim, and K. Amine, *J. Power Sources*, **104** (2002) 33.

[11]. G. Prado, A. Rougier, L. Fournes, and C. Delmas, *J. Electrochem. Soc.*, **147** (2000) 2880.

[12]. C. Pouillerie, L. Croguennec, Ph. Biensan, P. Willmann, and C. Delmas, *J. Electrochem. Soc.*, **147** (2000) 2061.

[13]. D. Caurant, N. Baffier, V. Bianchi, G. Gregoire, and S. Bach, *J. Mater. Chem.*, **6** (1996) 1149.

[14]. M. E. Spahr, P. Novak, B. Schnyder, O. Haas, and R. Nesper, *J. Power Sources*, **68** (1997) 629.

[15]. M. E. Spahr, P. Novak, B. Schnyder, O. Haas, and R. Nesper, *J. Electrochem. Soc.*, **145** (1998) 1113.

[16]. T. Ohzuku, and Y. Makimura, *Chem. Lett.*, **2001,** 744.

[17]. Y. Makimura, and T. Ohzuku, *J. Power Sources*, **119** (2003) 156.

[18]. K. M. Shaju, G. V. Subba Rao, and B. V. R. Chowdari, *Electrochim. Acta*, **48** (2002) 145.

[19]. T. Ohzuku, and Y. Makimura, *Chem. Lett.*, **2001**, 642.

[20]. N. Yabuuchi, and T. Ohzuku, *J. Power Sources*, **119–121** (2003) 171.

[21]. I. Belharouak, Y.-K. Sun, J. Liu, and K. Amine, *J. Power Sources* **123** (2003) 247.

[22]. Z. Lu, D. D. MacNeil, and J. R. Dahn, *Electrochem. Solid-State Lett*., **4** (2001) A200.

[23]. D. D. MacNeil, Z. Lu, and J. R. Dahn, *J. Electrochem. Soc.*, **149** (2002) A1332.

[24]. M.-H. Lee, Y.-J. Kang, S.-T. Myung, and Y.-K. Sun, *Electrochim. Acta*, **50** (2004) 939.

[25]. T. Roisnel, and J. Rodriguez-Carjaval, *Fullporf Manual*, Institut Laue-Langevin, Grnoble (2000).

[26]. K. M. Shaju, G. V. Subba Rao, and B. V. R. Chowdari, *Electrochim. Acta*, **48** 1505 (2003).

[27]. S. Gopukumar, K. Y. Chung, and K. B. Kim, *Electrochim. Acta*, **49** (2004) 803.

[28]. J.-M. Kim, and H.-T. Chung, *Electrochim. Acta*, **49** (2004) 937.

Chapter 3

Effect of Synthesis Condition on the Structural and Electrochemical properties of $Li[Ni_{1/3}Mn_{1/3}Co_{1/3}]O_2$ Prepared by Carbonate Co-precipitation Method

3.1 Background of this research

Recently, layered $LiMn_{1/2}Ni_{1/2}O_2$–$LiCoO_2$ solid solution is believed to be one of the most interesting lithium intercalation materials [1-5]. It attracts significant interest because the combination of nickel, manganese and cobalt can provide advantages such as higher reversible capacity with milder thermal stability at charged state [2], lower cost and less toxicity than $LiCoO_2$, Thus, this solid solution could be one of the promising cathode materials. Unfortunately, it is difficult to prepare this complicated material and this material could show low rate capability depending on the synthetic route. Therefore, it is important to select suitable preparation method.

In previous chapter, I have successfully introduced one of the simplest synthetic methods, viz. carbonate co-precipitation method, to prepare a $LiNi_{1/2}Mn_{1/2}O_2$ cathode material. Homogeneous $LiNi_{1/2}Mn_{1/2}O_2$ material could be readily obtained by applying the method.

I have already described the advantage of new method named carbonate co-precipitation method. Therefore, in this chapter, I have applied the method to prepare one of $LiMn_{1/2}Ni_{1/2}O_2$–$LiCoO_2$ solid solution, $LiMn_{1/3}Ni_{1/3}Co_{1/3}O_2$. It is necessary to study that the effect of preparation condition on the structural and electrochemical properties. Here, therefore, I report structural, morphological and electrochemical properties of layered $LiNi_{1/3}Mn_{1/3}Co_{1/3}O_2$ cathode materials synthesized under various condition by carbonate co-precipitation method.

3.2 Experimental

For preparing transition metal carbonate powder, $Mn_{1/3}Ni_{1/3}Co_{1/3}CO_3$, I used $MnSO_4 \cdot 4\text{-}5H_2O$, $NiSO_4 \cdot 6H_2O$, $CoSO_4 \cdot 7H_2O$ and Na_2CO_3 as the starting materials. The detail co-precipitation route was described in previous chapter. The co-precipitated carbonate powder $Mn_{1/3}Ni_{1/3}Co_{1/3}CO_3$ was pre-heated at 500 ^oC for 5 h in air and changed to spinel compound. I have applied EDTA titration to determine exact amount of transition metal ions in spinel powder. A stoichiometric amount of lithium was mixed with the spinel and calcined at various temperatures for 15h in air.

X-ray diffraction measurements for the precursor and the synthesized $Li[Mn_{1/3}Ni_{1/3}Co_{1/3}]O_2$ materials were carried out using Rigaku Rint 1000 diffractormeter with a CuKα radiation. The XRD data for the cathode materials were carefully collected by step of 0.03° with a constant counting time of 10 seconds per step. I applied Rietveld refinements analysis using the FullProf 2000 program [6] in order to investigate the structural information. The metal ion content in products were determined by an inductively coupled plasma spectrometer (ICP : SPS 7800, Seiko instruments, Japan). The specific surface areas of the sample materials measured using a Micromeritics Gemini 2375 (USA) and analyzed by the B.E.T method. Observation by scanning electron microscopy (SEM : JSM-5300E, JEOL, Japan) was carried out to know the morphologies of the synthesized materials. X-ray photoelectron spectra of the transition metals in the synthesized materials were measured using PHI 5800 spectrometer (ULVAC-PHI INC, USA) spectrometer with monochromated Al-Kα radiation. Charge referencing was done with carbon C_{1s} binding energy of 284.5 eV.

The electrochemical characterizations were carried out using the CR-2032-type coin cell. A cathode was prepared by pressing active material film, which is consist of 20 mg active material and 12 mg conducting binder (Teflonized acetylene black), on the stainless steel mesh. The cell was composed of the cathode, the lithium foil as an anode and 1M $LiPF_6$-EC/DMC (1:2 in volume) electrolyte. The electrochemical cycling tests were performed at room temperature. Cyclic voltammetry (CV) was conducted using a three-electrode cell, where lithium foil was used as both counter and reference electrode in 1M $LiPF_6$-EC/DMC (1:2 in volume) electrolyte. CV experiments were carried out at a scan speed of 0.1 mV s^{-1} between 2.8 and 4.6 V vs. Li/Li^+.

3.3 Results and Discussions

I have obtained pink colored powder as a precursor through the co-precipitation process. An X-ray diffraction experiment, SEM observation and ICP spectroscopy were employed in order to characterize the precursor. The XRD pattern of the precursor and standard $MnCO_3$ (JCPDS 07-0268) are given in Fig. 3.1.

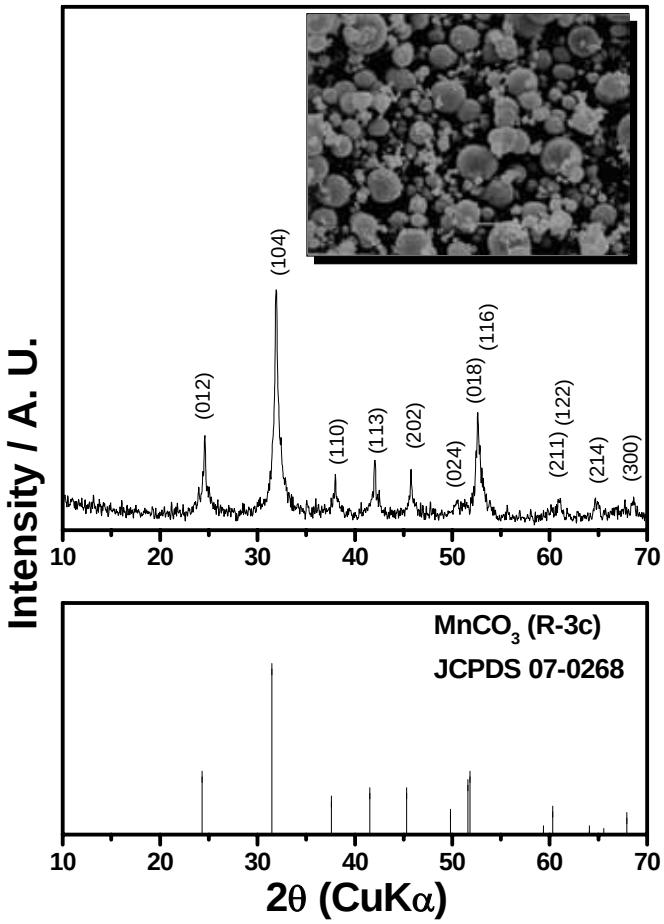

Figure 3.1 SEM photograph and X-ray diffraction pattern for co-precipitated powder and $MnCO_3$.

The diffraction pattern of the precursor is resemble with that of standard manganese carbonate pattern though there are slightly difference in both peak position and sharpness. Such deviation and broad diffraction lines can be attributed to mixing of three transition metal ion, Mn^{2+}, Ni^{2+}, and Co^{2+}. The particle morphology of the precursor is spherical with average secondary particle diameter about 5㎛, but primary particle size is less than 1㎛. The chemical composition of the precursor, that is calculated from the result of the ICP analysis, could be described as $Mn_{0.34}Ni_{0.33}Co_{0.33}CO_3$. Therefore, I could successfully prepare transition metal carbonate precursor by co-precipitation process.

Figure 3.2 shows typical XRD patterns of all synthesized $Li[Mn_{1/3}Ni_{1/3}Co_{1/3}]O_2$ materials at different calcination temperatures, viz., 750, 800, 850, 900 and 950 ^oC. Hereafter the materials synthesized at 750, 800, 850, 900 and 950^oC were referred as S75, S80, S85, S90 and S95, respectively. The XRD patterns of them can be indexed on the basis of the α-$NaFeO_2$ structure (space group : 166 , $R\bar{3}m$) and no remarkable secondary phase can be observed in the patterns. Peak splitting for (006)/(102) and (018)/(110) peaks are known to an indicator of developed layered in $LiNiO_2$ [7-9]. Regardless of low calcination temperature, the peak splits of (006)/(102) and (018)/(110) observed in all XRD patterns which indicate the layered $Li[Ni_{1/3}Mn_{1/3}Co_{1/3}]O_2$ cathode material successfully synthesized at all calcination temperature. Although S75 shows broader diffraction lines than the others, the XRD pattern of S75 shows the clear peak splits and there are no impurity phases. These results could be interpreted that homogeneous precursor obtained by carbonate co-precipitation method can form the layered compound even at low temperature of 750 ^oC. It would be due to the presence of Co.

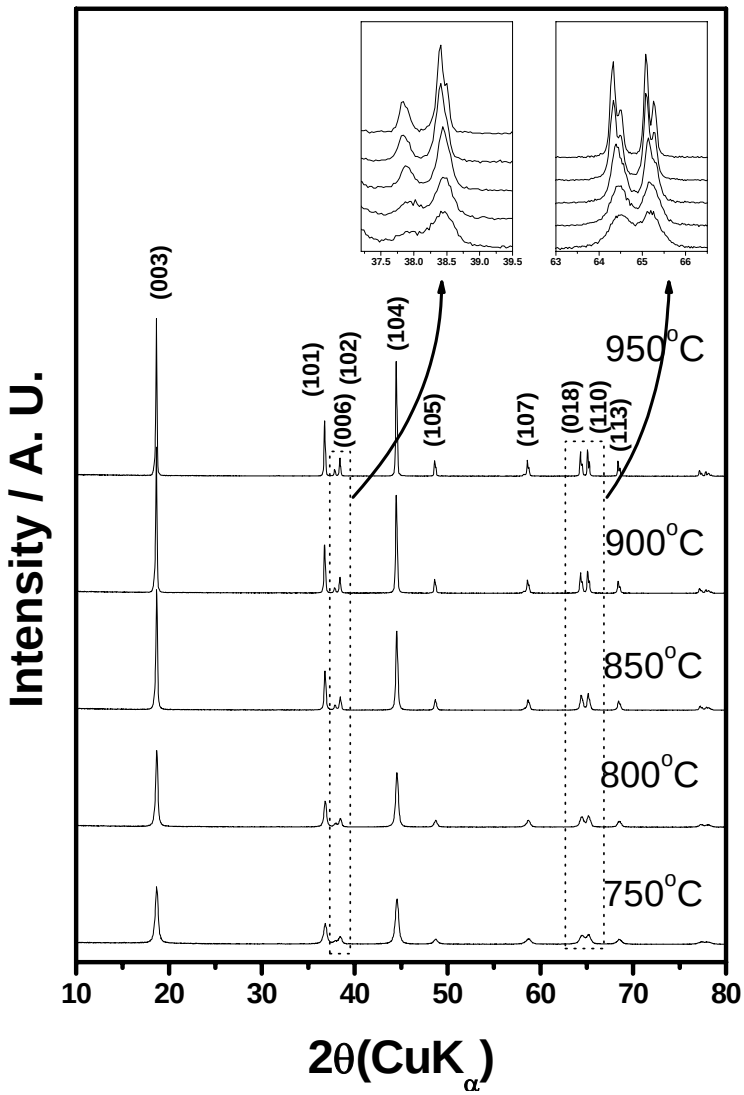

Figure 3.2 X-ray diffraction patterns of the synthesized $Li[Mn_{1/3}Ni_{1/3}Co_{1/3}]O_2$.

Lattice parameters of the synthesized $Li[Mn_{1/3}Ni_{1/3}Co_{1/3}]O_2$ materials were determined by the Rietveld refinement. The result of refinement for S90 was presented in Fig. 3.3 and refined parameters are summarized together with the specific surface area and the chemical composition in the Table 3.1.

Tabel 3.1 Chemical analysis, refined structure parameters and specific surface area for the synthesized compounds.

Calcination Temp. (^{o}C)	Composition	Lattiec parameter		c/a	Vol.	Z_{oxy}	Ni in Li_{3b} site	Reliable factor		Specific surface area (m^2/g)
		a (Å)	*c* (Å)					R_{WP}	R_B	
750	$Li_{1.01}Mn_{0.34}Ni_{0.32}Co_{0.34}O_2$	2.861	14.232	4.97	100.89	0.2594(2)	0.029(3)	13.1	1.96	11.3
800	$Li_{1.01}Mn_{0.34}Ni_{0.32}Co_{0.34}O_2$	2.860	14.234	4.97	100.87	0.2592(1)	0.023(1)	12.5	2.04	9.0
850	$Li_{1.01}Mn_{0.34}Ni_{0.32}Co_{0.34}O_2$	2.861	14.241	4.98	100.97	0.2594(2)	0.015(1)	13.6	3.05	3.0
900	$Li_{1.00}Mn_{0.34}Ni_{0.32}Co_{0.34}O_2$	2.862	14.248	4.98	101.06	0.2593(1)	0.014(1)	13.2	3.22	1.4
950	$Li_{0.98}Mn_{0.34}Ni_{0.32}Co_{0.34}O_2$	2.863	14.253	4.98	101.16	0.2593(2)	0.020(2)	13.1	3.33	0.7

Calculated lattice parameter were somewhat increased with increasing calcination temperature. While *c/a* values that indicate hexagonal structure disorder [10] were virtually unchanged. These results indicate that the specific surface area and lithium content decrease but hexagonal ordering do not change with calcination temperature. Therefore, I believe that the lower calcination temperature could give more advantage in terms of larger surface area.

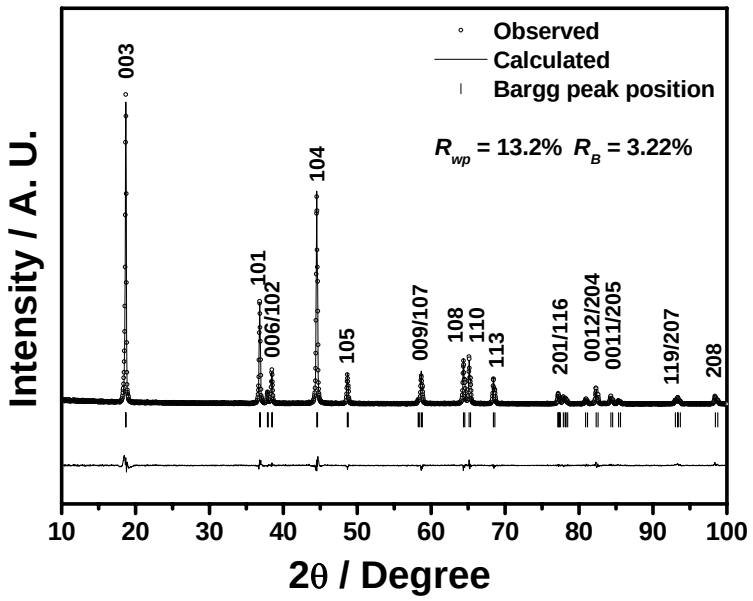

Figure 3.3 Rietveld refinement result of X-ray diffraction pattern for the S90.

In order to confirm the oxidation state of the transition metal species in the synthesized $Li[Mn_{1/3}Ni_{1/3}Co_{1/3}]O_2$ materials, XPS study was carried out. Figure 3.4 shows XPS spectra for $Mn_{2p3/2}$, $Ni_{2p3/2}$ and $Co_{2p3/2}$ binding energy. The binding energies of Mn, Ni and Co for the S75 are 641.9, 854.5 and 779.9 eV, respectively. From the related studies [5, 11], I could confirm that these binding energies of 641.9, 854.5 and 779.9 eV are well coincided with binding energy of Mn^{4+}, Ni^{2+} and Co^{3+},

respectively. Thus I could say the valence states of Mn, Ni and Co in the S75 are 4+, 2+ and 3+, respectively. Binding energies of all transition metal species in the samples were almost same until calcination temperature up to 900 ^{o}C. On the other hand, binding energy of Mn and Ni are suddenly increased up to 644 and 857.4 eV when the sample prepared at 950^{o}C and whereas binding energy of Co was decreased to 778.4 eV in the S95. I could not index the binding energy of Mn and Co because those binding energies are not coinciding with any transition metal species of Mn and Co. Only Ni could be indexed to the Ni^{3+} (Ni_2O_3 : 857.3 eV). This result indicates that higher calcination temperature, i.e., 950 ^{o}C, leads unexpected change of valence state for all the transition metal species. The specific reasons for the change of valence state of transition metals at 950 ^{o}C without structure transformation and emerging new phases is not clear yet in this study. However, I assume that these unexpected changes could be attributed by lithium and oxygen vaporization at high temperature.

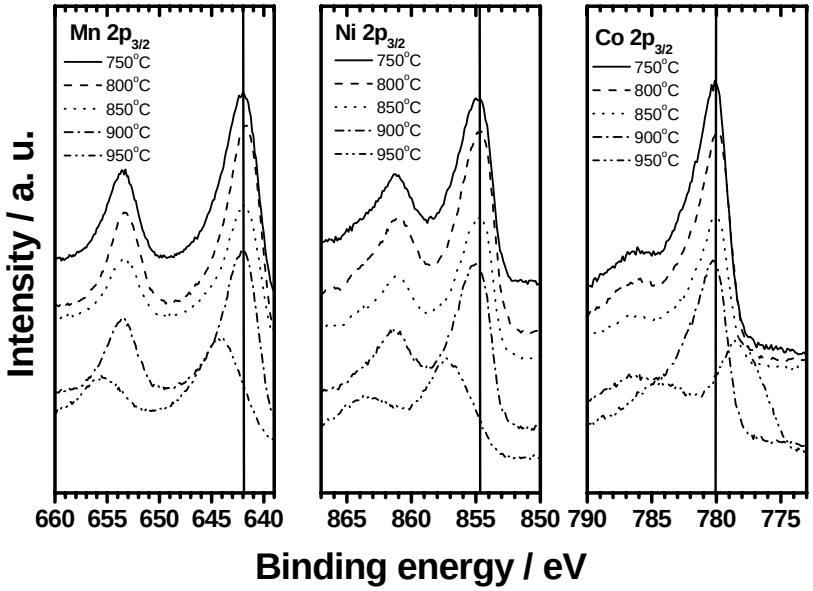

Figure 3.4 XPS spectra of $Mn2p_{3/2}$, $Ni2p_{3/2}$ and $Co2p_{3/2}$ for the synthesized $LiMn_{1/3}Ni_{1/3}Co_{1/3}O_2$ cathode materials.

In order to observe morphology of the synthesized $Li[Mn_{1/3}Ni_{1/3}Co_{1/3}]O_2$ materials at various calcination temperature, I applied SEM observation at different magnification. Scanning electron micrographs of materials with various calcination temperatures are given in Fig. 3.5 (a), (c) and (e). Fig. 3.5 show the micro morphologies of S75, S85 and S95, respectively. The primary particle size is less than 1㎛ in diameter and these small particles aggregated each other to form spherical secondary particle. This kind of morphology could be thought to enhance high rate capability with respect to high surface area and tapping density would be kept high level because of its larger secondary particle size. With increasing calcinations temperature, the primary particles increased up to 1㎛ in diameter (e), which leads decrease of surface area. Fig. 3.5(b), (d) and (f) show semi-micro morphology of the materials. Generally, increase in calcination temperature leads to crystal growth, however semi-micro morphologies of the materials are almost same and similar to original powder (see Fig. 3.1).

Since particle shape and its size could affect energy density for practical use, controlled particle morphology is very important. As shown in the Fig. 3.5(b), (d) and (f), the shape and size of secondary particle could be directly controlled by those of precursor powder. Therefore, I believe that carbonate co-precipitation process is practical method for the preparation of cathode material.

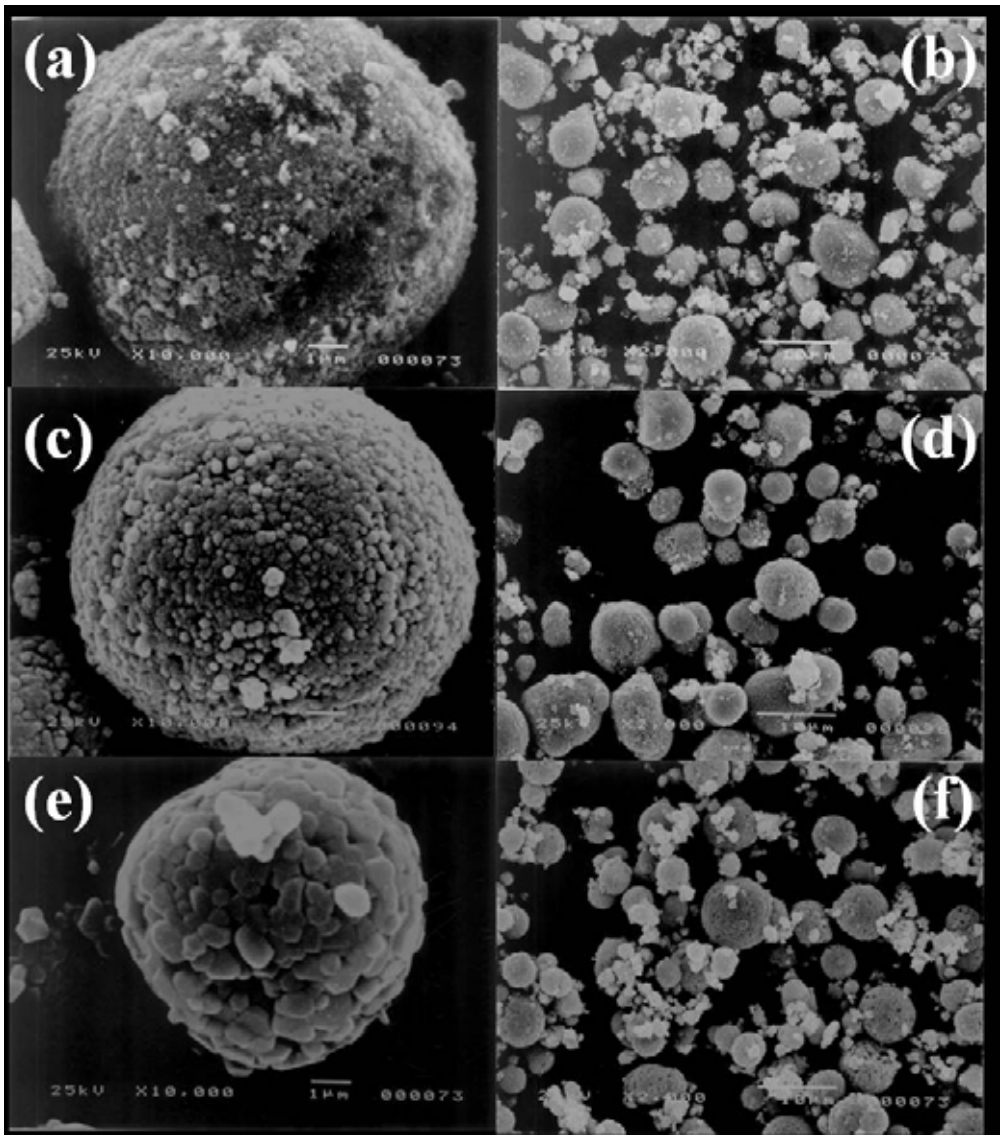

Figure 3.5 SEM Photographs for synthesized $Li[Mn_{1/3}Ni_{1/3}Co_{1/3}]O_2$ compounds at 750 ^oC (a and b), 850^oC (c and d) and 950^oC (e and f).

Electrochemical charge-discharge experiments for $Li[Mn_{1/3}Ni_{1/3}Co_{1/3}]O_2$ materials have been performed at room temperature in the voltage range 2.8 to 4.5 V with applying constant current density of 20 mA g^{-1}. Figure 3.6 shows initial charge/discharge curves (a) and cycling performance for all the samples during 30 cycles (b). The voltage profiles of all samples are similar to those reported profiles [2,5]. The S75 shows the charge capacity of 205.4 mAh g^{-1} and the discharge capacity of 179.4 mAh g^{-1} at the initial cycle and gives stable cycle performance in the subsequent cycles. Although the S75 has lower crystallinity than the other samples, it could deliver higher discharge capacity of 179.4 mAh g^{-1}. On increasing calcination temperature, discharge capacities of samples were gradually decreased except S80. The initial discharge capacity of the samples S85, S90 and S95 were 179.3, 175.7 and 174.3 mAh g^{-1}, respectively. The highest initial discharge capacity of 186.7 mAh g^{-1} was obtained by the S80. Moreover, the irreversible capacity, which leads energy loss in practical use, also slightly increased with increasing calcinations temperature. The irreversible capacity of S75, S85, S90 and S95 were 12.7, 11.5, 13.3 and 13.8 %, respectively. The smallest irreversible capacity of 10.7 % was achieved by S80.

Average capacity retention ratio, which was suggested by Yoshio et al. [12], was slightly increased with increasing calcinations temperature. The average capacity retention ratios of S75, S80, S85, S90, S95 were 99.64, 99.69, 99.75, 99.76 and 99.77% per each cycle, respectively. I thought that S80 shows best electrochemical properties because of moderate crystallity, large surface area and ideal chemical composition.

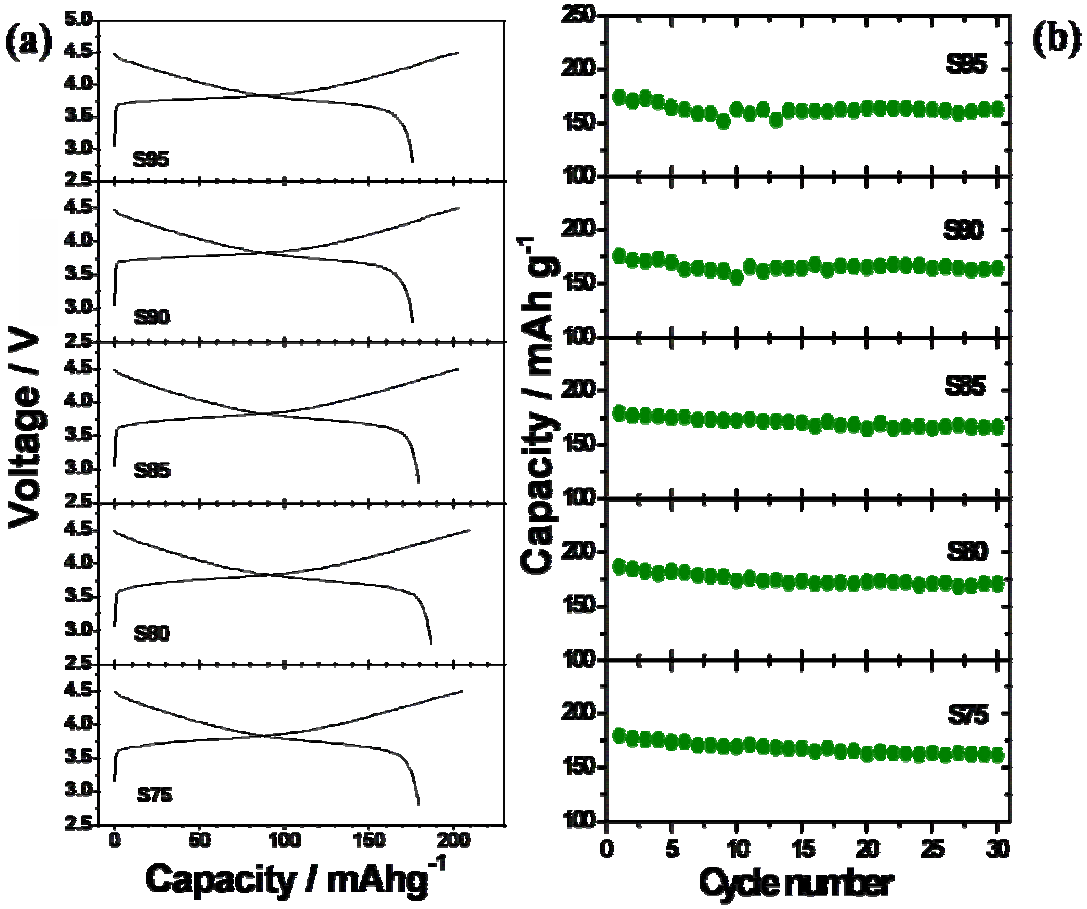

Figure 3.6 Charge and discharge curves for initial cycles (a) and charge-discharge capacities as a function of cycle number (b) in the voltage range 2.8 to 4.5 V (vs. Li/Li^+).

Figure 3.7 shows typical cyclic voltammogram of the S75, S85 and S95. As shown in the Fig. 3.7, major oxidation peak of S75 is 3.83 V and it shifted to the higher voltage with increasing calcination temperature. It means that the polarization of samples increased with increasing calcinations temperature. Thus, I thought that the increase in the polarization of the samples probably due to increase of electrode

resistance with respect to specific surface area because the samples calcined at high temperature have smaller specific surface area.

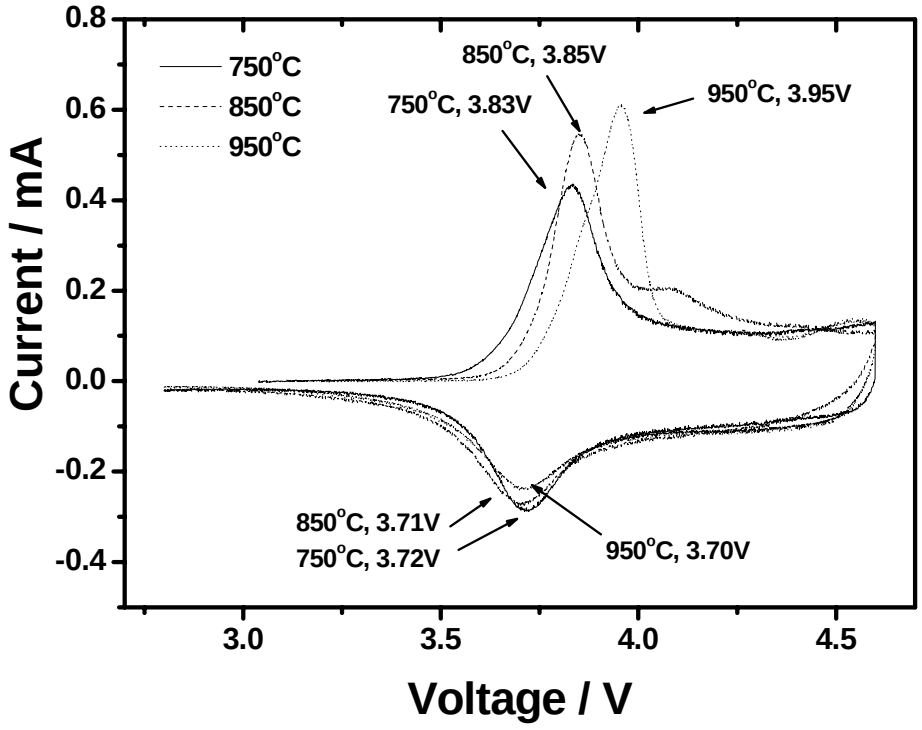

Figure 3.7 Cyclic voltammogram of $Li[Mn_{1/3}Ni_{1/3}Co_{1/3}]O_2$ cathode prepared at 750, 850 and 950 °C in the voltage range from 2.8 to 4.6 V.

It is well known that rate capability can be affected strongly by surface area of cathode material. In order to elucidate the dependence of rate capability on the surface area (primary particle size) and secondary particle size, I applied 20 mA g^{-1} for charging and 20, 90, 180, 360 and 450 mA g^{-1} for discharge currents across the $Li[Ni_{1/3}Mn_{1/3}Co_{1/3}]O_2$ electrode in the voltage range from 2.8 to 4.5 V. These current densities can be calculated to be 0.11(20 mA g^{-1}), 0.5(90 mA g^{-1}), 1(180 mA g^{-1}),

2(360 mA g^{-1}), 2.5C(450 mA g^{-1}), where the C-rate was determined using 180mAh g^{-1} as a capacity. Figure 3.8 shows the results of rate capability experiments. The delivered discharge capacities of S75, S80, S85, S90 and S95 at 2.5C (450 mA g^{-1}) were 144.0, 145.7, 142.3 144.8 and 127.1 mAh g^{-1}, respectively. Surprisingly, S75, S80, S85 and S90 show similar capacity retention ratio at each C-rate in spite of large difference in their specific surface area as summarized in Table 3.1, i. e., S75 has more than 8 times larger specific surface area than S90. Our results suggest that the rate capability depends on not the surface area (primary particle size) but the diffusion rate of Li in particle. From the above electrochemical charge/discharge and rate capability tests, I consider that 800 ^{o}C is the proper calcination temperature to obtain excellent cycle stability and rate capability and 950 ^{o}C is too high calcination temperature to obtain good rate capability.

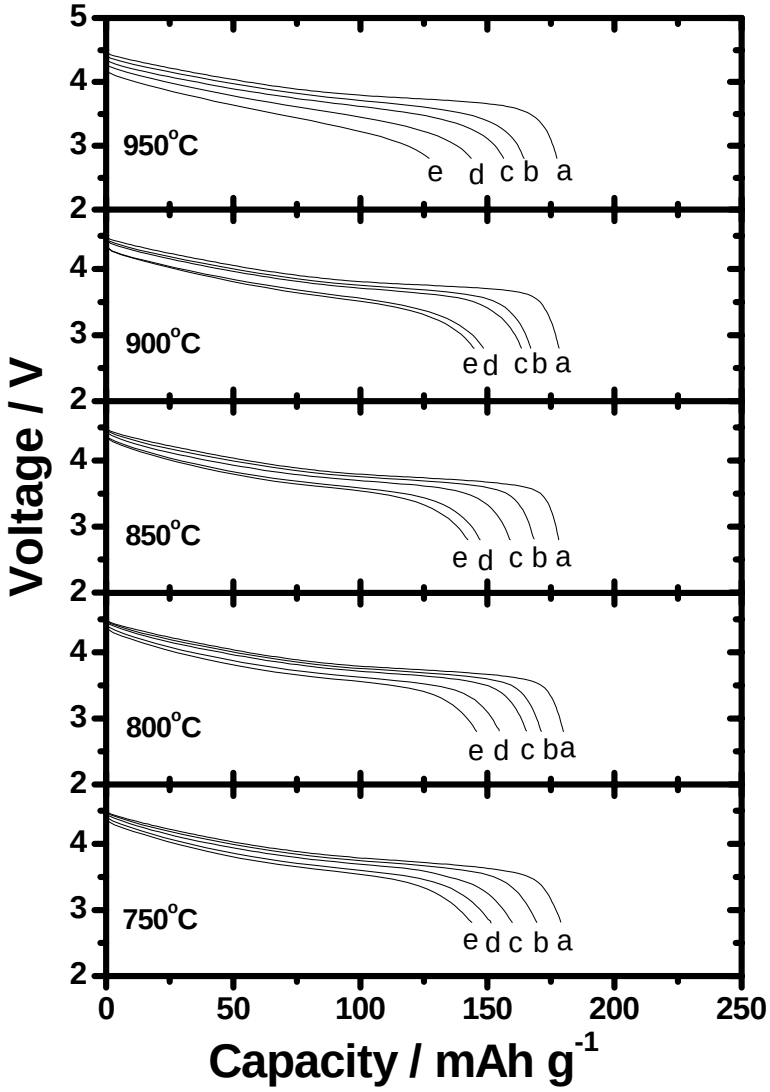

Figure 3.8 Rate capability tests for the samples in the voltage range 2.8 to 4.5 V.(a = 20 mA/g ; b = 90 mA/g ; c = 180 mA/g ; d = 360 mA/g ; e = 450 mA/g).

3.4 Conclusion

The layered $Li[Ni_{1/3}Mn_{1/3}Co_{1/3}]O_2$ cathode material with spherical particle shape was successfully synthesized through carbonate co-precipitation method under different calcinations temperature. I could synthesize the homogeneous material even at low temperature of 750 ^{o}C and control morphology of particles using the co-precipitation process. All the materials with hexagonal structure show clear XRD peak splits of (006)/(102) and (018)/(110) for the sake of high *c/a* value about 4.97. XPS study indicate that the transition metals in the materials are Ni^{2+}, Mn^{4+} and Co^{3+} except sample calcined at 950 ^{o}C. From electrochemical experiments, it can be concluded that 800 ^{o}C is an optimal calcination temperature in this experiment and the rate capability of these materials depends on not the surface area (primary particle size) but diffusion rate of Li in particle.

References

[1] T. Ohzuku, and Y. Makimura, *Chem. Lett.*, **2001** 642.

[2] N. Yabuuchi, and T. Ohzuku, *J. Power Sources*, **119–121** (2003) 171.

[3] Z. Lu, D. D. MacNeil, and J. R. Dahn, *Electrochem. Solid-State Lett.*, **4** (2001) A200.

[4] D. D. MacNeil, Z. Lu, and J. R. Dahn, *J. Electrochem. Soc.*, **149** (2002) A1332.

[5] K. M. Shaju, G. V. Subba Rao, and B. V. R. Chowdari, *Electrochim. Acta*, **48** (2002) 145.

[6] T. Roisnel, and J. Rodriguez-Carjaval, *Fullprof Manual*, Institut Laue-Langevin, Grnoble, 2000.

[7] J. R. Dahn, U. von sacken, and A. V. Chadwick, *Solid State Ionics*, **44** (1990) 87.

[8] T. Ohzuku and A. Ueda, and M. Nagayama, *J. Electrochem. Soc.*, **140** (1993) 1862.

[9] Y. Gao, M.V. Yakovleva, and W.B. Ebner, *Electrochem. Solid-State Lett.*, **1** (1998) 117.

[10] J.-M. Kim, and H.-T. Chung, *Electrochim. Acta*, **49** (2004) 937.

[11] S. Gopukumar, K. Y. Chung, and K. B. Kim, *Electrochim. Acta*, **49** (2004) 803.

[12] M. Yoshio, Y. Xia, N. Kumada, and S. Ma, *J. Power sources*, **101** (2001) 79.

Chapter 4

Novel Surface Modification Technique to Improve Electrochemical Performance of $LiCoO_2$ at High Voltage

4.1 Background of this research

Layered $LiCoO_2$ has been the most widely used in commercial Li-ion batteries as cathode material because of easiness of production and excellent electrochemical performance with high theoretical capacity of 274 mAh g^{-1}. Although it has high theoretical capacity, only about 137 mAh g^{-1} of capacity is used in the voltage range from 3 to 4.2 V in practical lithium ion battery. In order to obtain higher capacity, the cathode materials have to be charged beyond 4.2 V. However, charging the cathode material up to high voltage, i.e. above 4.2 V, results in significant deterioration of the cycle stability due to phase transformation [1] and dissolution of Co^{4+} ions [2]. Furthermore, Z. Chen and J. R. Dahn suggested that impedance growth could be a reason of the rapid capacity fading of $LiCoO_2$ cycled to 4.5 V [3].

Trials to overcome the capacity fading through suppression of phase transformation by doping of foreign elements have been reported by Zou et al.[4] They had shown that doping of foreign elements was effective to improve cycle stability at higher voltage. Especially, Mg doped $LiCoO_2$ delivered stable capacity of 160 mAh g^{-1} in the voltage range 3.5 to 4.5 V [4]. As an alternative approach, it has been reported that modifying the surface of the cathode material by coating with some metal oxides [5-9]. Surface coating plays a protective role in keeping the active material from direct contact with the acidic electrolyte, thereby $LiCoO_2$ coated with ceramic materials can deliver stable capacities for such high voltage cycling [6-9]. These researches suggest that doping and coating techniques are helpful to improve the capacity fading at high voltage.

From the above researches, I got a new concept of surface modification method, and here I would like to introduce a novel surface modification technique. One of the

features of this technique is that all the modification process can be achieved during co-precipitation process. In this study, I applied the technique to improve the cycle stability of $LiCoO_2$ for high voltage cycling and reported structural and electrochemical properties of the material. In order to modify the surface of $LiCoO_2$, I selected $Li[Ni_{1/2}Mn_{1/2}]O_2$ because it is well known as a cathode material which has good cycle ability even up to 4.5 V vs. Li/Li^+ [10-12] and it is confirmed that the preparation of selected one is easy as described in previous chapter.

4.2 Experimental

In order to form surface modified $LiCoO_2$ by $LiMn_{1/2}Ni_{1/2}O_2$, I have applied two-step precipitation method. In the first step, I precipitate a transition metals carbonate powder, $CoCO_3$, as core material using $CoSO_4 \cdot 7H_2O$ and Na_2CO_3. In the second step, the $CoCO_3$ powder was dispersed in another precipitation bath then precipitate again with transition metal aqueous solution (Mn:Ni = 1:1) in order to cover surface of $CoCO_3$ by $Mn_{1/2}Ni_{1/2}CO_3$. The surface modified precursor was heated at 400 ^oC for 5hr to form oxide compound, and then EDTA titration was carried out to determine exact concentration of transition metal element in the oxide compound. A stoichiometry amount of lithium hydroxide was mixed with oxide precursor, and then heated at 900 ^oC for 15h in air. In order to confirm the effect of this technique, I separately prepared reference Mn and Ni doped $LiCoO_2$ having same chemical composition with surface modified $LiCoO_2$. Schematic diagram of preparation procedures of precursor by one (reference material) and two step co-precipitation (surface modified material) are given in Fig. 4.1.

X-ray diffraction data of the calcined powder were carefully collected in the 2θ range of 10 to 80° using a CuKα radiation of Rigaku Rint 1000 diffractormeter. The lattice parameters of the calcined powders were calculated by least square method using strongly ten diffraction lines. The chemical composition of the synthesized cathode materials was determined by an inductively coupled plasma spectrometer (ICP : SPS 7800, Seiko instruments, Japan). The specific surface area was measured using a Micromeritics Gemini 2375 (USA) by the B.E.T method. Scanning electron microscopy (SEM : JSM-5300E, JEOL, Japan) was carried out to observe the morphologies of the synthesized cathode material. In order to confirm the Mn and Ni concentration on the surface, I carried out an electron probe micro analyzer (EPMA : JXA-8900RLS, JEOL, Japan) of cross section of coated particle.

The electrochemical characterizations were carried out using the CR-2032-type coin cell. Electrode were made by coating a slurry, which was prepared by mixing the cathode materials, KS-6 carbon as a conducting additive and a polyvinylidene fluoride (PVdF) as a binder with a weight ratio of 91:4:5 in *N*-methyl-2-pyrrolidene (NMP), on an Al foil. The loading amount of active material was about 7 mg cm^{-2}. The coin type cell was composed of the cathode, the lithium foil as an anode and 1M $LiPF_6$-EC/DMC (1:2 in volume) as an electrolyte. The electrochemical cycling tests were performed at room temperature.

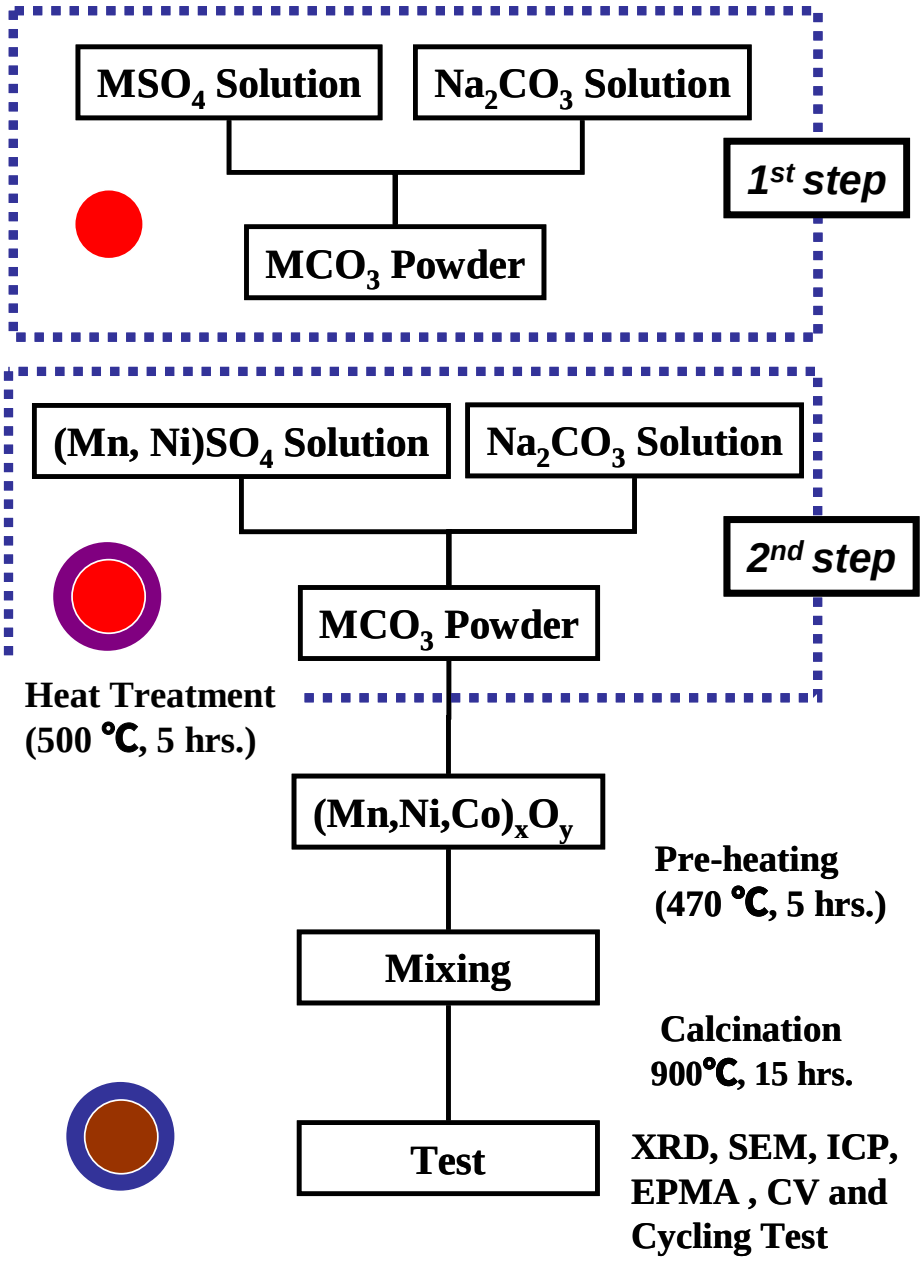

Figure 4.1 Schematic diagrams of one and two-step co-precipitation procedure.

4.3 Results and Discussion

I carried out XRD experiment in order to investigate structure of surface modified and doped $LiCoO_2$. Fig. 4.2 shows the XRD patterns of the synthesized Li[Ni, Co, Mn]O_2 coated $LiCoO_2$ (M3-C2, M3-C4 and M3-C6) and doped samples (M3-N2, M3-N4 and M3-N6). All the peaks of the two groups can be indexed based on the α-$NaFeO_2$ structure and secondary phases were not observed in the whole scan range. All the samples show clear peak splits of (006)/(102) and (108)/(110). XRD diffraction patterns of M3-C series gradually become broad with increase in Mn and Ni content. On the other hand, the broadness of diffraction pattern was not observed in M3-N series. The lattice parameters, *a* and *c,* were calculated by least square method using 10 diffraction lines and calculated parameters are summarized in Table 4.1. The chemical composition and specific surface area obtained by ICP spectroscopy and B.E.T methods are also described together in the Table. The determined chemical compositions of two groups are almost same, so it could be consider that difference in electrochemical performance between two groups basically can be attributed to effect of surface modification. It was found that there is an increase in lattice parameters, *a* and *c*, with increase in substitution amounts. The increase of lattice parameter might be caused by the substitution of lager Ni^{2+} ion for Co^{3+} [13].

I carried out EPMA experiment for the polished cross section of M3-C2 particle in order to investigate manganese and nickel distribution on the surface of the modified $LiCoO_2$. Distribution of metal elements in particles is presented in the Fig. 4.3. Ni and Mn ions were observed both the surface and the core of the particle. However, higher Mn and Ni concentration were observed on the surface of the particle. This result indicates that surface modification was successfully carried out through co-precipitation

method and some of the Mn and Ni ions diffused into the core of the particle to form $LiCo_{1-x-y}Mn_xNi_yO_2$. Moreover, broadening of XRD diffraction pattern of M3-C series can be explained by existence of two phases in a cathode material.

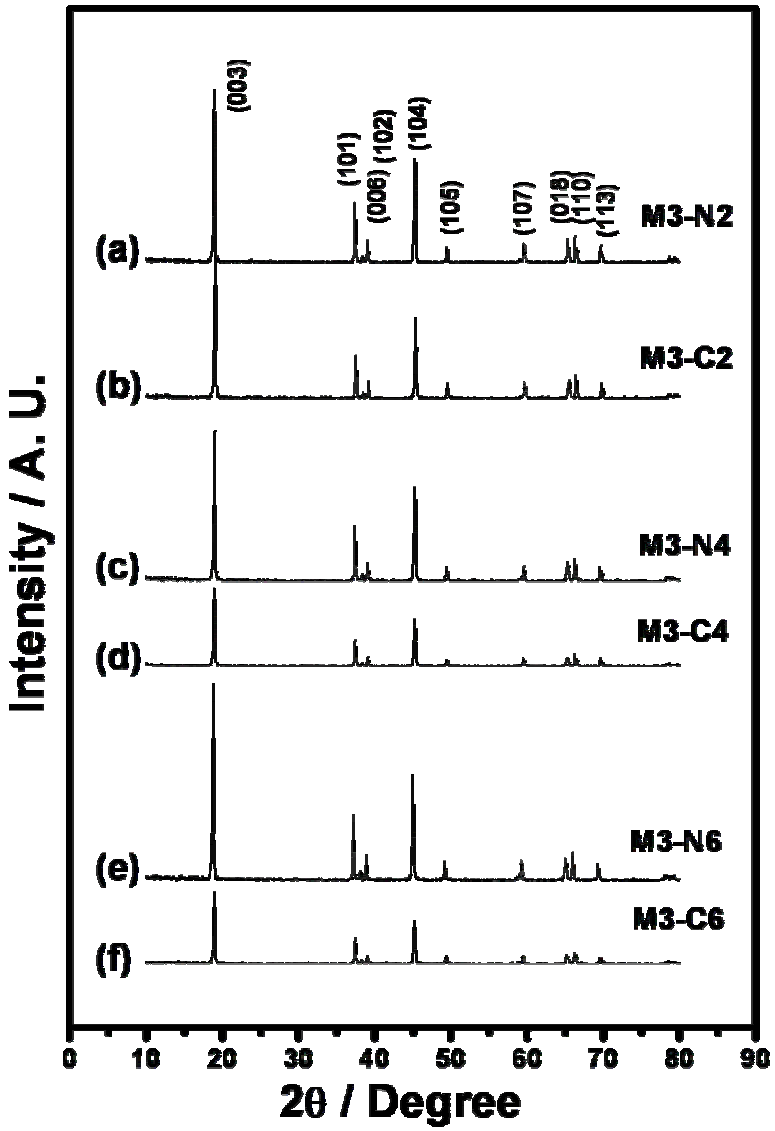

Figure 4.2 XRD patterns of (a), (c) and (e) were obtained from the doped $LiCoO_2$ and (b), (d) and (f) were obtained from the surface modified $LiCoO_2$.

Table 4.1 Chemical analysis, lattice parameter and specific surface area for the materials synthesized by different method

Sample	Chemical composition	Lattice parameters		*c*/*a*	Specific surface area ($m^2\ g^{-1}$)
		a (Å)	*c* (Å)		
$LiCoO_2$	$LiCoO_2$	2.810(2)	14.017(5)	4.988	–
M3-C2	$Li_{1.01}Ni_{0.01}Co_{0.96}Mn_{0.03}O_2$	2.816(1)	14.063(4)	4.994	1.33
M3-N2	$Li_{1.01}Ni_{0.01}Co_{0.96}Mn_{0.03}O_2$	2.818(2)	14.079(8)	4.996	1.23
M3-C4	$Li_{0.99}Ni_{0.05}Co_{0.88}Mn_{0.07}O_2$	2.821(1)	14.120(6)	5.002	3.29
M3-N4	$Li_{1.01}Ni_{0.06}Co_{0.87}Mn_{0.07}O_2$	2.823(2)	14.106(8)	4.996	2.39
M3-C6	$Li_{1.02}Ni_{0.08}Co_{0.81}Mn_{0.11}O_2$	2.823(1)	14.140(6)	5.008	3.33
M3-N6	$Li_{1.02}Ni_{0.09}Co_{0.80}Mn_{0.11}O_2$	2.826(1)	14.120(7)	4.997	2.02

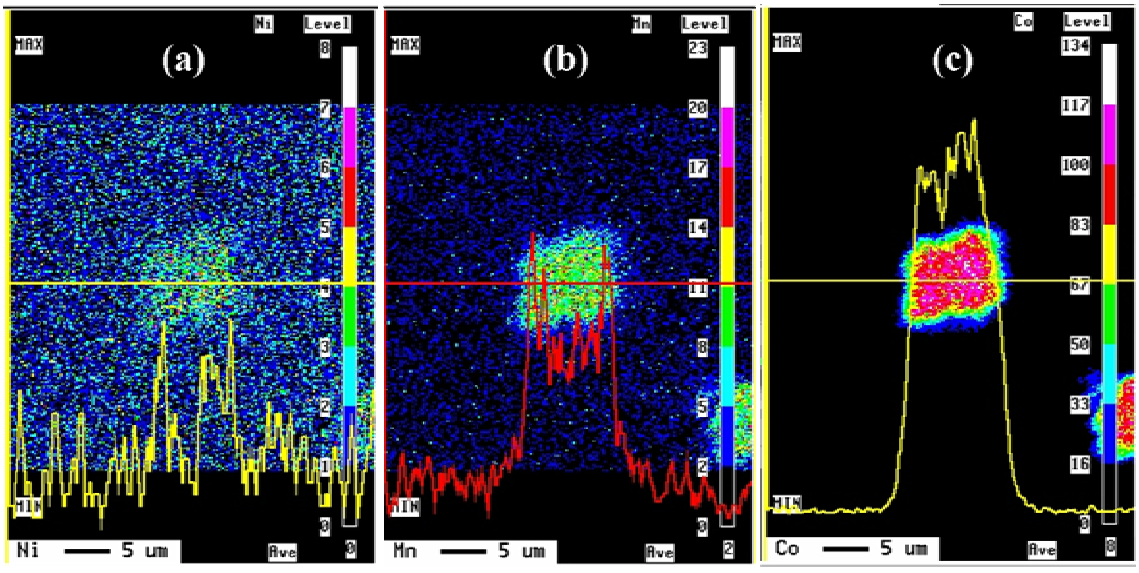

Figure 4.3 EPMA mapping of (a) Ni, (b) Mn and (c) Co ions in a single particle of the M3-C2 compound.

According to the Dahn et al. [14], increased substitution of nickel and manganese for the cobalt leads decrease in primary particle size. SEM observation was carried out in order to confirm morphology changes. Fig. 4.4 shows the SEM photographs of two groups. The primary particles of both groups (M3-C and M3-N) become smaller with increase in the Ni and Mn content. This phenomenon was also reported by Dahn et al. [14]. However, the primary particles of the M3-C group are smaller than those of the M3-N group. Therefore, I can deduce that the reason of the smaller primary particle size is due to the higher concentration of the Ni and Mn on the surface of the group M3-C. This is well agreed with results of XRD and EPMA experiments.

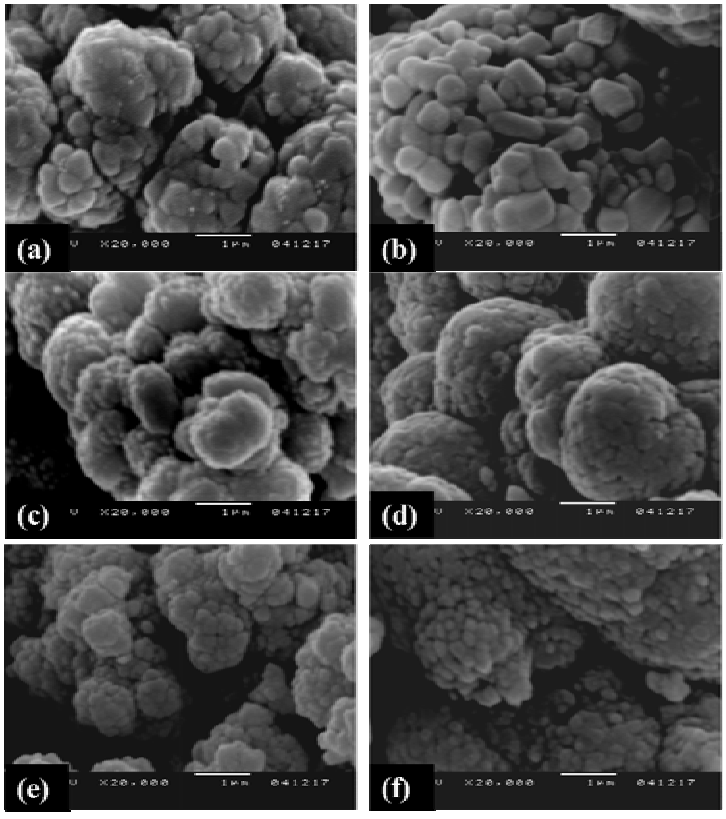

Figure 4.4 SEM images; (a) M3-C2, (c) M3-C4 and (e) M3-C6 are obtained from the surface modified $LiCoO_2$, and (b) M3-N2, (d) M3-N4 and (f) M3-N6 were obtained from the doped $LiCoO_2$.

Figure 4.5 shows initial charge/discharge curves of two groups between 2.8 and 4.4V with constant current of 80 mAh g^{-1}. The group M3-C delivers reversible capacity of about 167 mAh g^{-1} that is slightly higher than that of the group M3-N. The group, M3-C, also exhibits smaller irreversible capacity loss than those of the M3-N group. The cycle performances of all the samples are shown in Fig. 4.6. The sample M3-N2 could deliver 80.6 % of 5^{th} discharge capacity after 150 cycles and capacity retention was increased with increasing substituted amounts of the Ni and Mn, whereas the M3-N6 shows about 89 % of 5^{th} discharge capacity after 150 cycles. Whereas M3-C2 delivered about 90 % capacity retention ratio after 150 cycles. The capacity retention ratio was almost unchanged by increase in Ni and Mn content. This result indicates that surface treatment is excellent technique to improve cycling performance. The initial charge-discharge curve and the cycle performance of the M3-C2 and the M3-N2 in the cut voltage of 2.8 to 4.5 V were also given in the Fig. 4.5 (d) and 4.6 (d), respectively. The M3-C2 compound shows a slightly higher initial discharge capacity of 182.3 mAh g^{-1} than that of the M3-N2 (177.5 mAh g^{-1}) and better cycle stability. The retained discharge capacity of the M3-C2 and the M3-N2 were 91.5 % and 87.2 % of the initial discharge capacity, respectively. It is well known that the surface composition is important because the surface contacts with the electrolyte directly and electrochemical reaction of active material occurs at its surface. For the M3-C series, the surface of $LiCoO_2$ is covered uniformly with a Li-Mn-Ni-Co-O compound and it could be thought that it would prevent the direct contact of the $LiCoO_2$ core with electrolyte.

An increase in Ni and Mn amount is very helpful to increase the cycling performance, however it deteriorates rate capability. Fig. 4.7 shows rate capability of samples. The obtained rate capability decreased with increase in doping or coating

amount despite of higher specific surface area. Ni and Mn amount should be decreased in order to obtain higher rate capability. In this view point, therefore, coating method is excellent preparation route because it can give stable cycling performance without the deterioration of the rate capability by coating with small amount of nickel and manganese.

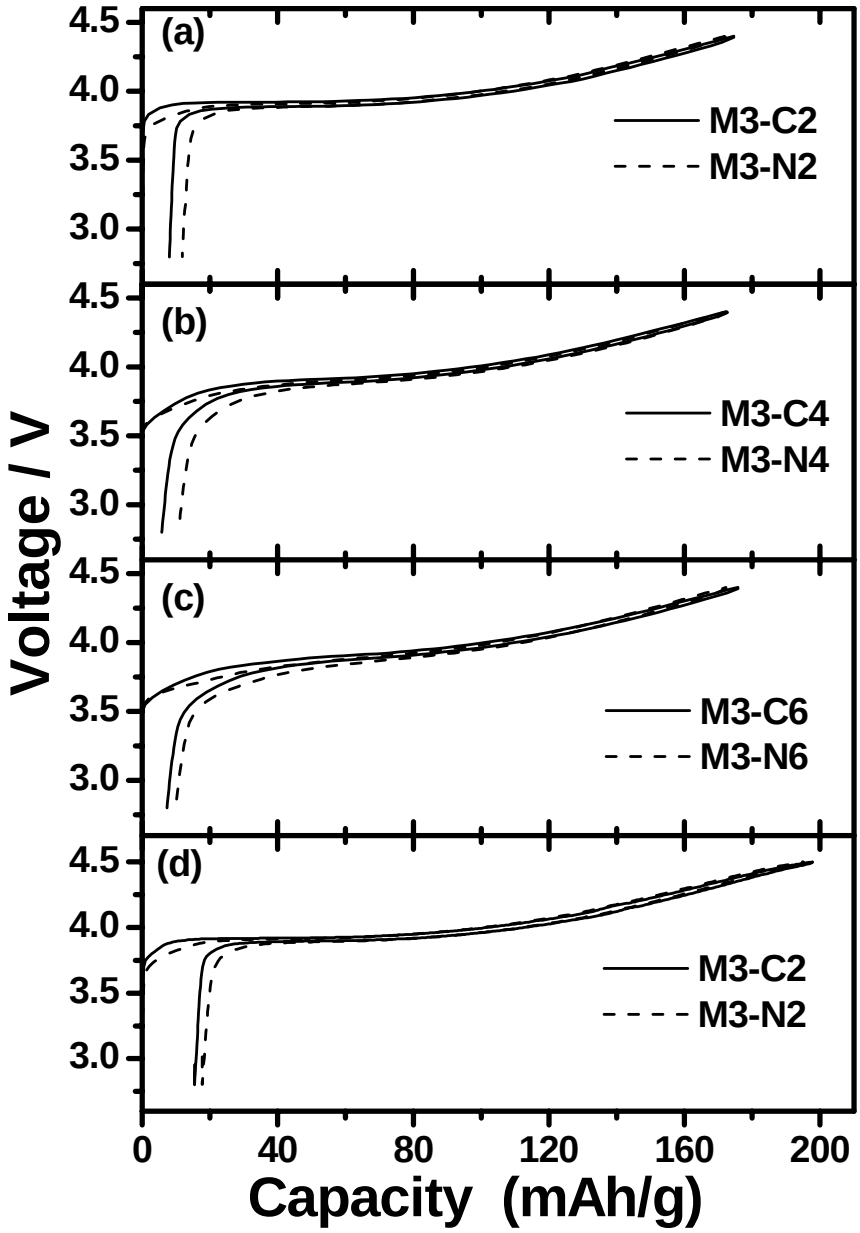

Figure 4.5 Initial charge-discharge curves of group the M3-C and M3-N operated in voltages 2.8- 4.4 V (a to c) and 2.8-4.5 V (d) at C/2 rate (80 mA g^{-1}).

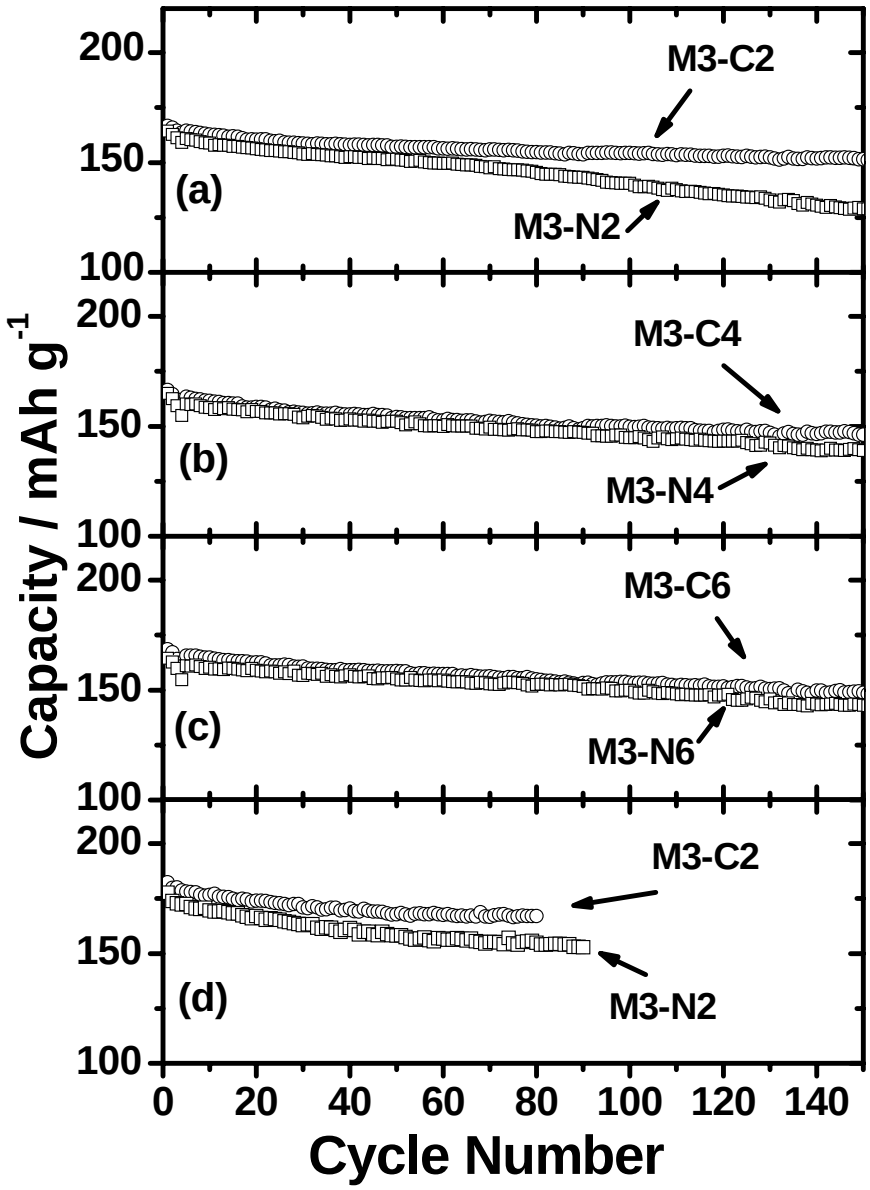

Figure 4.6 Cycle performance of group the M3-C and M3-N operated in voltages 2.8-4.4 V (a to c) and 2.8-4.5 V (d) at C/2 rate (80 mA g^{-1}).

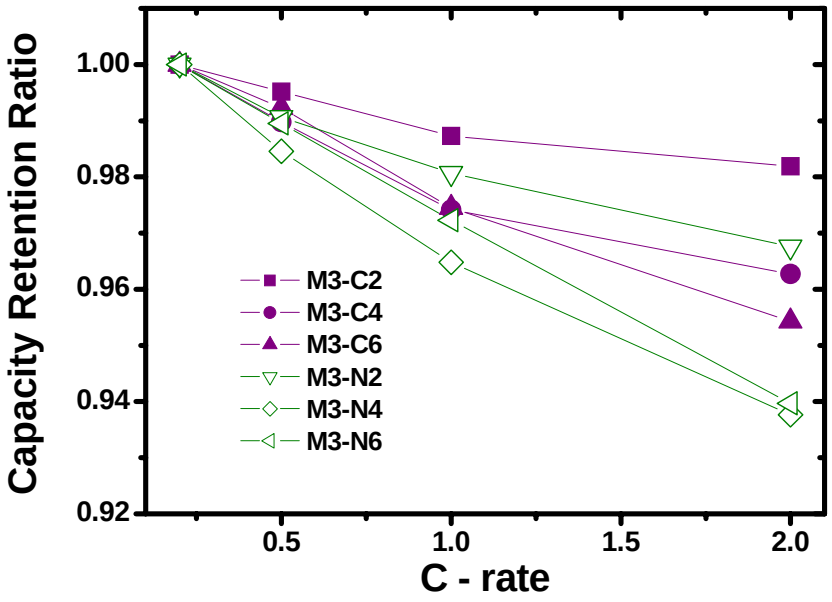

Figure 4.7 Rate capability for the samples in the voltage range 2.8 to 4.4V.

4.4 Conclusion

In this study, I have tried the preparation of Li[Ni, Mn]O_2 coated $LiCoO_2$ as one example to certify the possibility of co-precipitation technique as a novel surface modification method. I successfully synthesized Li[Ni, Mn]O_2 coated $LiCoO_2$ through this method. By comparing the two groups (M3-C and M3-N), I could find that the coated materials show a slightly higher initial discharge capacity with a lower irreversible capacity than the doped materials at the initial cycle. Furthermore, the coated materials exhibited better cycle stability than those of the doped compounds at each cut-off voltage of 4.4 and 4.5 V. These results suggest that the surface modification is better than the doping for the enhancement of the cycling performance of the cathode

material at a higher cut-off voltage. It is also confirmed that co-precipitation is very useful method to modify the surface of the cathode material. Here, I believe this method has more merits such as the easiness and the cost down to prepare variety of surface modified cathode materials and possibility to apply mass production.

References

[1] T. Ohzuku, and A. Ueda, *J. Electrochem. Soc.*, **141** (1994) 2972.

[2] Z. Wang, C. Wu, L. Liu, F. Wu, L. Chen, and X. Huang, *J. Electrochem. Soc*., **149** (2002) A466.

[3] Z. Chen, and J. R. Dahn, *Electrochim. Acta*, **49** (2004) 1079.

[4] M. Zou, M. Yoshio, S. Gopukumar, and J. Yamaki, *Electrochem. Solid-State Lett.*, **7** (2004) A176.

[5] Z. Chen, and J. R. Dahn, *Electrochem. Solid-State Lett.*, **5** (2002) A213.

[6] J. Cho, Y. T. Kim, and B. Park, *Angew. Chem., Int. Ed. Engl.*, **40** (2001) 3367.

[7] J. Cho, Y. J. Kim, and B. Park, *Chem. Mater.*, **12** (2000) 3788.

[8] J. Cho, Y. J. Kim, and B. Park, *Electrochem. Soc*., **148** (2001) A1110.

[9] Y. J. Kim, J. Cho, T.-J. Kim, and B. Park, *Electrochem Soc.*, **150** (2003) A1723.

[10] N. Yabuuchi, and T. Ohzuku, *J. Power Sources*, **119** (2003) 171.

[11] S. H. Park, C. S. Yoon, S. G. Kang, H.-S. Kim, S.-I. Moon, and Y.-K Sun, *Electrochim. Acta*, **49** (2004) 557.

[12] T. Cho, S. Park, and M. Yoshio, *Chem. Lett*., **33** (2004) 704.

[13] D. D. Macneil, Z. Lu, and J. R. Dahn, *J. Electrochem. Soc.*, **149** (2002) A1332.

[14] S. Jouanneau, D. D. Macneil, Z. Lu, S. D. Beattie, G. Murphy, and J. R. Dahn, *J. Electrochem. Soc*., **150** (2003) A1299.

Chapter 5

Enhancement of rate capability of a layered $LiMn_{1/2}Ni_{1/2}O_2$ cathode material by surface treatment with cobalt element

5.1 Background of our research

During past decay, many researchers have been intensively studied to find suitable alternative cathode materials (i.e., $LiMn_2O_4$[1-4], $LiNiO_2$[5-7], and $LiMnO_2$ [8,9]) for lithium ion secondary battery caused by drawbacks of lithium cobalt oxide such as high cost and toxicity of cobalt element. In recent year, a lot of attention has been paid to a nickel based layered $LiMn_{1/2}Ni_{1/2}O_2$, which is substitution in compound of $LiNiO_2$, $2Ni^{3+} = Ni^{2+} + Mn^{4+}$, as an alternative to $LiCoO_2$. Electrochemical redox process is occurred based on two electron reaction between Ni^{2+} and Ni^{4+} [10,11]. The cathode material show high reversible capacity of about 180 mAh g^{-1} in the voltage range between 2.5 and 4.5 V. Moreover, it shows very stable cycle performance due to the Mn^{4+}, which is electrochemically inactive, thus the manganese ion may provide structural stability by stable electronic configuration.

However, one of its drawbacks is lower rate capability due to lower electronic conductivity. On the other hand, it was reported that the $LiMn_{1/3}Ni_{1/3}Co_{1/3}O_2$, which is a solid solution between $LiMn_{1/2}Ni_{1/2}O_2$ and $LiCoO_2$, shows excellent battery performance, such as high rate capability, milder thermal stability and high reversible capacity. Although the cathode shows excellent battery performances, the higher price of the cathode prevent it from commercial use. In order to decrease price of the cathode, cobalt amount should be reduced. There are several reports for the dependence of rate capability of $Li[Mn_xCo_{1-2x}Ni_x]O_2$ solid solution on the Co amount. According to Sun et al. [12], rate capability increase linearly with increasing Co amount up to 30 % then almost constant with further increase of cobalt amount up to 50 %.

Therefore, I have tried to improve electrochemical performance of $LiMn_{1/2}Ni_{1/2}O_2$ by the addition of cobalt as small as possible. In our previous study [13],

I have introduced a new application of carbonate co-precipitation method as a surface modification technique and succeed to improve cycling performance of $LiCoO_2$ at high cut-off voltage of 4.4 or 4.5 V. Here, I try to apply carbonate co-precipitation method to improve electrochemical performance of $LiMn_{1/2}Ni_{1/2}O_2$ by analogous procedure. The main concept of our research is surface modification of $LiMn_{1/2}Ni_{1/2}O_2$ with $LiCoO_2$, which can give higher rate capability. Here, I report the structural and electrochemical performance of cathode materials prepared by carbonate co-precipitation method.

5.2 Experimental

In order to prepare surface modified $LiMn_{1/2}Ni_{1/2}O_2$, I firstly precipitated a transition metals carbonate powder, $Mn_{1/2}Ni_{1/2}CO_3$, using $MnSO_4 \cdot 4–5H_2O$, $NiSO_4 \cdot 6H_2O$ and Na_2CO_3. Then, the powder was coated by $CoCO_3$ through a precipitation route using $CoSO_4 \cdot 7H_2O$ and Na_2CO_3. The co-precipitated carbonate powders were pre-heated at 500 ^oC for 5 h in air. The carbonate powder converted to spinel compound by pre-heating. After pre-heating, I applied EDTA titration to decide exact amount of transition metal ions in the pre-heated powder. A stoichiometric amount of lithium hydroxide was mixed with the pre-heated powder and calcined at 900 ^oC for 15h in air in order to make surface modified $LiMn_{1/2}Ni_{1/2}O_2$ powder,.

X-ray diffraction data of the calcined powder were carefully collected in the 2θ range of 15 to 100° using Rigaku Rint 1000 diffractormeter using CuKα radiation. The lattice parameters of the calcined powders were calculated by profile fitting method using *Fullprof* software [15]. Scanning electron microscopy (SEM : JSM-5300E, JEOL, Japan) was carried out to observe the morphologies of the synthesized cathode material. The distribution of Mn, Ni and Co in a particle of cathode material were confirmed by

an electron probe micro analyzer (EPMA : JXA-8900RLS, JEOL, Japan) for the cross section of coated particle. X-ray photoelectron spectroscopy measurements were performed to get information on the surface modified $LiMn_{1/2}Ni_{1/2}O_2$ as a function of etching time.

The electrochemical characterizations were carried out using the CR-2032-type coin cell. Electrode were made by coating a slurry, which was prepared by mixing the cathode materials, acetylene black as a conducting additive and a polyvinylidene fluoride (PVdF) as a binder with a weight ratio of 90: 5: 5 in *N*-methyl-2-pyrrolidene (NMP), on an Al foil. The loading amount of active material was about 10 mg cm^{-2}. The cell was composed of the cathode, the lithium foil anode and 1M $LiPF_6$-EC/DMC (1:2 in volume) electrolyte. The electrochemical cycling tests were performed at room temperature.

5.3 Results and discussions

Figure 5.1 shows XRD patterns of bare and surface modified $LiMn_{1/2}Ni_{1/2}O_2$ with 5 % and 15 % cobalt. The XRD pattern of $LiMn_{1/3}Ni_{1/3}Co_{1/3}O_2$, reference material, is also presented in the Fig. 5.1. Hereafter I refer the bare $LiMn_{1/2}Ni_{1/2}O_2$, surface treated $LiMn_{1/2}Ni_{1/2}O_2$ with 5 % and 15 % of Co to B-$LiMn_{1/2}Ni_{1/2}O_2$, C5-$LiMn_{1/2}Ni_{1/2}O_2$ and C15-$LiMn_{1/2}Ni_{1/2}O_2$, respectively.

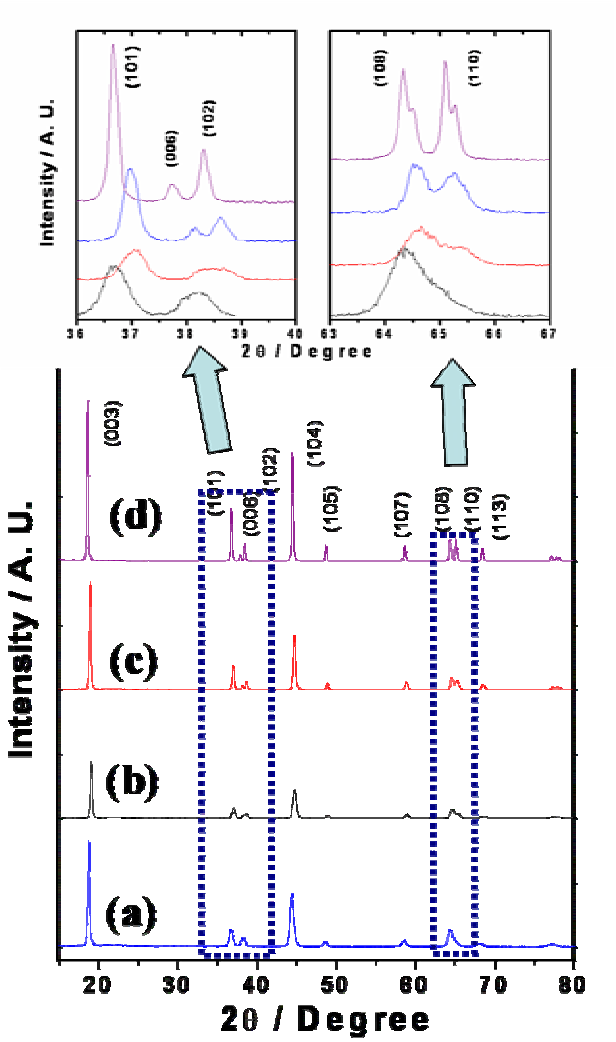

Figure 5.1 XRD patterns of (a) B-$LiMn_{1/2}Ni_{1/2}O_2$, (b) C5-$LiMn_{1/2}Ni_{1/2}O_2$ (c) C15-$LiMn_{1/2}Ni_{1/2}O_2$ and (d) $LiMn_{1/3}Ni_{1/3}Co_{1/3}O_2$.

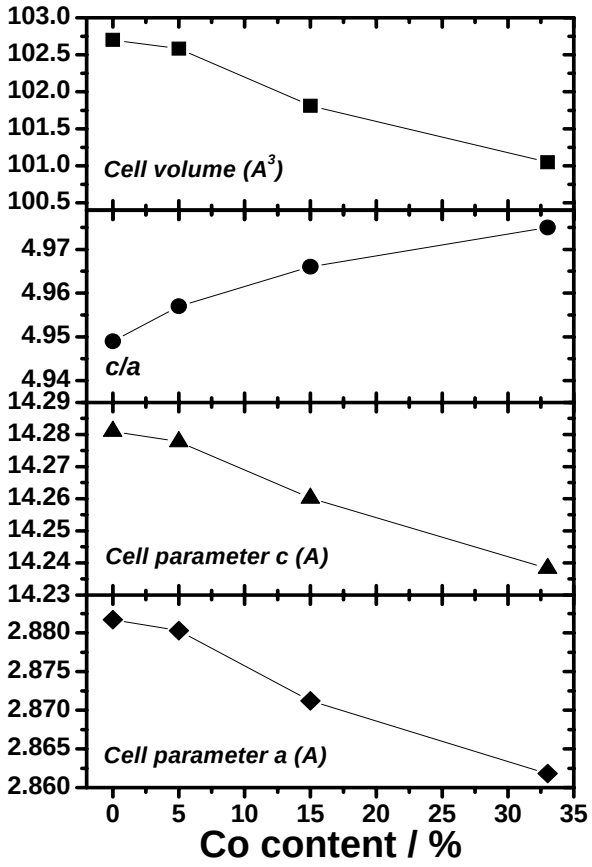

Figure 5.2 Structural parameters of the cathode materials.

The X-ray diffraction patterns can be indexed based on the hexagonal α–$NaFeO_2$ structure with space group $R\bar{3}m$. The XRD pattern revealed that these materials have typical hexagonal structure.

The unit cell parameter for the cathode materials were calculated by profile refinement method using Fullprof software and the results were given in Figure 5.2. On increasing of cobalt amount in the compounds, the unit cell parameter *a* and *c* were gradually decreased. The decrease of unit cell parameters can be ascribed by difference in ionic radius between Ni^{2+} (0.69 Å) and Co^{3+} (0.545 Å) [16].

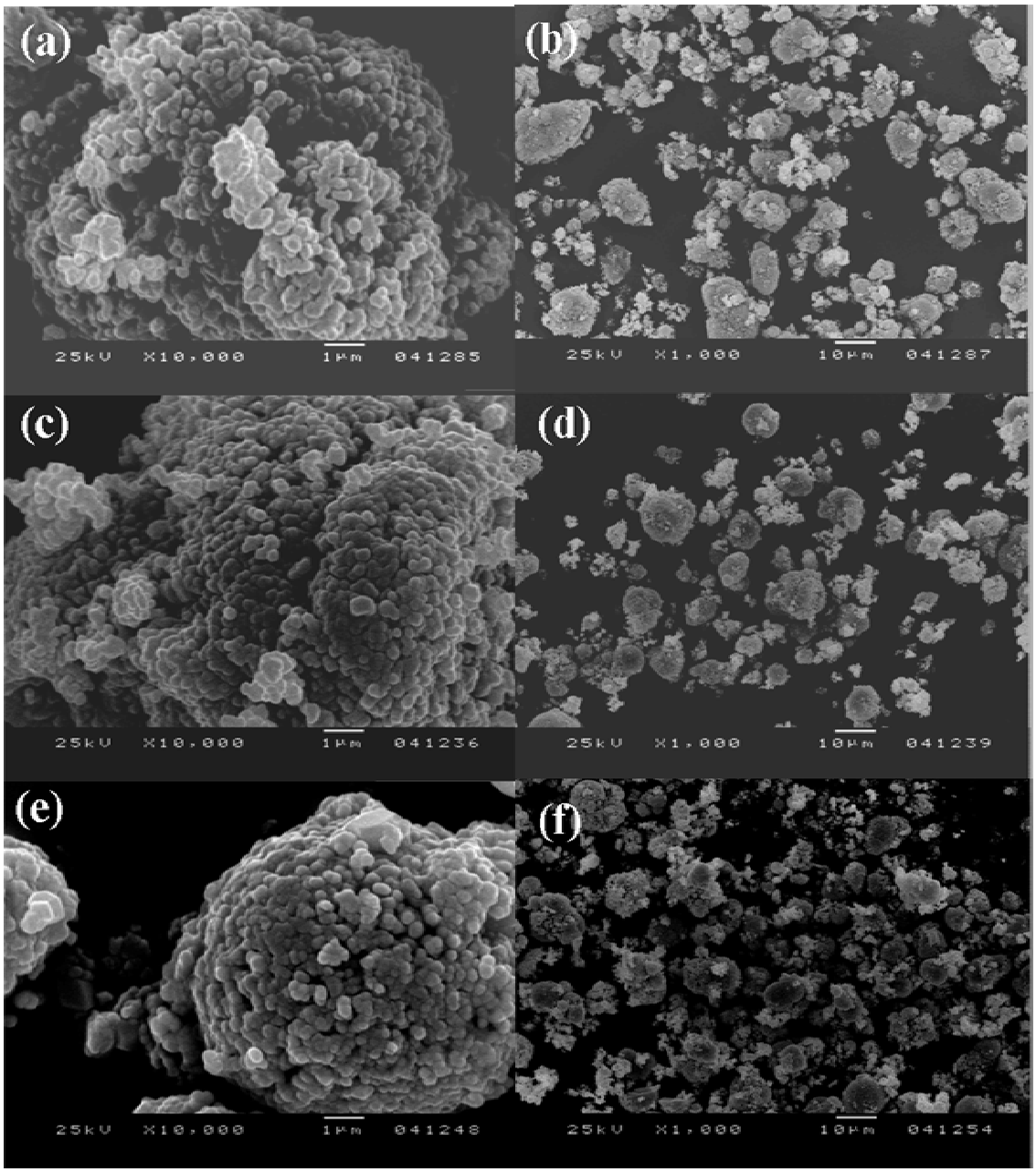

Figure 5.3 SEM photographs of B-$LiMn_{1/2}Ni_{1/2}O_2$ (a and b), C5- $LiMn_{1/2}Ni_{1/2}O_2$ (c and d) and C15- $LiMn_{1/2}Ni_{1/2}O_2$ (e and f).

It is well known that rate capability is affected strongly by particle size and morphology. Thus morphologies of the cathode materials were confirmed by SEM observation at different magnification. Figure 5.3 shows morphologies of cathode materials. The three samples show similar primary particle size of less than 0.5 μm. The secondary particle distribution in each samples are also almost same. Therefore, I believe that the effect of particle distribution on rate capability is negligible in this experiment.

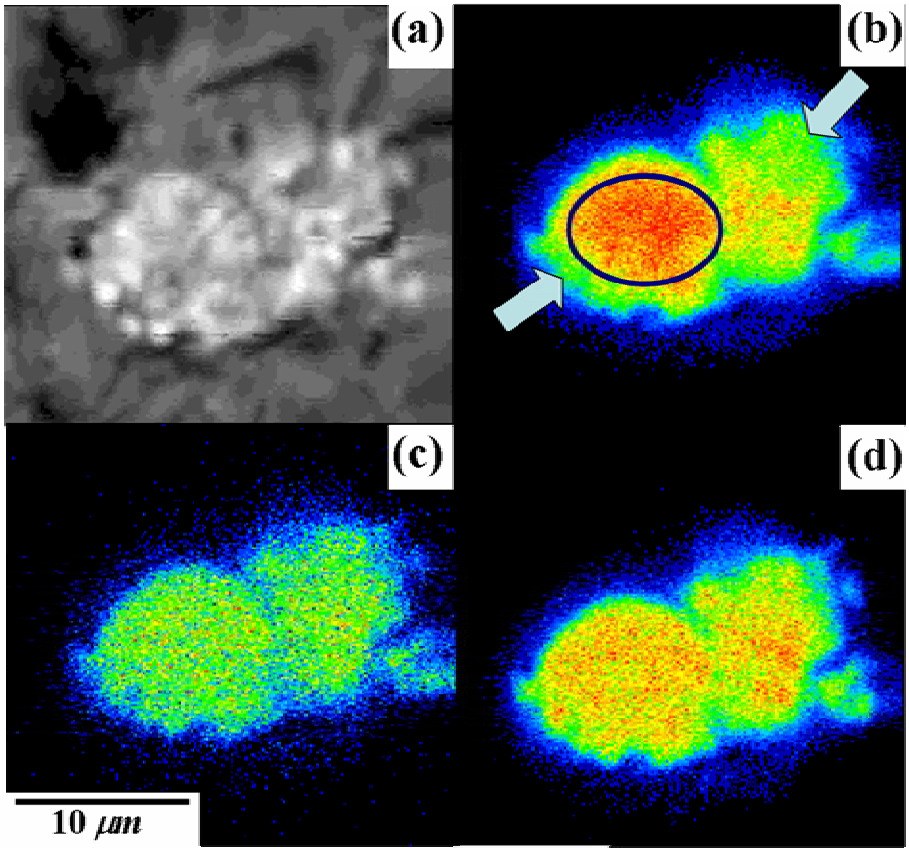

Figure 5.4 (a) SEM image of cross section and EPMA mapping of (b) Mn, (c) Ni and (d) Co ions in a particle of the C15-$LiMn_{1/2}Ni_{1/2}O_2$.

In order to investigate distribution of cobalt, manganese and nickel on the surface of the modified $LiMn_{1/2}Ni_{1/2}O_2$, I carried out EPMA experiment for the polished cross section of particle of cathode material coated with 15 % cobalt and result was presented in the Fig. 5.4. I obtained unexpected result, i.e. I could confirm that cobalt ions are not observed only on the surface but whole particle. This EPMA result indicates that the cobalt ions on the surface of precursor particle seem to be diffused into the core of the particle through calcination at high temperature (900 ^oC) for 15h. Moreover, the nickel and manganese distribution are quite different as shown in Fig. 5.4 (b) and (d). The Fig. 5.4 (d) shows homogeneous distribution of nickel ion whereas manganese ions are less homogeneous than that of nickel ions. The arrow marks in Fig. 5.4 (b) indicate low concentration of Mn ions and circle mark indicates high concentration of Mn ions. From this EPMA surface analysis of the cross section, I could deduce that there are two different phases of Li-Mn-Ni-Co-O solid solution, i.e. one is nickel rich and the other is manganese rich phase and the manganese rich solid solution is likely to be surrounded by nickel rich phase.

I applied XPS analysis in order to confirm the assumption obtained by EPMA analysis. The XPS spectroscopy was carried out using MgKα radiation in order to avoid overlapping of XPS profile between Ni Äuger spectrum and Mn and Co $2p_{3/2}$ spectra. Fig. 5.5 (a) and (b) show the XPS spectra and variation of atomic ratio as a function of etching time, respectively. At the beginning, higher nickel concentration was observed. The atomic ratios of Mn, Ni and Co were 36, 4.5 and 59 %, respectively. The manganese ion concentration is rapidly increased up to about 47 % with increasing etching time. On the other hand, nickel concentration was getting lower with increasing

of etching time whereas the concentration of Co was almost unchanged during XPS analysis. Therefore, this result well support the assumption obtained by EPMA analysis.

Electrochemical charge-discharge experiments were carried out at room temperature in the voltage range 2.8 to 4.5 V with applying current density of 40 mA g^{-1}. Fig. 5.6 shows first charge/discharge curves and Fig. 5.7 shows cycling performance for the all samples as a function of cycle number.

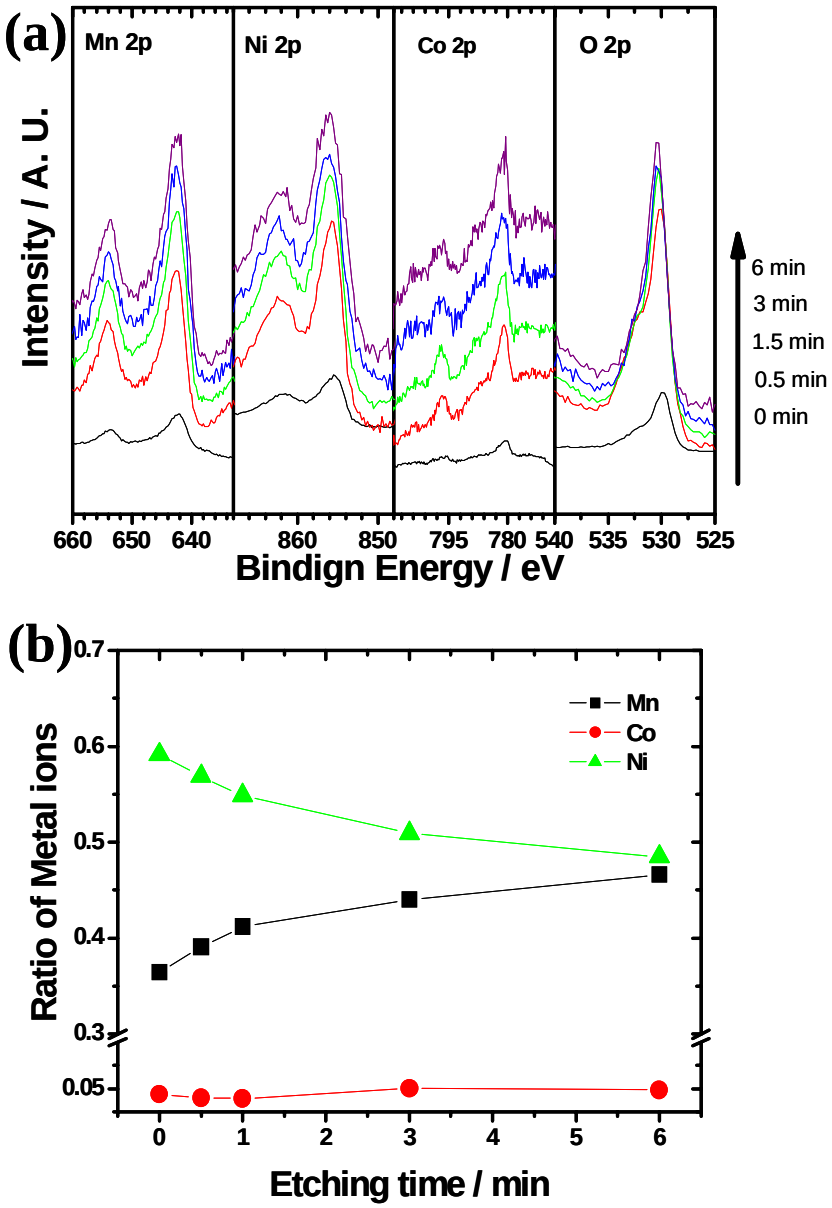

Figure 5.5 (a) XPS spectra for Mn, Ni, Co and O and (b) related atomic ratio for the C15-$LiMn_{1/2}Ni_{1/2}O_2$.

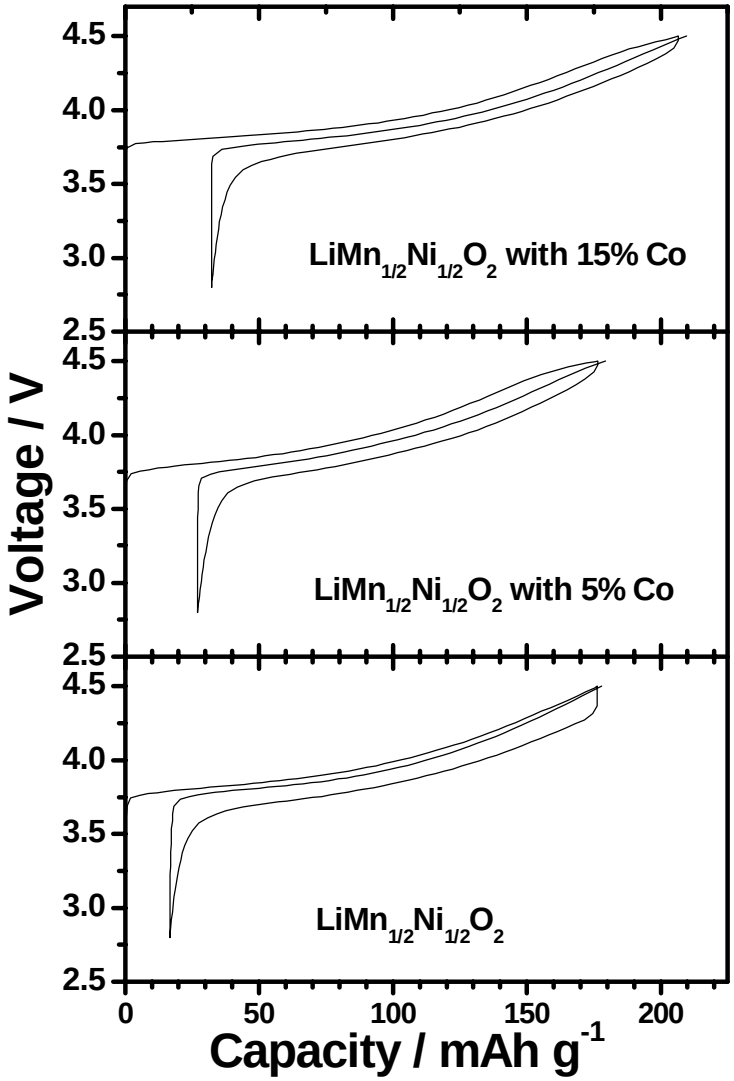

Figure 5.6 Initial charge discharge curves for the cathode materials.

All the samples show monotonous voltage increase up to 4.5 V. The C15-$LiMn_{1/2}Ni_{1/2}O_2$ delivered the highest charge and discharge capacity of 203.2 mAh g^{-1} and 173.4 mAh g^{-1}, respectively, at the initial cycle as well as excellent cycle performance. The cathode retained 93.5 % of initial discharge capacity after 75 cycles. B-$LiMn_{1/2}Ni_{1/2}O_2$ delivers 159.5 mAh g^{-1} as initial discharge capacity and 76.2% of the

capacity was obtained after 60 cycles. By surface treatment with 5 % of cobalt, capacity retention ratio was greatly increased up to 90.2 % after 60 cycles. The increases of reversible capacity and cycle stability are due probably to increase of structural integrity as shown in the XRD analysis.

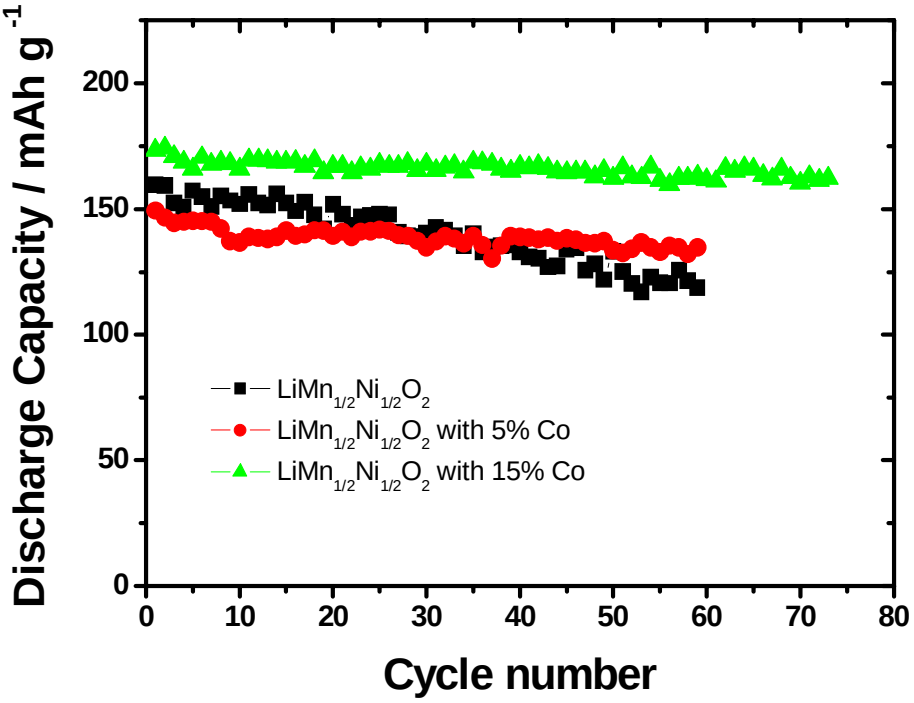

Figure 5.7 Discharge capacities as a function of cycle numbers.

In order to investigate the rate capability of the cathode materials, I applied constant current of 34 mA g^{-1} (0.2 C) for charging and various current densities of 0.2, 0.5, 1, 2 and 4 C for discharging in the voltage range of 2.8 to 4.5 V and data are presented in Fig. 5.8. The C rates were calculated using 170 mA h g^{-1} as a capacity. B-$LiMn_{1/2}Ni_{1/2}O_2$ delivered 165 mAh g^{-1} at 0.2 C (34 mA g^{-1}). With increasing current density, the obtained discharge capacity was gradually decreased thus only 65.4 % of

initial capacity was retained at 4 C (680 mA g^{-1}). The rate capability was greatly increased in C5-$LiMn_{1/2}Ni_{1/2}O_2$.

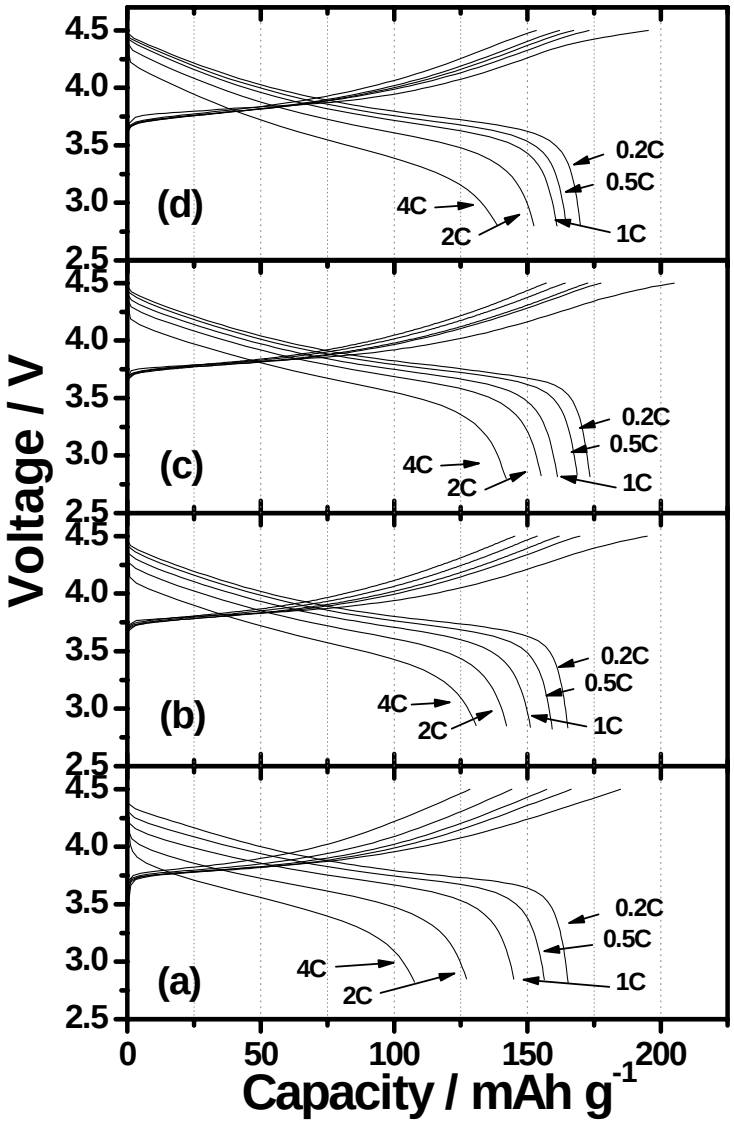

Figure 5.8 Rate capability for the (a) $LiMn_{1/2}Ni_{1/2}O_2$, (b) C5-$LiMn_{1/2}Ni_{1/2}O_2$, (c) C15-$LiMn_{1/2}Ni_{1/2}O_2$ and (d) $LiMn_{1/3}Ni_{1/3}Co_{1/3}O_2$.

The C5-$LiMn_{1/2}Ni_{1/2}O_2$ delivered 165 mAh g^{-1} at 0.2 C and it showed about 83 % of initial capacity at 4 C. For the C15-$LiMn_{1/2}Ni_{1/2}O_2$ and $LiMn_{x/2}Ni_{x/2}Co_{1-x}O_2$ (x

= 2/3), they delivered 82.1 and 81.7 % of initial discharge capacity at 4 C, respectively. This result is quite surprise because, according to previously reported studies [17], more than 20 % of cobalt have to be doped to get similar rate capability to $LiMn_{1/3}Ni_{1/3}Co_{1/3}O_2$ cathode material. To our knowledge, it is the first time to show the excellent rate capability with only 5 % of cobalt. The high rate capability of the surface treated $LiMn_{1/2}Ni_{1/2}O_2$ without difference of particle size may be enhancement of electron conductivity by surface treatment with cobalt. Outer nickel rich Li-Mn-Ni-Co-O seems to play an important role to enhance the rate capability of cobalt treated $LiMn_{1/2}Ni_{1/2}O_2$.

A GITT (Galvanostatic intermittent Titration Technique) was carried out in order to investigate lithium diffusion coefficient for the cathode materials. Fig. 5.9 shows the GITT curves for the synthesized cathode material as a function of time at room temperature. For GITT measurement, the cells were charged at a constant current density of 10 mA g^{-1} for a capacity interval of 15 mAh g^{-1}. The cells were then allowed relaxing to their open circuit voltage. The procedure was repeated for the cut-off voltage of 4.5 V and 2.8 V. The lithium diffusion coefficient for the cathode materials were determined by using the formula [17,18] as follow:

$$D_{Li}=\frac{4}{\pi\tau}\left(\frac{m_B V_m}{M_B A}\right)^2\left(\frac{\Delta E_s}{\Delta E_\tau}\right) \qquad \left(\tau << L^2/D_{Li}\right) \tag{5.3.1}$$

Where V_m is the molar volume of the compound, M_B and m_B are its molecular weight and mass, respectively, A is the total contact area (surface area of electrode) between the electrolyte and the electrode and L is thickness of the electrode. ΔE_τ and ΔE_s (see inset

of Fig. 5.9) are total transient change in cell voltage and the change in the steady-state voltage during the respective single titration.

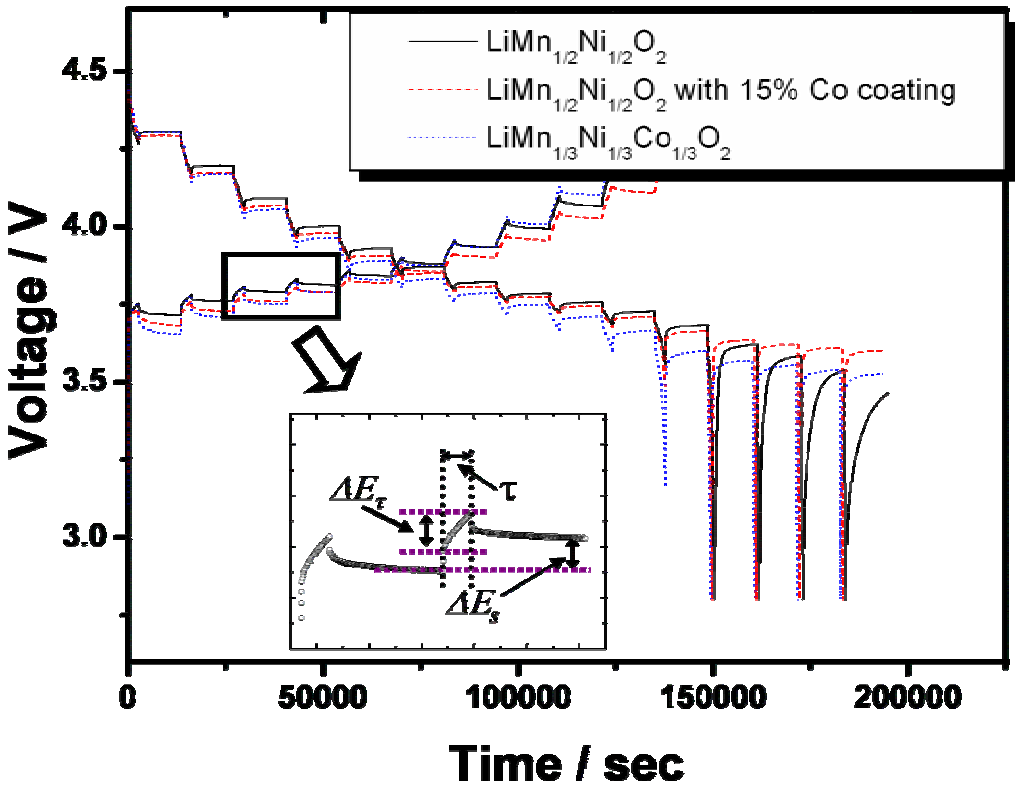

Figure 5.9 GITT curves for the cathode materials.

The lithium diffusion coefficient (D_{Li}) as a function of lithium extract amount for the cathode materials are given in the Fig. 5.10 (a) and (b). Fig. 5.10 (a) shows lithium diffusion coefficients for the cathode materials during charge. At the beginning, the $LiMn_{1/2}Ni_{1/2}O_2$ show higher D_{Li} than others. With increase of extraction amount of lithium more than 0.6 mol from host, the D_{Li} of the $LiMn_{1/2}Ni_{1/2}O_2$ with surface treated by 15% of cobalt shows higher Li diffusivity than other cathode materials. Moreover, the cathode shows slightly higher Li diffusivity during lithium insertion to the host

structure. Therefore, it could be thought that surface treated with cobalt could increase lithium diffusion coefficient as well as improve of electron conductivity.

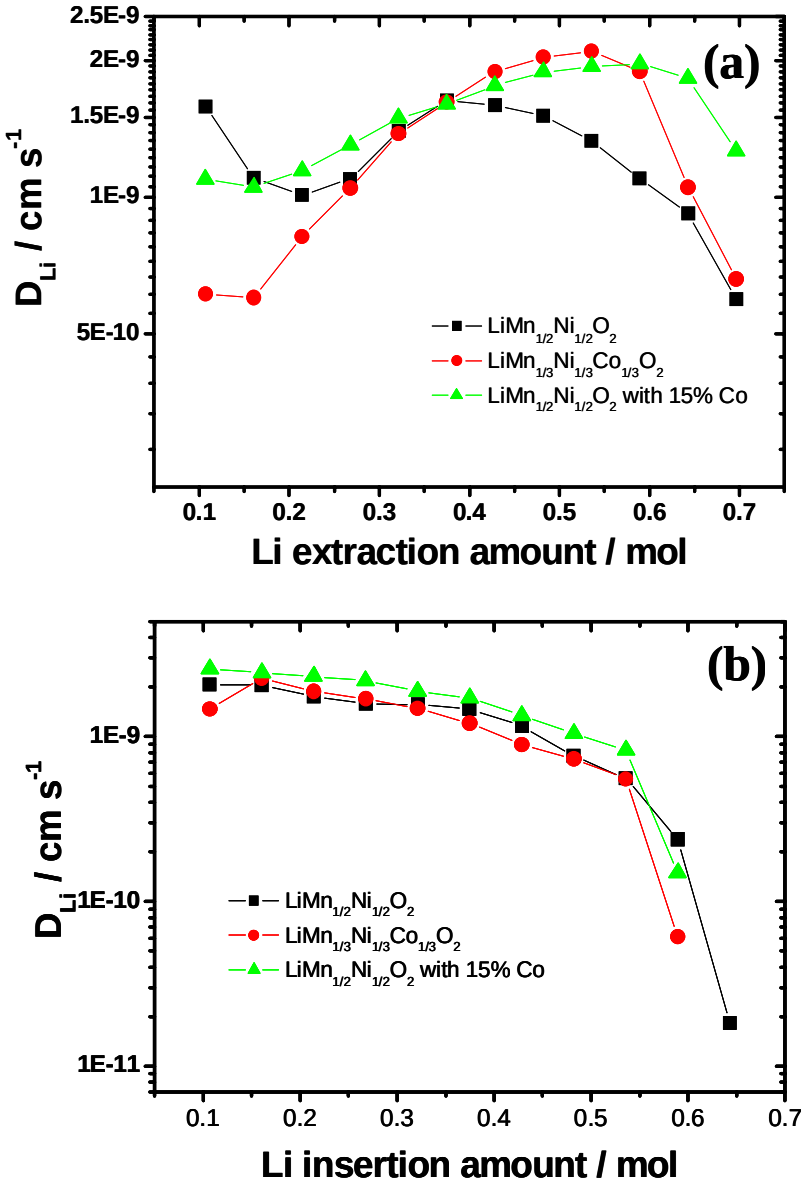

Figure 5.10 Variation of diffusion coefficient, D_{Li}, as a function of extraction/insertion of lithium form/to cathode materials during first (a) charge and (b) discharge.

5.4 Conclusion

Surface modified $LiMn_{1/2}Ni_{1/2}O_2$ with cobalt was synthesized by carbonate co-precipitation process. XRD analysis showed that layered cathode materials are successfully synthesized and structural integrity was increased with increasing cobalt amount, whereas primary particle size and secondary particle distribution were unchanged with increasing cobalt amount. By surface analysis of the cross section with EPMA, it was found that two different phases of Li-Mn-Ni-Co-O solid solution, i.e. one is nickel rich and the other is manganese rich phase were co-exist in a particle of cathode material. The manganese rich phase is likely to be surrounded by nickel rich phase. It was confirmed that surface treatment by cobalt is more effective for rate capability than doping of cobalt ingredient.

References

[1]. Y. Xia, Y. Zhou, and M. Yoshio, *J. Electrochem. Soc.*, **144** (1997) 2593.

[2]. J. M. Tarascon, and D. Guyomard, *J. Electrochem. Soc*., **138** (1991) 2864.

[3]. T. Ohzuku, M. Kitagawa, and T. Hirai, *J. Electrochem. Soc*., **137** (1990) 769.

[4]. M. M. Thackeray, A. de Kock, M. H. Rossouw, and D. Liles, *J. Electrochem. Soc*., **139** (1992) 363.

[5]. C. Delmas, J. P. Peres, A. Rougier, A. Demourgues, F. Iill, A. Chadwick, M. Broussely, F. Perton, Ph. Biensan, and P. Willmann, *J. Power Sources*, **68** (1997) 120.

[6]. J. R. Dahn, E. W. Fuller, M. Obrovac, and U. VonSacken, *Solid State Ionics*, **69** (1994) 265.

[7]. A. Rougier, P. Gravereau, and C. Delmas, *J. Electrochem. Soc*., **143** (1996) 1168.

[8]. W. D. Johnston, and R. R. Keikes, *J. Am. Chem. Soc*., **78** (1956) 3255.

[9]. R. Armstrong, and P. G. Bruce, *Nature,* (1996) 381.

[10]. K. M. Shaju, G. V. Subba Rao, and B. V. R. Chowdari, *Electrochim. Acta*, **49** (2004) 1565.

[11]. W.-S. Yoon, M. Balasubramanian, X.-Q. Yang, Z. Fu, D.A. Fisher, and J. McBreen, *J. Electrochem. Soc*., **151** (2004) A246.

[12]. Y. Sun, C. Ouyang, Z. Wang, X. Huang, and L. Chen., *J. Electrochem. Soc.*, **151** (2004) A504.

[13]. S. M. Park, T. H. Cho, Y. M. Kim, and M. Yoshio, *Electrochem. Solid–State Lett.*, **8** (2005) A299.

[14]. T. Roisnel, and J. Rodriguez-Carjaval, *Fullporf Manual*, Institut Laue-Langevin, Grnoble (2000).

[15]. D. Li, H. Noguchi, and M. Yoshio, *Electrochim. Acta,* **50** (2004) 425.

[16]. D.D. Macneil, Z. Lu, and J.R. Dahn, *J. Electrochem. Soc.,* **149**, A1332 (2002)

[17]. K. M. Shaju, G. V. Subba Rao, and B. V. R. Chowdari, *J. Electrochem. Soc.*, **150** (2003) A1.

[18]. K. M. Shaju, G. V. Subba Rao, and B. V. R. Chowdari, *Electrochim. Acta,* **48** (2003) 2691.

Chapter 6

General conclusions

General Conclusion

The practical capacity of lithium ion battery has been increased gradually by intensive research for both cathode and anode materials. However, the newly developed multi functional portable devices need more volumetric energy density over $LiCoO_2$, major cathode material, moreover cobalt price became more expensive nowadays.

A solid solution $LiMn_{1/2}Ni_{1/2}O_2$-$LiCoO_2$ was introduced as an alternative cathode material. But it suffers from difficulty of preparation. Therefore, this thesis is focused on development of a novel preparation technique to overcome the drawback. I have proposed carbonate co-precipitation method as a solution of drawback and applied the process as surface modification technique to enhance electrochemical performance of the cathode materials. This research contributes as follows:

1) It was confirmed that the layered $LiMn_{1/2}Ni_{1/2}O_2$ cathode materials were successfully synthesized by carbonate co-precipitation process by mean of XRD, SEM-EDX and XPS spectroscopy. In the cathode material, Ni and Mn are homogeneously distributed in the cathode material with the valence state of 2+ and 4+, respectively. Temperature range between 850 ^oC and 900 ^oC is determined to be proper calcination temperature. The sample prepared at 850 ^oC shows the highest discharge capacity as well as the highest rate capability due to higher structural integrity and larger specific surface area. The XRD experiment and SEM observation revels that structural integrity and morphology of the cathode materials synthesized by carbonate method depends slightly on the lithium sources. Sample prepared from lithium nitrate delivered better structural integrity and homogeneous particle distribution than those from lithium

hydroxide and lithium carbonate.

2) By applying the carbonate co-precipitation, The layered $Li[Ni_{1/3}Mn_{1/3}Co_{1/3}]O_2$ cathode material with spherical particle shape was successfully synthesized even at low temperature of 750 ^oC. In this study I could control morphology of particles using the co-precipitation process. By means of XRD analysis, it was confirmed that all the materials show similar hexagonal ordering despite of different calcinations temperature. From electrochemical experiments, it can be concluded that 800 ^oC is an optimal calcination temperature in this experiment and the rate capability of these materials depended on not the surface area (primary particle size) but diffusion rate of Li in particle.

3) I have introduced a new concept of surface modification by applying carbonate co-precipitation. In this study, I have selected the $LiCoO_2$ and tried to modify its surface by $LiNi_{1/2}Mn_{1/2}O_2$ as one example to certify the possibility of co-precipitation as a novel surface modification method. I successfully synthesized $LiNi_{1/2}Mn_{1/2}O_2$ coated $LiCoO_2$ through the method. The coated materials exhibited better cycle stability than that of the doped compounds at each cut-off voltage of 4.4 and 4.5 V. These results suggest that the surface modification is better than the doping to enhance the cycling performance of the cathode material at a higher cut-off voltage and co-precipitation is very useful method to modify the surface of the cathode material.

4) Surface modification technique, carbonate co-precipitation, has been applied to enhance rate capability of $LiMn_{1/2}Ni_{1/2}O_2$. XRD analysis showed that layered cathode

materials were successfully synthesized and structural integrity was increased with increasing cobalt amount. From the EPMA surface analysis of the cross section, it was found that two different phases of Li-Mn-Ni-Co-O solid solution, i.e., nickel rich and manganese rich phase, were co-exist in a particle of cathode material, and the manganese rich solid solution is likely to be surrounded by nickel rich phase. It also confirmed by XPS analysis. From the rate capability test, it was confirmed that surface treatment by cobalt is more effective than doping of cobalt ingredient.

Appendix

Analytical Techniques.

A.1. Analytical Techniques

In order to understand characteristics of the as-prepared powders and phenomena that occur during charge and discharge process in batteries, different kinds of analysis techniques, such as, physical, physicochemical, chemical methods, have been used to examine surface and bulk composition, crystallinity, etc..

Some of them, used for our study, will be presented briefly hereafter.

A.1.1. X-ray Powder Diffraction

An X-ray powder diffraction pattern is a set of lines or peaks, each of different intensity and position (d-spacing or Bragg angle, θ), on either a strip of photographic film or on a length of chart paper. For a given substance, the line positions are essentially fixed and are characteristic of that substance. The intensities may vary somewhat from sample to sample, depending on the method of sample preparation and the instrumental conditions. For identification purposes, principal note is taken of line positions together with a semi-quantitative consideration of intensities. Some applications of X-ray diffraction are now given.

A.1.1.1. Phase identification

Each crystalline substance has its own characteristic powder diffraction pattern which may be used for its identification. Standard patterns are given in the Powder Diffraction File (known as the JCPDS File or formerly, as the ASTM File). T

he inorganic section of the File now contains over 35,000 entries and is increasi ng at the rate of about 2,000 per year. The file also contains a section for orga nic compounds.

A.1.1.2. Determination of Accurate Unit Cell Parameters

The positions (d-spacings) of the lines in a powder pattern are governed by the values of the unit cell parameters (a, b, c, α, β, γ). Unit cell lattice parameters are normally determined by single crystal methods but the values obtained are of ten accurate to only two or three significant figures. More accurate cell paramete rs may be obtained from the powder pattern, provided the various lines have bee n assigned Miller indices *hkl* and their positions have been measured accurately. Using a least square minimization procedure, unit cell parameters accurate to for or fine significant figures may usually be obtained. Accurate unit cell parameter are particularly useful (a) for enabling complex powder patterns to be indexed, (b) for studying the effects of composition on cell parameters and (c) for measur ing thermal expansion coefficients.

A.1.2. Rietveld Refinement Method

A.1.2.1. General

Materials are essential to our technological society: semiconductors in the electronic

industry, zeolites as catalysts in the petrochemical industry, ceramics in medicine and engineering, proteins in biochemistry and, possibly in the future, high-temperature superconductors in electrical engineering.

In order to understand the properties of these materials and to improve them, the atomic structure has to be known. An effective way to do this is by means of diffraction techniques using neutrons from nuclear reactors and particle accelerators or X-rays from X-ray tubes and synchrotrons. The single crystal diffraction technique, using relatively large crystals of the material, gives a set of separate data from which the structure can be obtained.

However, most materials of technical interest cannot grow large crystals, so one has to resort to the powder diffraction technique using material in the form of very small crystallites. The drawback of this conventional powder method is that the data grossly overlap, thereby preventing proper determination of the structure. Between 1964 and 1966 at the Reactor Centre Netherlands in Petten, the Netherlands, Dr. Rietveld developed the "*Rietveld Method*" which creates an effective separation of these overlapping data, thereby allowing an accurate determination of the structure. The method was first reported by him at the IUCr Congress in Moscow (1966).

It has been so successful that nowadays the structure of materials, in the form of powders, is routinely being determined, nearly as accurately as the results obtained by single crystal diffraction techniques. The method is widely used, resulting yearly in more than a thousand scientific papers applying it.

A.1.2.2. History and the Acceptance of the Rietveld Method

The method was first reported at the seventh Congress of the IUCr in Moscow in 1966 [1]. The response was slight, or, rather, non-existent, and it was not until the full implementation of the method was published [2], that reactions came. At this time, the method was mainly used to refine structures from data obtained by fixed wavelength neutron diffraction; a total of 172 structures were refined in this way before 1977 [3]. In the previously mentioned paper [2], it had been suggested that the method could also be applied to X-ray data, but it was not until 1977 that the method became generally accepted for X-ray as well as neutron powder diffraction [4], first with fixed wavelength and then also with fixed angle (energy dispersive data). This is reflected in an increasing number of citations to the original papers [2,5] as published in the Science Citation Index. Figure A.1 shows the number of citations between the years 1967 and 1994.

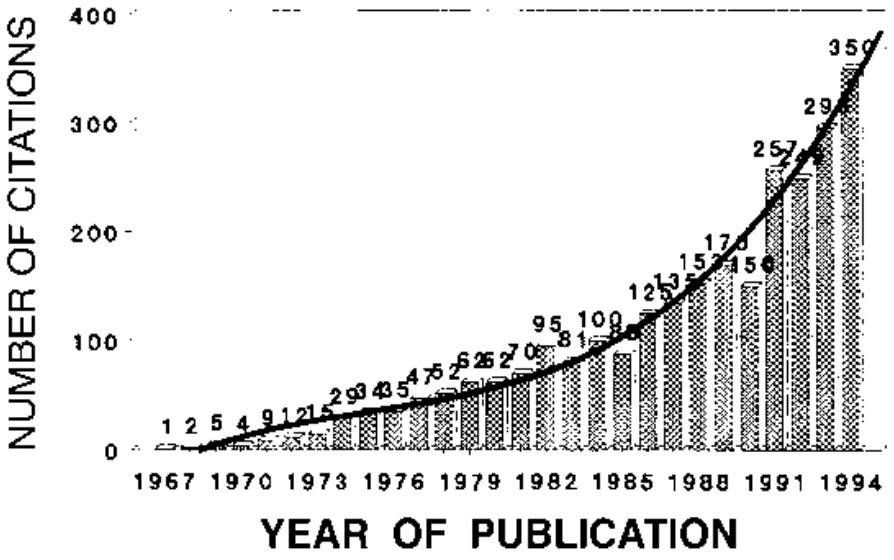

Fig. A.1. Number of publications, in the Science Citation Index, citing as reference the original papers (Rietveld 1967 [5], 1969 [2]) on the Rietveld method or having the name Rietveld in their title.

In the period January 1987 to May 1989 a total of 341 papers were published with reference to or using the Rietveld Method, of which nearly half used neutron diffraction. The review article of Albinati and Willis [6] gives a good impression of the state of the method at that moment. Many more papers on the method have appeared since, often with unexpected applications.

A.1.2.3. Principles of the Rietveld Method

In order to perform the refinement, data of X-ray powder diffraction should be digitized in a fixed step mode. The fixed step mode is usually used for the measurement of position and relative intensity of diffraction peaks accurately. Normal data collection range in 2θ is between 0.01 to 0.05^{o}.

The refinement is proceeded by indexation of the observed diffraction peaks using appropriate Bragg reflection angle, and therefore precise lattice constants are calculated based on the diffraction pattern. It needs a great extent of effort to refine, if a material has a large unit volume or low symmetry. Further, a suitable space group and a careful examination of occupation sites of atoms should be chosen to refine well. Then, if the structural model is selected properly, the observed pattern, *yi*, is compared to the calculated pattern, *yi*(c). Each parameter which organizes structural model can be minimized by a least square method following equation, *S*;

$$S = \sum wi\left|yi - yi(c)\right|^2 \quad \text{(A.1)}$$

where *wi* is a statistical aggravation parameter. Here, the calculated intensity, *yi(c)* is given as below;

$$yi(c) = \sum_k s\left|F_k\right|^2 m_k P_k L(\theta) G(\Delta\theta_{i_k}) + y_{i_k}(c) \quad \text{(A.2)}$$

, where *yi(c)* = calculated intensity,

k = reflection number,

s = scale factor,

F_k = structure factor,

m_k = multiplicity,

P_k = correction factor for preferred orientation,

$L(\theta)$ = Lorentz and polarization factor,

$G(\Delta\theta_{i_k})$ = profile shape factor,

y_{i_k} = background intensity,

θ_i = scattering angle at *i*th step,

θ_k = Bragg angle,

$\Delta\theta_{i_k} = \theta_i - \theta_k$,

Then, the structural parameter can be expressed as follow;

$$F_k = \sum \exp[2\pi i(hx_j + hy_j + hz_j)]\exp(-M_j) \quad \text{(A.3)}$$

, where *h, k, l* : Miller indices,

M_j = site occupancy of *j*th atom,

x_j, y_j, z_j = coordinates of *j*th atom in unit cell,

$M_j = 8\pi^2 \overline{U^2} \sin^2\theta / \lambda^2$,

$\overline{U^2}$ = thermal vibration

Therefore, refinement parameters contain position of each atom, peak profile, thermal vibration factor and background parameters, as can be seen in the above equations.

Rietveld refinement was usually employed to refine neutron diffraction data, because profile function for neutron diffraction is expressed with Gaussian function. In case of X-ray diffraction, however, the shapes of diffracted peaks are rather complex than that of neutron and are difficult to find proper profile of X-ray diffraction so that the application of refinement for X-ray diffraction could not grow prosper than that of neutron diffraction. As a result, Gaussian, Lorentzian, Pseudo-Voigt functions that show peak profile of X-ray diffraction should be necessary to obtain reliable refinement results.

A full width of the half maximum (FWHM) which decides the broadness of diffraction

peaks is given as below;

$$FWHM^2 = H_k{}^2 = U\tan^2\theta + V\tan\theta + W \tag{A.4}$$

Background intensity can be expressed;

$$y_{ib} = \sum_n b_n (2\theta_j)^n \tag{A.5}$$

The above enumerated all parameters are used to Rietveld refinement, and the follow parameters are directly referred as the measurement of appropriateness between observed and calculated patterns.

I) Profile *R* factor

$$R_p = \frac{\sum |y_i - y_{ic}|}{\sum y_i} \tag{A.6}$$

$$R_{wp} = \left[\frac{\sum w_i |y_i - y_{ic}|}{\sum w_i y_i{}^2} \right]^{\frac{1}{2}} \tag{A.7}$$

Provided that background intensity becomes high, *Rwp* may appear small. The above two factor are usually used to decide the refinement results, if the value becomes less than 10 %, it is interpreted that the refinement was done successfully.

II) The Bragg *R* factor

$$R_B = \frac{\sum |I_k - I_{kc}|}{\sum I_k} \tag{A.8}$$

This is much more reliable factor than profile factors to examine the appropriateness of

structural parameters used for refinement.

III) Expected R factor

$$R_E = \left[\frac{(N-P)}{\sum w_i y_i^{\,2}} \right]^{\frac{1}{2}} \tag{A.9}$$

N: number of data points

P: number of refined parameters

This factor means statically expected minimum *R* factor. When intensity is considerably higher, the *RE* value is tending to decrease.

IV) Goodness of fit, S

$$S = \left[\frac{\sum w_i (y_i - y_{ic})^2}{N-P} \right]^{\frac{1}{2}} = \frac{R_{wp}}{R_E} \tag{A.10}$$

S = 1 means perfect refinement. Practically, smaller value of S factor results in much better refinement results, for example, 1.4.

A.1.2.4. Structural Calculation Parameters

I) Global parameters

(a) Zero point shift

Diffraction error in 2 . The error can be calibrated by using Si standard powder.

(b) Background parameter

b1, b2, b3

II) Phase dependent parameters

Parameters to adjust integrated intensities.

(a) Scale factor: s

Control total intensity of diffraction peaks

(b) Preferred orientation parameters: p1,p2

In case of the sample having a preferred orientation, this parameter is useful.

III) Profile parameters

(a) FWHM parameters: *u, v, w*

Control the broadness of each diffraction peak

(b) Gaussian factor: .

(c) FWHM ratio;

d) Asymmetry parameter: *A*

Calibrate asymmetry of peaks appeared below 35^{o} in 2

IV) Parameters determining peak position

(a) Lattice parameters: *a, b, c,* , ,

(b) Fractional coordinate: *xj,yj, zj*

(c) Occupation factor: *nj*

(d) Overall thermal parameter: *Q*

(e) Isotropic thermal parameter: *Bj*

(f) Anistropic thermal parameter: *11j, 22j, 33j*

A.1.3. Electron Microscopy

Electron microscopy is an extremely versatile technique capable of providing stru ctural information over a wide range of magnification. At one extreme, scanning electron microscopy (SEM) complements optical microscopy for studying the tex ture, topography and surface features of powders or solid pieces; features up to t ens of micrometers in size can be seen and, because of the depth of focus of S EM instruments, the resulting pictures have a definite three-dimensional quality.

With reflection instruments samples thickness is no longer causing a problem and special methods of sample preparation are not required. It is usually necessary o nly to coat the sample with a thin layer of metal, especially if the sample is a poor electrical conductor, in order to prevent the build-up of charge on the surfa ce of the sample. The main reflection instrument is SEM. It covers the magnific ation range between the lower resolution limit of optical microscopy (~ 1 m) and the upper practical working limit of transmission electron microscopy (TEM) (~ 0.1 mm) although, SEM can be used to study structure over a much wider ra nge from 10^{-2} to 10^{2} m. The approximate working ranges of different kinds of microscope are summarized in Fig. A. 2.

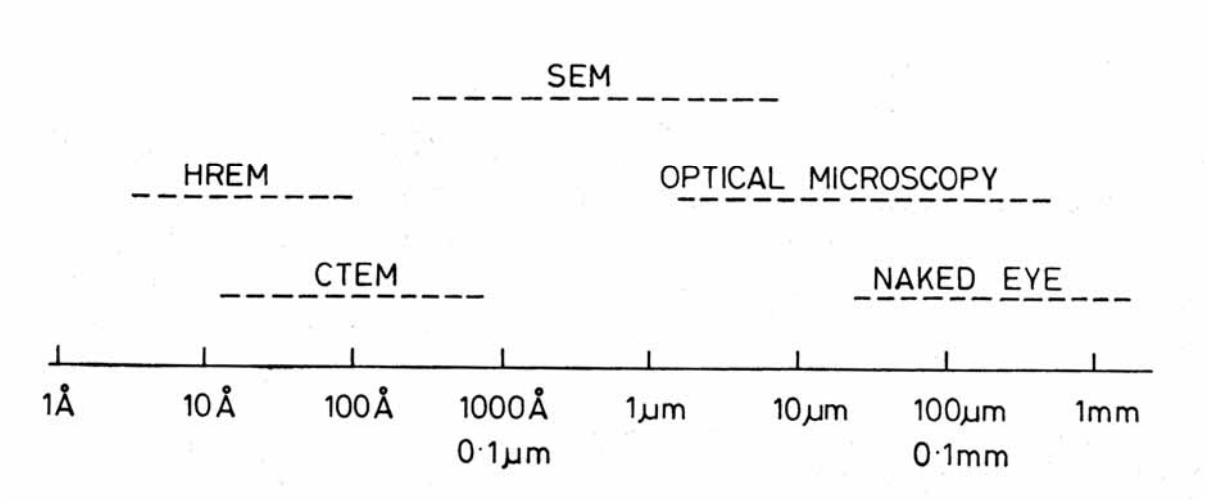

Figure A.2. Working ranges of various techniques used for viewing solids. CTEM; conventional transmission electron microscopy, HREM; high resolution electron microscopy, SEM; scanning electron microscopy.

Some SEM and TEM instruments have the very valuable additional feature of pr oviding an elemental analysis of sample composition. There are various names fo r the technique including electron probe microanalysis (EPMA), electron microsco py with microanalysis (EMMA) and analytical electron microscopy (AEM). The main mode of operation makes use of the fact that when a sample is placed in the microscope and bombarded with high energy electrons, many things can happ en including the generation of X-rays. These X-rays are characteristic emission s pectra of the elements present in the sample. By scanning either the wavelength (wavelength dispersive, WD) or the energy (energy dispersive, ED) of the emitte d X-rays, it is possible to identify the elements present. If a suitable calibration procedure has been adopted, a quantitative elemental analysis may be made.

In the scanning electron microscope, electrons from the electron gun are focused

to a small spot, 50 to 100 Å in diameter, in the surface of the sample. The el ectron beam is scanned systematically over the sample. Both X-rays and seconda ry electrons are emitted by the sample; the former are used for chemical analysi s and the latter are used to build up an image of the sample surface. A recent advance is the development of the scanning transmission electron microscope (ST EM). This combines the scanning feature of the SEM with the intrinsically highe r resolution obtainable with TEM.

A.1.4. X-ray Photoelectron Spectroscopy

XPS, also known as ESCA (electron spectroscopy for chemical analysis), is one of the most powerful tools used for surface analysis technique. This technique consists in bombarding a solid sample under vacuum with a monoenergetic beam of X photons. The photon, with an energy of exciting radiation, *hv*, interacts with one electron of the sample. If *hv* is higher than the binding energy of the electron, the photon gives all its energy to the electron, which is then ejected; it is the photoelectric effect.

The Kinetic energy of emitted photoelectrons, *Ec*, detected using an electron spectrometer, gives access to the binding energy, *Eb*, by $Eb = hv - Ec - s$

Where s is the spectrometer work function. The identification of the photoelectric peaks using the binding energy values is possible using data available in the literature. In addition, the binding energies of electrons are affected by the valence electrons and therefore, by the chemical environment of the atom. For a given atom, a range of *Eb* values is possible, corresponding to the ionization of electrons from different inner and outer shells, and these *Eb* values are characteristic for each element.

The principal use of ESCA for studying surfaces, mainly because it is one of the few techniques that is surface selective. It may be used purely as an analytical method for detecting which elements are present at a surface and in particular for detecting layers of adsorbed molecules on, for example, the surface of metals.

This technique only allows analyzing the composition of the surface sample, the analyzed thickness depends on the nature of the sample; it is usually lower than 20 nm.

A.2. Electrochemical analysis

The electroanalytical methods use electrically conductive probes, called electrodes, to make electrical contact with the electrolyte. The electrodes are used in conjunction with electric or electronic devices to which they are attached, to measure an electrical parameter of the solution. The measured parameter is related to the identity or to the quantity of the electroactive species present in the solution. The electroanalytical methods are divided into categories according to the electric parameters that are measured. The major electroanalytical methods include potentiometry, amperometry, conductimetry, voltamperometry and coulmetry. The names of the methods reflect the measured electric property or its units.

In case of voltamperometry, typically the potential is initially adjusted to a value at which no electrochemical reaction occurs at the working electrode. The potential is scanned in a direction that makes an electrochemical reaction more favorable. In the most common case, the potential varies linearly with time but triangular voltamperometry wave (cyclic voltammetry) is more used.

A.2.1. Cyclic Voltammetry

The study of an electrochemical system can be carried out by measuring a couple of intensity-time curves for different applied potentials. Through this method, one can build a three dimensional intensity-time-potential surface. However, because of the quantity of information measured, it becomes quite hard to analyze them, especially when a stationary electrode is used. Moreover, if many species are present in the solution, it becomes difficult to determine their presence through I-t curve. In practice, more information can be obtained easily through one experiment if a scanning potential function of the time is applied. The scanning mode used is usually a linear variation of the potential function of the time and the scan speed used comprised between 0.01 and 100 V/s.

Let us consider the following electrochemical reaction;

$Ox + ne^- \rightarrow Red$

If the initial potential is positive enough, the current produced by the reduction of the species is negligible at the start of the scan, only the residual current can be observed. When the potential decreases, the reduction speed of the oxidant compounds increases with increasing current value. When the reduction speed is too high, the concentration of the oxidant species becomes null at the electrode surface and the current is limited by diffusion, at this time, the current decreases as a function of time and potential.

The theoretical analysis consists of resolving the Fick's equations, taking into account boundary conditions. For a reduction step, the potential is function of the scan speed following this equation;

$E = E_i - vt$

where v sweep rate, and E_i starting potential. When the final potential, E_f, is reached, a reverse sweep is applied: $E + E_f + vt$. This technique can be used for qualitative analysis because substances exhibit characteristic peaks or waves at different potentials. Theoretical considerations permit to access to parameters like diffusion coefficient, D, concentration, c, through the peak intensity, and the peaks potential values. However, the detailed analysis of the voltammograms is difficult because it leads to integral equation which must be solved numerically.

References

[1] H.M. Rietveld, *Acta Crystallogr*., **20** (1966) 508.

[2] H.M. Rietveld, *J.Appl. Crystallogr.,* **2** (1969) 65.

[3] A.K. Cheetham, and J.C. Taylor, *J. Solid State Chem*., **21** (1977) 253.

[4] G. Malmros, and J.O. Thomas, *J. Appl. Crystallogr*., **10** (1977) 7.

[5] H.M. Rietveld, *Acta Crystallogr*., **22** (1967) 151.

[6] A. Albinati, and B.T.M. Willis, *J. Appl. Crystallogr*., **15** (1982) 361.

Acknowledgement

The author would like to heartfelt thank to Professor Masaki Yoshio of Saga University for his fruitful supervision and encouragement throughout my doctoral course. The author also would like to express grateful to Professor Hideyuki Noguchi of Saga University for his solicitous care and valuable discussion. Without their patient instruction, this work could not be fulfilled.

The author would especially like to express special thank to Professor Hoon-Taek Chung of Dongshin University for his guidance of my life and encouragement

The author sincerely acknowledges valuable discussion and unselfish help of Dr. Hiroyoshi Nakamura and Mr. Kenichi Isono during three years.

The author wishes to thank Prof. Watari and Prof. Nagano of Saga University for their kind reviewing and valuable comments.

The author would like to express his appreciation to Dr. Y. S. Lee, Dr. H. Wang, Dr, N. Dimov, Dr. D. Li, Mr. S. M. Park, Dr. P. Gimire, Mr. Q. Zhang, Mrs. M. Zou, Mr. A. Thapa, Mr. Y, Xia and all other students in this laboratory for their kind help in this work.

The author specially tank to Jung-min Kim and Seung-taek Myung for their best friendship and valuable discussion. Without their discussion, this work could not be fulfilled so smoothly.

The author wishes to thank the Japanese Government for the financial support during the doctoral course.

Finally, the author would like to express his family for their unselfish help, patience, and incentive support during this work.

PUBLICATIONS

1. Synthesis and Characterization of $LiNi_{0.8}Co_{0.2}O_2$ Synthesized by an Emulsion Drying Method, J. Applied Electrochemistry, Resubmitted revised manuscript.

   Tae-Hyung Cho and Hoon-Taek Chung

2. Novel Surface Modification Technique to Improve Electrochemical Performance of $LiCoO_2$ at High Voltage, *Electrochemical Solid-State Letter*, **8** (2005) A229

   Sang-mok Park, Tae-hyung Cho, You-mee Kim, and Masaki Yoshio

3. Effect of Synthesis Condition on the Structural and Electrochemical properties of $Li[Ni_{1/3}Mn_{1/3}Co_{1/3}]O_2$ Prepared by Carbonate Co-precipitation Method, *Journal of Power Sources*, **142** (2005) 306

   T. H. Cho, S. M. Park, M. Yoshio, T. Hirai, and Y. Hideshima

4. Novel Synthesis Method for Preparing Layered $Li[Mn_{1/2}Ni_{1/2}]O_2$ as a Cathode Material for Lithium Ion Secondary Battery, *Chemistry Letters* **33** (2004) 748

   Sang-Mok Park, Tae-Hyung Cho, and Masaki Yoshio

5. Preparation of Layered $Li[Ni_{1/3}Mn_{1/3}Co_{1/3}]O_2$ as a Cathode for Lithium Secondary Battery by Carbonate Co-precipitation Method, *Chemistry Letters* **33** (2004) 704

   Tae-hyung Cho, Sang-mok Park, and Masaki Yoshio

6. Synthesis of Olivine Type $LiFePO_4$ Compound by Emulsion Drying Method, *Journal of Power Sources* **133** (2004) 272

   Tae-Hyung Cho and Hoon-Taek Chung

7. Synthesis and electrochemical behavior of spinel structure of $Li_{1+x}M_yMn_{2-x-y}O_4$(M=Co, Ni) obtained by carbonate co-precipitation method, Electrochemistry 71 (2003) 1087

   Tae-Hyung Cho, Masami Makidera, Hiroyoshi Nakamura, and Masaki Yoshio

8. Nano-crystalline $LiNi_{0.5}Mn_{1.5}O_4$ synthesized by emulsion drying method, Electrochimica Acta 47 (2002) 2543

S. T. Myung, S. Komaba, N. Kumagai, H. Yashiro, H. T. Chung and T. H. Cho\

9. Lattice Parameter as a meawure of electrochemical properties of LiMn2O4, Journal of Power Sources 97-98 (2001) 454

Hoon-Taek Chung, Seung-Taek, Myung, Tae-Hyung Cho and Jong-Tae Son -457

Academic Activities

1. Synthesis of Ni – Based Layered Compounds by Carbonate Co-precipitation Method for Li-ion Battery Cathode Material.
   Tae-Hyung Cho, Sang-mok Park and Masaki Yoshio
   The 5th Korea-Japan Joing Seminar on Advanced Batteries, Seoul, Korea, Septemper 25-27, 2003.

2. Characterization of Li[Ni1/2Mn1/2]O2 Synthesized by Carbonate Co-precipitation Method
   S. M. Park, T. H. Cho, H. Noguchi, M. Yoshio and T. Hirai
   The 71th Meeting of Electrochemical Society of Japan, Yokohama, Japan, April 24-26, 2004.

3. Synthesis and Characterization of Layered Li[Ni1/3Mn1/3Co1/3[O2 by Carbonate Co-precipitation Method.
   Tae-Hyung Cho, Sang-Mok Park, Hideyuki Noguchi and Masaki Yoshio
   The 205th Meeting of the Electrochemical Sodiety, San Antonio, Texas, May 9-14, 2004.

4. Structural and Electrochemical Properties of Li[Ni1/3Mn1/3Co1/3]O2 Prepared by Carbonate Co-precipitation Method
   Tae-Hyung Cho, Sang-Mok, Park, Hiroyoshi Nakamura, and Masaki Yoshio
   The 45th Battery Symposium in Japan, Kyoto, November 27-29, 2004.

5. Novel Surface Modification Technique to Improve Electrochemical Performance of $LiCoO_2$ at High Voltage
   Tae-Hyung Cho, Sang-Mok Park, Hiroyoshi Nakamura and Masaki Yoshio
   The 72nd Meeting of Electrochemical Society of Japan, Kumamoto, Japan, April, 1-3, 2005.